

Dissertation zur Erlangung des Doktorgrades  
der Fakultät für Chemie und Pharmazie  
der Ludwig-Maximilians-Universität München

# Characterization of a cytoplasmic mRNA-transport complex from yeast



Roland Gerhard Heym  
aus  
Frankenthal (Pfalz)

2011

## **Erklärung**

Diese Dissertation wurde im Sinne von § 13 Abs. 3 der Promotionsordnung vom 29. Januar 1998 (in der Fassung der sechsten Änderungssatzung vom 16. August 2010) von Herrn Prof. Dr. Roland Beckmann betreut.

## **Ehrenwörtliche Versicherung**

Diese Dissertation wurde selbständig, ohne unerlaubte Hilfe erarbeitet.

München, 19. Dezember 2011

Roland Heym

Dissertation eingereicht am 19. Dezember 2011

1. Gutachter: Prof. Dr. Roland Beckmann

2. Gutachter: Prof. Dr. Klaus Förstemann

Mündliche Prüfung am 1. März 2012

# TABLE OF CONTENTS

<b>SUMMARY</b> .....	<b>1</b>
<b>1 INTRODUCTION</b> .....	<b>3</b>
<b>1.1 mRNA localization in eukaryotes</b> .....	<b>3</b>
1.1.1 Active mRNA transport involves multiple steps.....	5
1.1.2 Examples of mRNA localization in different model systems.....	6
1.1.3 Zip-code elements direct mRNA localization .....	8
1.1.4 RNA-binding proteins with a function in mRNA localization .....	9
1.1.5 Motor molecules drive mRNA transport.....	11
1.1.6 Kinesin and dynein motors .....	11
1.1.7 Type V myosin motors .....	13
1.1.8 Regulation and coordination of motor molecules.....	14
<b>1.2 mRNA localization in budding yeast</b> .....	<b>16</b>
1.2.1 The steps of <i>ASH1</i> mRNA localization .....	17
1.2.2 Zip-code elements of localizing mRNAs from yeast.....	19
1.2.3 The RNA-binding protein She2p.....	20
1.2.4 The adapter protein She3p .....	22
1.2.5 The type V myosin Myo4p.....	22
1.2.6 Translational regulation of localizing transcripts.....	24
<b>1.3 Active transport of endoplasmic reticulum in yeast</b> .....	<b>25</b>
<b>1.4 Objectives</b> .....	<b>25</b>
<b>2 RESULTS</b> .....	<b>27</b>
<b>2.1 In vitro reconstitution of the SHE complex</b> .....	<b>27</b>
2.1.1 Expression and purification of SHE components .....	27
2.1.2 Reconstitution of the SHE-core complex <i>in vitro</i> .....	29
<b>2.2 Analysis of zip-code RNA recognition by She2p and She3p</b> .....	<b>30</b>
2.2.1 She2p and She3p form a complex .....	30
2.2.2 She3p binds RNA unspecifically.....	31
2.2.3 She2p and She3p synergistically recognize <i>ASH1</i> -E3 zip-code RNA .....	32
2.2.4 Mapping of RNA-protein binding sites in the ternary complex of <i>ASH1</i> -E3 RNA, She2p, and She3p .....	33
2.2.5 The C-terminus of She3p mediates synergistic RNA binding with She2p....	36

2.2.6	Point mutations in the C-terminus of She3p impair synergistic RNA binding with She2p.....	38
2.2.7	Helix E of She2p mediates synergistic RNA binding with She3p.....	40
2.2.8	Point Mutations around helix E of She2p impair synergistic RNA binding with She3p.....	43
<b>2.3</b>	<b>Structural studies on SHE sub-complexes.....</b>	<b>45</b>
2.3.1	Identification of a core-binding region in the <i>ASH1</i> -E3 zip-code element ...	45
2.3.2	Crystallization trials with She2p, She3p, and <i>ASH1</i> -E3 RNA.....	46
2.3.3	The ribosome as a structural scaffold for cryo-EM analysis of small RNA-protein complexes.....	48
2.3.4	She2p and She3p bind to zip-code containing ribosomes.....	49
2.3.5	Cryo-EM reconstruction of <i>ASH1</i> -E3 zip-code ribosomes in complex with She2p .....	50
<b>2.4</b>	<b>Size and stoichiometry analysis of SHE-complex assembly .....</b>	<b>53</b>
2.4.1	She3p oligomerizes via its N-terminus .....	53
2.4.2	A She3p dimer and a Myo4p monomer form a constitutive co-complex.....	53
2.4.3	A She2p tetramer binds two zip-code RNAs.....	55
2.4.4	Assembly of the SHE-core complex induces Myo4p dimerization.....	57
2.4.5	RNAs with two zip-code elements induce clustering of SHE-core complexes .....	61
2.4.6	Assembly of SHE-core complexes does not influence the actin-activated ATPase activity of Myo4p .....	63
<b>3</b>	<b>DISCUSSION.....</b>	<b>66</b>
3.1	Specific recognition of zip-code RNA is mediated by the co-complex of She2p and She3p .....	66
3.2	Structural studies on the SHE-core complex .....	77
3.3	SHE-core complex assembly induces motor multimerization .....	79
<b>4</b>	<b>MATERIALS &amp; METHODS .....</b>	<b>87</b>
4.1	Consumables and chemicals .....	87
4.2	Oligonucleotides .....	87
4.2.1	DNA oligonucleotides for cloning.....	87
4.2.2	DNA oligonucleotides to generate templates for <i>in vitro</i> transcription .....	89
4.2.3	RNA oligonucleotides .....	89
4.3	Plasmids.....	91
4.3.1	Plasmids for protein expression in <i>E. coli</i> .....	91

4.3.2	Plasmids for protein expression in insect cells .....	92
4.3.3	Plasmids for expression of tRNA-tagged RNAs in <i>E. coli</i> .....	92
4.3.4	Plasmids for rRNA modification in <i>M. smegmatis</i> .....	93
<b>4.4</b>	<b>Bacterial strains .....</b>	<b>93</b>
<b>4.5</b>	<b>Insect cell lines .....</b>	<b>93</b>
<b>4.6</b>	<b>Media and supplements.....</b>	<b>94</b>
<b>4.7</b>	<b>Molecular biology .....</b>	<b>94</b>
4.7.1	Molecular cloning.....	94
4.7.2	Transformation and selection of <i>M. smegmatis</i> cells .....	95
<b>4.8</b>	<b>Protein expression and purification .....</b>	<b>96</b>
4.8.1	Protein expression in <i>E. coli</i> .....	96
4.8.2	Protein expression in insect cells.....	96
4.8.3	Purification of She2p, She3p (1-234), and Myo4p (978-1471).....	97
4.8.4	Purification of full-length She3p constructs.....	97
4.8.5	Purification of C-terminal She3p constructs .....	98
4.8.6	Purification of full-length Myo4p .....	99
4.8.7	Purification of actin from rabbit muscle .....	100
<b>4.9</b>	<b>RNA expression and purification .....</b>	<b>101</b>
4.9.1	Expression and purification of tRNA-tagged RNAs .....	101
4.9.2	<i>In vitro</i> transcription and RNA purification.....	101
<b>4.10</b>	<b>Ribosome expression and purification .....</b>	<b>102</b>
<b>4.11</b>	<b>Biochemistry .....</b>	<b>103</b>
4.11.1	Concentration determination.....	103
4.11.2	Gel electrophoresis .....	104
4.11.3	Circular dichroism spectroscopy.....	104
4.11.4	Chemical cross-linking of proteins.....	105
4.11.5	<i>In vitro</i> pull-down assay.....	105
4.11.6	Analytical size-exclusion chromatography .....	105
4.11.7	Density gradient centrifugation of SHE-core complexes.....	106
4.11.8	Dynamic light scattering.....	106
4.11.9	Static light scattering .....	106
4.11.10	Surface plasmon resonance.....	107
4.11.11	Isothermal titration calorimetry .....	108
4.11.12	Electrophoretic mobility shift assay .....	108
4.11.13	UV cross-linking followed by mass spectrometry .....	109
4.11.14	Quantitative mass spectrometry .....	109

4.11.15	Regenerative ATPase assay .....	110
4.11.16	Radioactive ATPase assay .....	111
4.11.17	Ribosome pelleting assay .....	112
<b>4.12</b>	<b>Structural biology .....</b>	<b>112</b>
4.12.1	Crystallization .....	112
4.12.2	Cryo-electron microscopy.....	113
4.12.3	Calculation of single-particle cryo-EM reconstructions .....	114
<b>5</b>	<b>ABBREVIATIONS.....</b>	<b>116</b>
<b>6</b>	<b>SUPPLEMENTARY INFORMATION .....</b>	<b>118</b>
<b>7</b>	<b>REFERENCES .....</b>	<b>122</b>
	<b>PUBLICATIONS &amp; PRESENTATIONS .....</b>	<b>131</b>
	<b>ACKNOWLEDGEMENTS .....</b>	<b>132</b>

## SUMMARY

Asymmetric localization of mRNAs is an important mechanism to achieve spatially restricted gene expression in eukaryotes. In the budding yeast *Saccharomyces cerevisiae*, *ASH1* mRNA is actively transported during cell division from the mother cell to the tip of the daughter cell. There, the protein Ash1p is produced in a locally restricted manner and inhibits mating type switching of the daughter cell. The transport of *ASH1* mRNA is mediated by the SHE complex, consisting of the RNA-binding protein She2p, the adapter protein She3p, and the type V myosin Myo4p. In addition to *ASH1* mRNA, the SHE complex transports more than 30 other mRNAs to the bud tip. These transcripts contain stem-loop structures, so-called zip-code elements, that interact with the SHE complex.

Since She2p shows only weak specificity for zip-code elements, it was unclear how localizing transcripts are recognized by the SHE complex. Here, I demonstrate that the adapter protein She3p contributes to the specific recognition of zip-code elements. She2p and She3p act synergistically to bind zip-code RNAs with high specificity and affinity. Helix E of She2p and the C-terminus of She3p are crucial for this interaction. A key finding of this study is that a high-affinity complex between She2p and She3p is only formed in the presence of functional zip-code RNAs. Thus, the mRNA itself is indispensable for stable assembly of the SHE complex.

The motor protein Myo4p is monomeric and thus not capable to support processive transport along actin filaments. It was not known how many Myo4p molecules are incorporated into one SHE complex and how this assembly affects transport activity. Here, I demonstrate that two Myo4p molecules assemble with one RNA-bound She2p tetramer via She3p. Since She2p and She3p only form a stable complex in the presence of zip-code elements, dimerization of Myo4p is directly coupled to specific RNA recognition. Although SHE complex assembly does not stimulate the ATPase activity of Myo4p, it is likely that dimerization of Myo4p enables processive transport along the cytoskeleton. I further show that one She2p tetramer binds two zip-code elements and that RNAs with multiple

zip-code elements induce multimerization of SHE complexes into large ribonucleoprotein particles (RNPs) with variable size. These RNPs contain several RNA molecules and multiple Myo4p dimers. Such higher-order assemblies might enhance sustained transport to the bud tip and help to coordinate localization of different transcripts.

## 1 INTRODUCTION

### 1.1 mRNA localization in eukaryotes

mRNA localization and localized translation are important processes to achieve spatially and temporally regulated gene expression in eukaryotes. They are crucial for a variety of cellular processes (Figure 1.1), including the asymmetric distribution of cell fate determinants in yeast (Chartrand et al. 2001; Gonsalvez et al. 2005) and *Xenopus* oocytes (King et al. 2005), determination of body axes during embryonic development of *Drosophila* (Becalska and Gavis 2009; Kugler and Lasko 2009), migration of fibroblasts (Condeelis and Singer 2005), and neuronal plasticity as the basis for memory and learning (Martin and Zukin 2006; Bramham and Wells 2007).

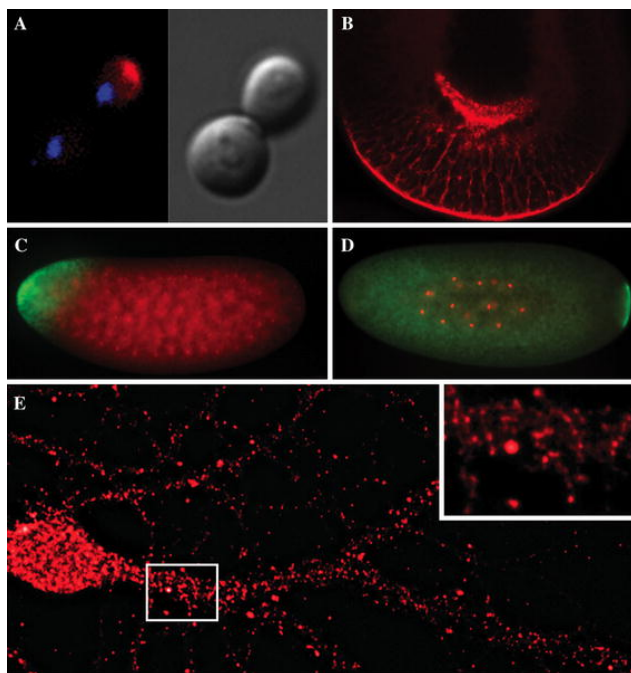


**Figure 1.1: Examples of mRNA localization in eukaryotic cells.** **A)** Localization of *ASH1* mRNA (red) to the bud tip of a dividing *S. cerevisiae* cell. Left panel shows FISH with *ASH1* mRNA in red and nuclei in blue. Right panel shows Normarski image. **B)** Localization of *Vg1* localization element RNA (red) to the vegetal pole of a *Xenopus* oocyte. **C)** Localization of *bicoid* mRNA (green) to the anterior pole of a *Drosophila* embryo. Nuclei are stained red. **D)** Localization of *nanos* mRNA (green) to the posterior pole of a *Drosophila* embryo. Nuclei are stained red. **E)** *CamKII $\alpha$*  mRNA granules (red) in dendrites of a hippocampal neuron. Magnification of the boxed region is shown in the upper right panel. The figure was taken from Shahbadian and Chartrand 2011.

In recent years, several large-scale approaches showed that mRNA localization is a widespread phenomenon. Screening for localized mRNAs in mouse fibroblasts identified at least 50 transcripts that were enriched in pseudopodial protrusions upon migration stimuli (Mili et al. 2008). High-throughput fluorescent *in situ* hybridization (FISH) of over 3000 transcripts in *Drosophila* embryos revealed that 71% of them were subcellularly localized (Lecuyer et al. 2007). The high

frequency and variety of localization patterns underlines the importance of mRNA localization for cellular architecture and function.

mRNA localization restricts gene expression to specific subcellular regions. Compared to localization of the protein itself, mRNA localization has several advantages. It is more cost-effective to localize the mRNA first and then produce several molecules of the respective protein from a single mRNA molecule (Martin and Ephrussi 2009). In addition, localized translation prevents proteins to act ectopically during transport. Another advantage of mRNA localization is that pre-deposition of translationally silenced transcripts allows for rapid local protein synthesis in responses to extrinsic cues (Holt and Bullock 2009). This is especially important in neurons, where the distance between the site of transcription and the site of response (i.e. the synapse) is large.

Localization of mRNA can be achieved by at least three different mechanisms (Meignin and Davis 2010). Common to all mechanisms is the presence of cis-acting regions in the mRNA (also termed zip-code elements or localization elements) that mediate its localization. Some mRNAs are selectively stabilized in a certain subcellular region, whereas rapid degradation occurs in the remainder of the cell. For example in *Drosophila* embryos, *nanos* mRNA is targeted for deadenylation and subsequent decay by binding of the protein Smaug to its 3' untranslated region (UTR) (Zaessinger et al. 2006). Only at the posterior pole, where the protein Oskar inhibits recruitment of Smaug, *nanos* mRNA is stabilized and translated. Another mRNA localization mechanism relies on diffusion and local entrapment of mRNAs. This mechanism contributes to *nanos* mRNA localization in late oogenesis, when cytoplasmic streaming supports its movement throughout the oocyte (Forrest and Gavis 2003). Upon association with the pole plasm, *nanos* mRNA is anchored at the posterior pole in an actin-dependent manner. The most common mechanism to achieve mRNA localization is active transport by motor proteins along the cytoskeleton (Martin and Ephrussi 2009).

### 1.1.1 Active mRNA transport involves multiple steps

Although active mRNA transport processes are complex and can be quite diverse in different organisms, they follow some general principles (Figure 1.2). All localizing mRNAs contain zip-code elements that determine the destination of the transcript (Jambhekar and DeRisi 2007). Zip-code elements are often recognized already in the nucleus by trans-acting RNA-binding proteins that function in transport and translational silencing of the transcript. For several mRNA localization events, nuclear processes, like co-transcriptional recruitment of RNA-binding proteins or pre-mRNA splicing, are crucial for cytoplasmic mRNA localization and translational repression (Giorgi and Moore 2007; Forget and Chartrand).

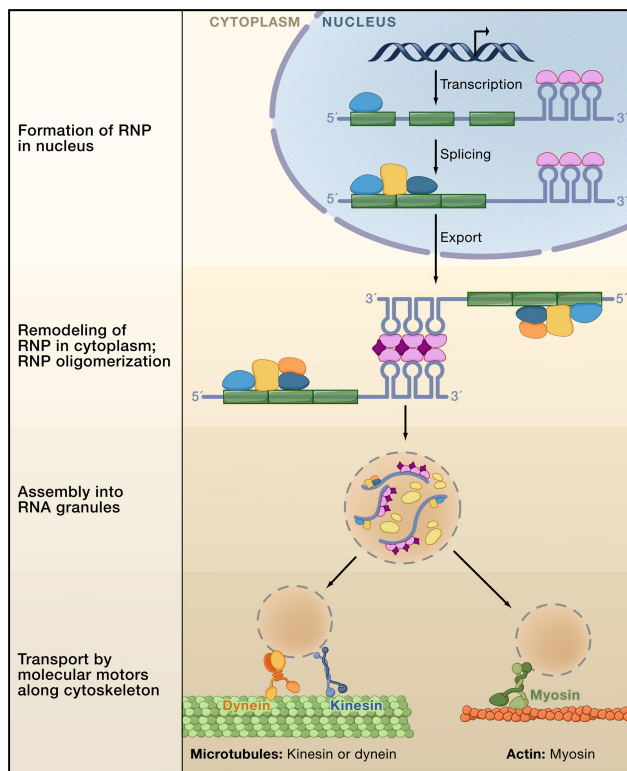


**Figure 1.2: Principle steps of active mRNA transport.** After transcription, trans-acting RNA-binding proteins (magenta) bind to the cis-acting localization elements in the 3' UTR of the localizing transcript. Additional RNA-binding proteins involved in translational repression and splicing (blue and yellow) are recruited. After nuclear export, further proteins (orange and purple) join the RNP. This remodeling may also induce oligomerization. Several RNPs are assembled into heterogeneous RNA granules containing diverse mRNAs, ribosomal subunits and proteins involved in translational control. Finally, motor proteins are incorporated into the complex and actively transport the mRNA to its destination. The figure was taken from Martin and Ephrussi 2009.

After nuclear export the messenger ribonucleoprotein particle (mRNP) recruits further proteins. This remodeling of the mRNP may include oligomerization as well as the formation of heterogeneous RNA transport granules containing several mRNA species (Martin and Ephrussi 2009). Finally, motor proteins are incorporated and mRNAs are actively transported along the cytoskeleton. All major types of motor molecules, i.e. kinesin, dynein, and myosin, can be involved

in the transport (Müller et al. 2007). However, in many cases the molecular linkage between the mRNA and the motor is not yet established. At its destination the mRNA is usually anchored and translational repression is relieved, resulting in local protein synthesis (Besse and Ephrussi 2008).

### 1.1.2 Examples of mRNA localization in different model systems

Over the years, active mRNA transport has been studied in several model organisms. In *Xenopus laevis* oocytes, *Vg1* mRNA is transported to the vegetal pole by kinesin (King et al. 2005). *Vg1* mRNA encodes a transforming growth factor  $\beta$  (TGF- $\beta$ ) family member that induces mesodermal development at the vegetal pole.

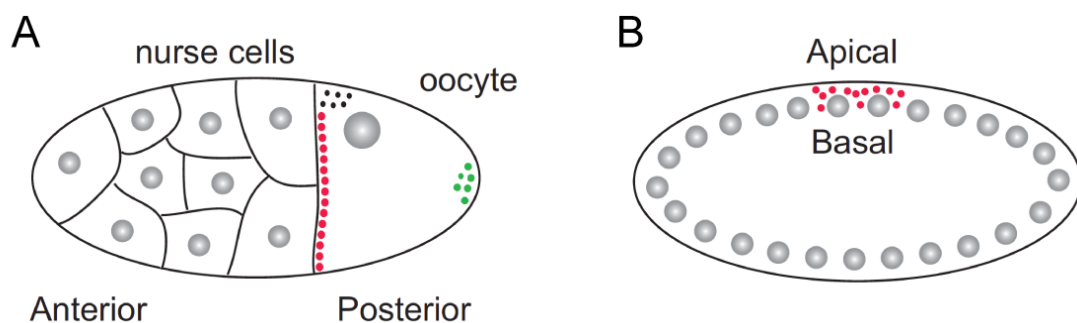


**Figure 1.3: Examples of mRNA localization in *Drosophila*.** **A)** In the *Drosophila* oocyte, *bicoid* mRNA (red dots) is localized to the anterior, *gurken* mRNA (black dots) to the dorsal anterior, and *oskar* mRNA (green dots) to the posterior pole. **B)** In the *Drosophila* syncytial blastoderm embryo, mRNAs from pair-rule genes are localized to the apical side of the nuclei. Nuclei are shown in grey. The figure was taken from Gagnon and Mowry 2011.

During *Drosophila* oogenesis, localization of four maternal mRNAs is crucial for the specification of anteroposterior and dorsoventral body axes of the embryo. *Gurken* mRNA is localized to the posterior of the oocyte, where signaling of the TGF- $\alpha$  homolog Gurken to the adjacent follicle cells induces reorganization of the cytoskeleton (Neuman-Silberberg and Schupbach 1993; Gonzalez-Reyes et al. 1995). Subsequently, *bicoid* mRNA is localized to the anterior, *oskar* mRNA to the posterior, and *gurken* mRNA to the dorsal anterior (Figure 1.3 A) (Becalska and Gavis 2009). Signaling by Gurken defines the dorsoventral axis of the embryo (Gonzalez-Reyes et al. 1995), whereas Oskar nucleates the assembly of the posterior pole plasm also containing *nanos* mRNA (Lehmann and Nusslein-

## INTRODUCTION

Volhard 1986). After fertilization, the translational repressor Nanos functions in abdominal and germline development, whereas the transcriptional regulator Bicoid defines head and thorax of the embryo (Becalska and Gavis 2009). Active transport of *gurken*, *bicoid*, and *oskar* mRNAs is mainly driven by dynein and kinesin along microtubules (Kugler and Lasko 2009). In the *Drosophila* syncytial blastoderm embryo, pair-rule transcripts (such as *fushi-tarazu* and *hairy*) as well as *wingless* mRNA are apically localized (Figure 1.3 B) (Bullock and Ish-Horowicz 2001; Bullock et al. 2006). This dynein-dependent process is important for proper segmentation of the embryo.

External stimuli trigger myosin-dependent transport of  $\beta$ -actin mRNA to the leading edge of fibroblasts to guide cell migration and the formation of cell protrusions (Latham et al. 2001; Condeelis and Singer 2005). Localized translation of  $\beta$ -actin provides a high local concentration of active monomers for fast and efficient polymerization of actin filaments (Holt and Bullock 2009).

Localization of  $\beta$ -actin mRNA also plays a role during axonal growth. Attractive signals induce  $\beta$ -actin mRNA localization at the site of stimulation to guide growth of the axon (Leung et al. 2006; Yao et al. 2006). In addition, mRNA transport is crucial for synaptic plasticity. Synaptic activation induces transcription of *arc* mRNA and its localization to the activated dendritic site (Steward et al. 1998). There, Arc impacts actin dynamics and dendritic spine morphogenesis (Bramham et al. 2008).  $Ca^{2+}$ /calmodulin-dependent protein kinase II  $\alpha$  (*CaMKII $\alpha$* ) mRNA also localizes to dendrites upon synaptic activation. Specific disruption of *CaMKII $\alpha$*  mRNA localization impairs long-term potentiation and memory in mice (Miller et al. 2002). Proteomic analysis of neuronal transport granules revealed great complexity (Kanai et al. 2004). A total of 42 proteins, as well as *Arc* and *CaMKII $\alpha$*  mRNA associate with conventional kinesin in such granules.

In contrast to the high complexity of mRNA localization in neurons, mRNA localization in the budding yeast *S. cerevisiae* is rather simple and involves only a limited number of proteins (Section 1.2.1). It is thus an excellent model system to study the molecular mechanisms of mRNA transport.

### 1.1.3 Zip-code elements direct mRNA localization

Zip-code elements direct localization of transcripts by recruiting trans-acting transport factors. If a zip-code element is placed into a reporter RNA, this RNA localizes to the same “address” as the donor mRNA (Jambhekar and DeRisi 2007). Zip-code RNAs typically reside in the 3' UTR of localizing transcripts, where they are unlikely to interfere with translation (St Johnston 2005). In some cases they are also found in the 5' UTR (Thio et al. 2000) or the coding region (Chartrand et al. 1999). The length of a zip-code element can vary between five and several hundred nucleotides (Jambhekar and DeRisi 2007).

How RNA-binding proteins recognize a zip-code element is still not very well understood. In few cases, the recognition is based on the primary structure of the RNA. For example, a linear motif of six nucleotides is critical for *Vg1* mRNA localization in *Xenopus* oocytes (Gautreau et al. 1997). In most cases however, zip-code elements form stem-loop structures that are crucial for their function (Hamilton and Davis 2007). Studies on *ASH1* mRNA from *S. cerevisiae* revealed that a combination of secondary structure and conserved nucleotides in certain positions defines functional zip-code elements (Section 1.2.2) (Jambhekar et al. 2005; Olivier et al. 2005). Further analyses indicated that these requirements are still not sufficient to explain zip-code recognition and localization (Jambhekar and DeRisi 2007). This suggests that structured zip-code elements might be recognized on the basis of their three-dimensional structure. To date, the only available tertiary structure of a zip-code element comes from the *fs(1)K10* mRNA (Bullock et al. 2010). The structure reveals a stem-loop with two helices adopting an unusual A'-form conformation. This gives rise to widened major grooves that are likely recognized by the transport machinery. Other zip-code elements even form a quaternary structure. For example, the *bicoid* zip-code element requires loop-loop mediated dimerization for proper recognition and localization by the RNA-binding protein Staufen (Ferrandon et al. 1997; Wagner et al. 2001). Recently, the *oskar* 3' UTR has been reported to dimerize in a similar manner (Jambor et al. 2011). A detailed understanding of zip-code recognition still awaits a high-resolution structure of a zip-code element in complex with its RNA-binding protein.

Many localizing transcripts contain multiple zip-code elements. These elements often have redundant function to ensure efficient localization, as in the case of *ASH1* mRNA from yeast (Chartrand et al. 1999; Gonzalez et al. 1999). Similarly, *Vg1* mRNA in *Xenopus* oocytes contains repetitions of redundant sequence motifs (Gautreau et al. 1997). On the other hand, distinct zip-code elements can mediate distinct steps of a localization event. For example, localization of *oskar* mRNA in *Drosophila* involves three steps: transport from the nurse cells to the oocyte, transient enrichment at the anterior, and finally localization to the posterior pole (Kugler and Lasko 2009). Each step is mediated by a distinct cis-acting region in the *oskar* 3' UTR (Kim-Ha et al. 1993).

Interestingly, zip-code element function can be conserved between different cell types or even across species. For example, *ASH1* mRNA from *C. albicans* expressed in *S. cerevisiae* is efficiently transported into the daughter cell (Münchow et al. 2002). Similarly, maternal transcripts that are involved in asymmetric localization in the *Drosophila* oocyte are also localized upon injection into blastoderm embryos (Bullock and Ish-Horowicz 2001). These experiments suggest conservation of the transport machinery in different cells types and species.

### **1.1.4 RNA-binding proteins with a function in mRNA localization**

Several trans-acting RNA-binding proteins have a conserved role in mRNA localization. For example, the protein Staufen is involved in several active mRNA-transport processes along microtubules and actin filaments in *Drosophila*, *Xenopus*, as well as mammalian dendrites (St Johnston 2005). Different regions of Staufen are responsible for the association with actin- and microtubule-based transport complexes. Staufen has five conserved double-stranded RNA-binding domains (dsRBDs), of which only three bind RNA (Micklem et al. 2000). A single dsRBD of Staufen binds indiscriminately to double-stranded RNA *in vitro* (St Johnston et al. 1992). However, if the *bicoid* 3' UTR – a native target of Staufen – is injected into *Drosophila* embryos, Staufen specifically associates with this RNA to form large mRNPs that are transported to the anterior pole (Ferrandon et al.

## INTRODUCTION

1994). Efficient interaction with Staufen requires dimerization of the *bicoid* 3' UTR (Ferrandon et al. 1997). The ability of Staufen to form multimers via protein-RNA and protein-protein interactions *in vivo* (Martel et al. 2010) might contribute to mRNP assembly.

The zip-code binding protein 1 (ZBP1) was first identified in chicken embryo fibroblasts, where it is involved in localization and translational silencing of  *$\beta$ -actin* mRNA by binding to a 54 nucleotides-long localization element in its 3' UTR (Kislauskis et al. 1994; Ross et al. 1997; Besse and Ephrussi 2008). Homologs of ZBP1 contribute to mRNA localization in *Xenopus*, *Drosophila*, mouse, and human (Martin and Ephrussi 2009). ZBP1 contains two RNA recognition motif (RRM) domains followed by four hnRNP K homology (KH) domains (Farina et al. 2003). The KH domains are required for the formation of  *$\beta$ -actin* mRNA-containing granules and association with the cytoskeleton. The RRM domains are necessary for localization of the granules to the leading edge of fibroblasts. It is clear that the KH domains mediate specific binding to the  *$\beta$ -actin* zip-code element but mechanistic details and the role of specific KH domains are still under debate (Farina et al. 2003; Atlas et al. 2007). Nevertheless, it has been shown that KH domains three and four recognize a bipartite single-stranded sequence motif in the 5'-half of the  *$\beta$ -actin* zip-code (Chao et al. 2010). The structure of KH domains three and four suggests that RNA binding induces a 180° turn in the RNA, which might be required for specific RNA recognition and assembly of the mRNP (Chao et al. 2010). Similar to the oligomerization of Staufen, ZBP1 is able to form dimers that are stabilized in the presence of RNA (Git and Standart 2002; Nielsen et al. 2004).

In contrast to Staufen and ZBP1, the protein Egalitarian (Egl) lacks a canonical RNA-binding motif (Dienstbier et al. 2009). Nevertheless, it binds zip-code elements from localizing pair-rule transcripts in *Drosophila* embryos. The affinity to functional zip-code elements is however only three to six-fold higher than to mutated, non-functional elements.

### 1.1.5 Motor molecules drive mRNA transport

Three types of motor molecules are utilized to transport mRNAs to different locations in various organisms and cell types (Figure 1.4) (Gagnon and Mowry 2011). Kinesins mediate transport towards the plus-end of microtubules, whereas cytoplasmic dynein moves to the microtubule minus-end. Type V myosin is responsible for plus-end directed transport along actin filaments. All molecular motors use energy from adenosine triphosphate (ATP) hydrolysis to undergo conformational changes that finally drive movement along cytoskeletal tracks (Vale and Milligan 2000; Tyska and Mooseker 2003; Sellers and Veigel 2006; Gennerich and Vale 2009). Most motors dimerize via coiled-coil domains to achieve processive movement meaning that the motor takes several steps on its track without dissociating. In addition to mRNA localization, molecular motors are involved in the transport of vesicles, organelles, intermediate filaments, viruses, and the mitotic spindle. (Vale 2003b).

To date, the molecular link between motor molecules and their mRNA cargo remains ambiguous for most transport processes. Only for *ASH1*-mRNA transport in yeast (Section 1.2.1) and for pair-rule transcripts in *Drosophila* embryos this linkage has been established. In *Drosophila*, the protein Egl recognizes pair-rule transcripts and links them to dynein by binding independently to dynein light chain and the dynein co-factor Bicaudal-D (BicD) (Navarro et al. 2004; Dienstbier et al. 2009).

### 1.1.6 Kinesin and dynein motors

Three types of kinesins are associated with intracellular cargo transport: kinesin I (or conventional kinesin), kinesin II (or heteromeric kinesin), and Unc104/KIF1 (Vale 2003b). Kinesin I is a heterotetramer comprised of two kinesin heavy chains (KHC) and two kinesin light chains (KLC) (Figure 1.4 A). The KHC is built up of an N-terminal motor domain responsible for microtubule binding and ATP hydrolysis, followed by a long coiled-coil for dimerization and a C-terminal cargo-binding domain (Vale 2003b). KLC binds to the C-terminus of

KHC and contributes to cargo recognition. Important examples of kinesin-transported transcripts include *oskar* mRNA in *Drosophila*, *Vg1* mRNA in *Xenopus*, *myelin basic protein* mRNA in oligodendrocytes, and several mRNAs in vertebrate neurons (Müller et al. 2007; Gagnon and Mowry 2011).

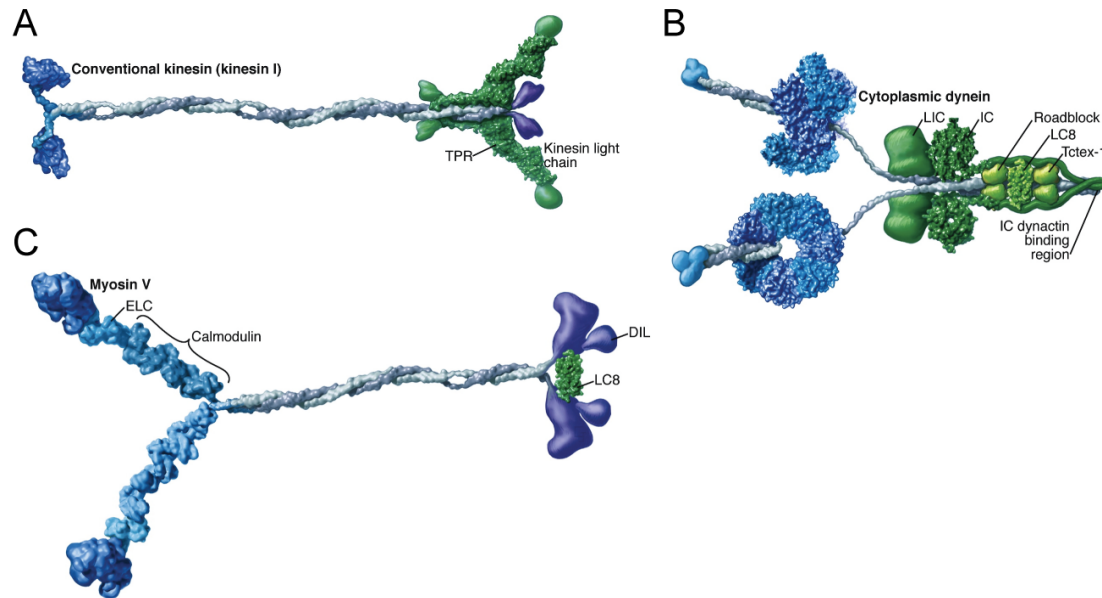


**Figure 1.4: Architecture of the three main classes of molecular motors for mRNA transport.** **A)** Kinesin I, also termed conventional kinesin. **B)** Cytoplasmic dynein. **C)** Type V myosin. Catalytical motor domains are shown in blue, mechanical elements (like lever arms) in light blue, coiled-coils in grey, cargo binding domains in purple and tightly associated subunits (light chains) in green. Surface features of existing atomic resolution structures are included. Smooth envelopes represent domains of unknown structure. The figure was taken from Vale 2003b.

Cytoplasmic dynein consists of a homodimeric dynein heavy chain (DHC) and several light chains that regulate cargo selection and dynein function (Figure 1.4 B) (Vale 2003b; Kardon and Vale 2009). The motor domain of the DHC is composed of six AAA domains that are arranged in an asymmetric ring (Carter et al. 2011). A coiled-coil is inserted into this ring and links it to a microtubule binding domain. Another coiled-coil extending at the N-terminus of the motor domain mediates dimerization and associates with additional subunits that establish interactions with various cargos (Vale 2003b). Cytoplasmic dynein mediates transport of *bicoid* and *gurken* mRNA during *Drosophila* oogenesis as well as localization of pair-rule mRNAs in *Drosophila* embryos (Gagnon and Mowry 2011).

### 1.1.7 Type V myosin motors

Myosins and kinesins evolved from a common ancestor and thus share general features (Vale and Milligan 2000). Type V myosin has an N-terminal motor domain (or head domain) for actin binding and ATP hydrolysis, a lever arm helix (or neck domain) that is stabilized by six calmodulins (CaM) or related light chains, a long coiled-coil (or rod region) for dimerization, and a C-terminal cargo-binding domain (or globular tail domain, GTD) (Figure 1.4 C) (Trybus 2008). Myosin V dimers move processively along actin filaments taking steps of 36 nm (Walker et al. 2000). The step size corresponds to the half-repeat distance of the actin double-helix and allows myosin V to walk straight without rotation around the filament axis.

The hand-over-hand model describes the processive movement of myosin V (Tyska and Mooseker 2003; Vale 2003a; Trybus 2008). The head domain of myosin V has high affinity for actin filaments in the adenosine diphosphate (ADP)-bound form, whereas ATP binding triggers dissociation. When both heads are ADP-bound and attached to the filament, the leading head is in a strained pre-power stroke state, whereas the trailing head adopts a post-power stroke conformation (Trybus 2008). ADP release is the rate-limiting step of the ATPase cycle preceding dissociation of the head upon ATP binding. A process, called kinetic gating, coordinates both heads to ensure that one head remains bound to the filament at all times (Vale 2003a; Sellers and Veigel 2006). Intramolecular strain between the heads slightly increases the rate of ADP release from the trailing head, whereas ADP release from the leading head is substantially slowed down. Thus, the trailing head dissociates upon binding of ATP, while the leading head remains bound and completes its power stroke. The dissociated head swings forward, hydrolyzes ATP, adopts the pre-power stroke state, and binds to the next binding site on its track (Trybus 2008). During the power stroke, the lever arm transfers small nucleotide-dependent conformational changes in the motor domain into a large step (Tyska and Mooseker 2003; Vale 2003a).

Myosin V is responsible for the transport of a subset of mRNAs into the bud of a dividing yeast cell (Müller et al. 2007) (Section 1.2.5). Recently, myosin V has

also been involved in short-range transport of *oskar* mRNA at the posterior pole of *Drosophila* oocytes (Krauss et al. 2009). In addition, type V myosins play an important role in the transport of membranes (Li and Nebenfuhr 2008). In mammalian melanocytes, MyoVa transports melanosomes to the cell periphery. During cell division of yeast, Myo2p delivers secretory vesicles and vacuoles to the bud. The binding sites for vacuoles and vesicles are simultaneously exposed on opposite sides of the Myo2p globular tail domain (Pashkova et al. 2006), suggesting that both cargos might be able to associate simultaneously with Myo2p.

The engagement of myosin V with its various cargos is tightly regulated by several mechanisms (Li and Nebenfuhr 2008; Trybus 2008). For example, alternative splicing of mammalian MyoVa controls the expression of exons that act as part of the cargo-binding site. Alternatively, cargo binding can induce a conformational change in the cargo-binding domain that reduces the affinity for another cargo. Phosphorylation of the globular tail domain has been implicated in cargo release (Karcher et al. 2001). Myosin adapter proteins can be regulated by differential expression, degradation, or conformational changes upon cargo binding (Li and Nebenfuhr 2008; Trybus 2008). For example, deposition of the vacuole at its final destination depends on degradation of the adapter protein Vac17p via its PEST sequence (Tang et al. 2003).

### **1.1.8 Regulation and coordination of motor molecules**

Processive motors are often regulated by auto-inhibition to prevent unnecessary ATP consumption when the motor is not engaged in transport. In the absence of  $\text{Ca}^{2+}$ , myosin V adopts its auto-inhibited form characterized by a compact conformation (Taylor 2007). Bending at the junction between lever arm and coiled-coil enables the cargo binding domains to interact with the motor domains and inhibit their ATPase activity (Figure 1.5) (Liu et al. 2006; Thirumurugan et al. 2006). In contrast,  $\text{Ca}^{2+}$  induces an extended conformation of myosin V and stimulates its actin-activated ATPase activity about 50-fold (Lu et al. 2006). Binding of the cargo adapter melanophilin also stimulates the actin-

## INTRODUCTION

activated ATPase activity of myosin V, albeit to a lesser extent than  $\text{Ca}^{2+}$  (Li et al. 2005). Nevertheless, it suggests that cargo binding triggers activation of the motor.

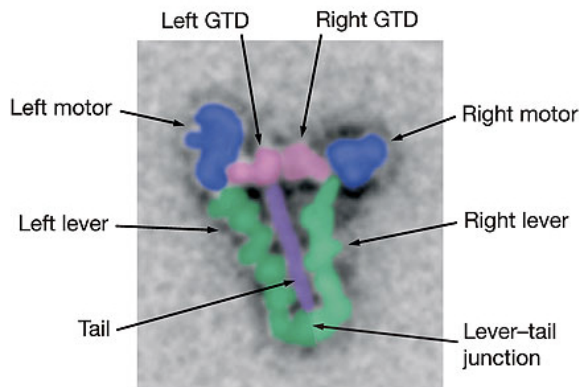


**Figure 1.5: Averaged electron microscopy image of the myosin V auto-inhibited state.** The globular tail domains (GTD) fold back onto the motor domains and inhibit their ATPase activity. Features corresponding to distinct domains are colored: motor domains (blue), lever arms (green), tail/coiled-coil (purple), GTD (magenta). The figure was taken from Thirumurugan et al. 2006.

Recently, the molecular basis for auto-inhibition of kinesin I has been revealed. A short peptide in the tail domain binds to a cleft between both motor domains and prevents conformational changes required for ADP release (Kaan et al. 2011). As for myosin V, release of kinesin I inhibition upon cargo binding has been demonstrated (Blasius et al. 2007).

Another mechanism to regulate motor activity is cargo-mediated oligomerization. For example, myosin VI involved in minus-end directed membrane transport is a monomer in isolation (Lister et al. 2004), but it dimerizes upon cargo binding (Phichith et al. 2009; Yu et al. 2009). Since dimerization is a prerequisite for kinetic gating and processive movement, cargo binding activates the motor. However, a recent study revealed that four or more myosin VI monomers coupled to a nanoparticle can move over long distances with similar speed than dimers (Sivaramakrishnan and Spudich 2009). Similarly, multimerization of the monomeric type V myosin Myo4p contributes to mRNA transport in yeast (Section 1.2.5) (Chung and Takizawa 2010).

Sequential or simultaneous association of different types of motors with an mRNA often regulates mRNA localization. During *Drosophila* oogenesis for example, *oskar* mRNA is first transported from the nurse cells into the oocyte by dynein, followed by kinesin I-dependent transport to the posterior pole (Bullock 2011). Myosin V also contributes to posterior localization of *oskar* mRNA by

counterbalancing kinesin function (Krauss et al. 2009). Such simultaneous association with different motors is also common in organelle transport and might help to navigate transport particles around roadblocks on their track (Welte 2004; Akhmanova and Hammer 2010).

Transcripts in the *Drosophila* blastoderm embryo undergo short bidirectional runs on microtubules without a net bias in either direction, suggesting engagement of competing motors (Bullock et al. 2006; Bullock 2011). The zip-code elements in localizing transcripts introduce a net bias towards long minus-end directed runs, possibly by recruiting a high copy number of dynein transport complexes (Bullock et al. 2006). Bidirectional movement has also been observed for neuronal transport granules that associate with kinesin and dynein simultaneously (Rook et al. 2000; Kanai et al. 2004; Elvira et al. 2006). Another mechanism has been suggested for *oskar* mRNA transport by kinesin I. Here, mRNPs move in all directions with a slight net bias towards the posterior (Zimyanin et al. 2007). This observation can be explained by plus-end directed transport along a weakly polarized microtubule network.

## 1.2 mRNA localization in budding yeast

The budding yeast *S. cerevisiae* can exist in a diploid and a haploid form (Cosma 2004). A haploid cell has either mating type a or  $\alpha$  representing a simple form of sexual differentiation. Two haploid cells of opposing mating types can mate to form a diploid cell. Unequal cell division of haploid yeast cells results in a mother cell that switches its mating type and a smaller daughter cell (or bud) that retains its original mating type. This process ensures equal distribution of mating types throughout a yeast population.

Mating-type switching of the mother cell relies on a genomic recombination at the MAT locus catalyzed by the HO endonuclease (Cosma 2004). In the daughter cell, the protein Ash1p inhibits the HO endonuclease and thereby suppresses mating-type switching (Bobola et al. 1996; Sil and Herskowitz 1996). Exclusive expression of Ash1p in the daughter cell is achieved by active transport and

localized translation of *ASH1* mRNA (Bobola et al. 1996; Sil and Herskowitz 1996; Long et al. 1997; Takizawa et al. 1997). *ASH1*-mRNA transport takes place during late anaphase of the cell cycle.

A genetic screen identified five genes, named SHE1-5 (for Swi5p-dependent HO expression), that are required for mother cell specific HO expression (Jansen et al. 1996). Further studies revealed that the proteins She1p/Myo4p, She2p and She3p are the main components of the *ASH1*-mRNA transport complex, also called locosome or SHE machinery (Gonsalvez et al. 2005; Müller et al. 2007).

In addition to *ASH1* mRNA, the SHE machinery transports more than 30 different mRNAs (Takizawa et al. 2000; Shepard et al. 2003; Oeffinger et al. 2007; Hogan et al. 2008). Interestingly, many of these mRNAs encode for membrane proteins. Live-cell imaging has revealed that different mRNAs are co-transported in the same particle (Lange et al. 2008).

Also in the fungal pathogen *C. albicans*, a set of 40 mRNAs is transported to the bud of yeast-form cells and to the tips of hyphae (Elson et al. 2009). A homolog of She3p (Figure S3) and a type V myosin motor have been identified in *C. albicans*, but no clear homolog of She2p is present. When *C. albicans* *ASH1* mRNA is expressed in *S. cerevisiae*, it accumulates in the bud (Münchow et al. 2002). Thus, the basic system of mRNA transport is conserved between *C. albicans* and *S. cerevisiae*.

### **1.2.1 The steps of *ASH1* mRNA localization**

Extensive research on *ASH1*-mRNA transport in yeast has yielded detailed insights into this process. In this chapter, I will provide an outline of the individual steps leading to *ASH1*-mRNA localization (Figure 1.6). Afterwards, the individual factors of the SHE machinery will be discussed (Section 1.2.2-1.2.6).

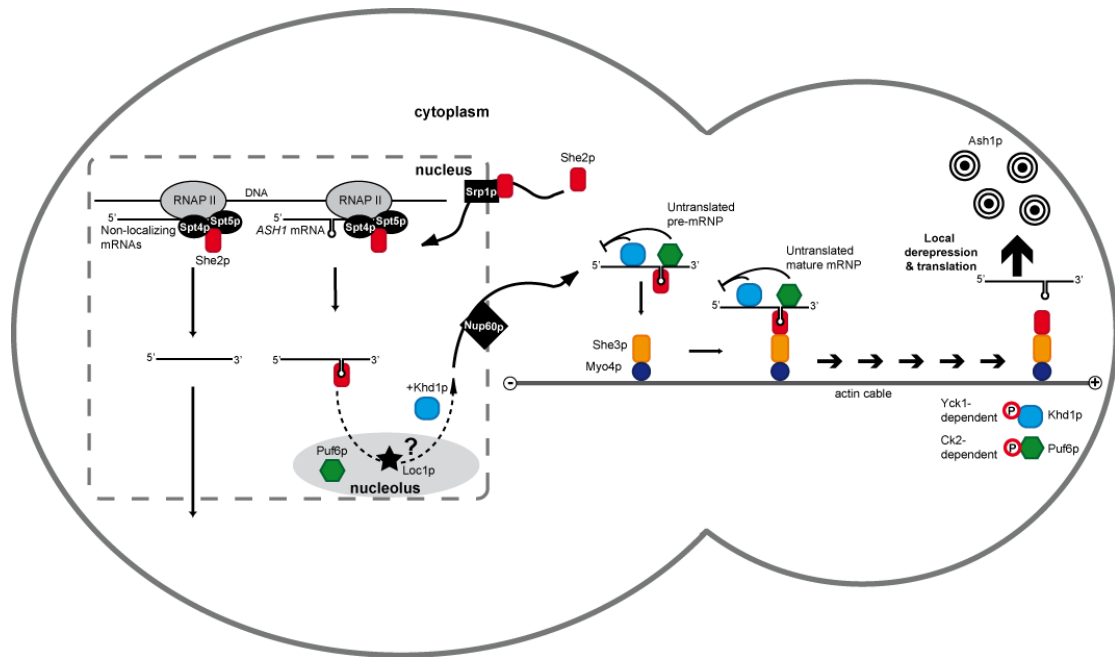


**Figure 1.6: Model of *ASH1*-mRNA localization in yeast.** The cartoon depicts the individual steps of *ASH1*-mRNA transport in a dividing yeast cell. After nuclear import, She2p binds co-transcriptionally to nascent *ASH1* mRNA. The RNA:She2p complex passes through the nucleolus and further assembles with the translational repressors Puf6p and Khd1p. After nuclear export, She2p binds to the co-complex of She3p and Myo4p and the assembled mRNP translocates along actin filaments. At the bud tip, the mRNP is likely anchored, translational repression is relieved by phosphorylation of Puf6p and Khd1p, and Ash1p is produced. RNAP II: RNA polymerase II, Yck1: yeast casein kinase 1, Ck2: casein kinase 2. For further details see main text.

The RNA-binding protein She2p is imported into the nucleus of the mother cell by the importin  $\alpha$  Srp1p (Shen et al. 2009). In the nucleus, She2p is recruited to sites of active transcription by binding to the transcription elongation factor Spt4-Spt5 (Shen et al. 2010). After binding to zip-code elements on the nascent *ASH1* mRNA, the RNA:She2p co-complex passes through the nucleolus, where Loc1p and pumilio-homology domain family 6 protein (Puf6p) are present (Urbinati et al. 2006; Du et al. 2008). Loc1p is required for efficient localization and localized translation of *ASH1* mRNA (Long et al. 2001). However, it remains unclear how Loc1p mediates this function. Puf6p and KH-domain protein 1 (Khd1p) bind to *ASH1* mRNA and repress its translation during transport (Irie et al. 2002; Gu et al. 2004; Paquin et al. 2007). Subsequent nuclear export of the pre-assembled nuclear mRNP is mediated by the nucleoporin Nup60p (Powrie et al. 2011).

In the cytoplasm, the adapter protein She3p simultaneously interacts with RNA-bound She2p and the type V myosin Myo4p (Böhl et al. 2000; Long et al. 2000).

This mature complex translocates along actin filaments towards the bud tip. A recent study revealed that an mRNP consisting of one *ASH1* zip-code element, She2p, She3p, and Myo4p has motile activity in an actin gliding assay, suggesting that these are the core components required for transport (Chung and Takizawa 2010). At the bud tip the *ASH1* mRNP is likely anchored (Beach et al. 2000; Gonsalvez et al. 2004). Phosphorylation of Puf6p and Khd1p at the plasma membrane induces their dissociation from the mRNA and enables translation of Ash1p (Paquin et al. 2007; Deng et al. 2008).

### **1.2.2 Zip-code elements of localizing mRNAs from yeast**

The *ASH1* mRNA contains four distinct zip-code elements, called E1, E2A, E2B, and E3 (Chartrand et al. 1999; Gonzalez et al. 1999). E1, E2A, and E2B are located in the coding region whereas E3 lies mainly in the 3' UTR of the transcript. Although each of these zip-code elements alone is sufficient to restrict an mRNA to the bud cell, the presence of multiple elements enhances localization to the bud tip (Long et al. 1997; Chartrand et al. 1999; Gonzalez et al. 1999; Chartrand et al. 2002). RNA constructs with four copies of one zip-code element localize almost as well as wild-type *ASH1* mRNA suggesting redundant function of the four *ASH1* zip-code elements.

Extensive mutagenesis studies showed that a combination of secondary structure and certain bases is required for a functional zip-code element (Chartrand et al. 1999; Gonzalez et al. 1999; Chartrand et al. 2002). The formation of stem-loop structures with internal loops and bulges has been confirmed by enzymatic secondary-structure mapping (Kertesz et al. 2010). A three-hybrid screen with partially randomized *ASH1* zip-code sequences led to the identification of a consensus motif required for She2p binding and mRNA localization (Olivier et al. 2005). The motif consists of a CGA sequence in one loop and a cytosine in a second loop, both separated by a double-stranded helix of four to five base pairs. Identification of the same motif in *IST2* and *EAR1* mRNA suggests conservation among some bud-localized transcripts. Another study used unbiased selection to confirm the importance of the CG dinucleotide for

interaction with the SHE machinery (Jambhekar et al. 2005). Although other nucleotides contributed to recognition, the sequence requirements were flexible. Attempts to identify new zip-code elements that contain the determined motifs failed for many bud-localized transcripts, showing that these sequence motifs only insufficiently describe zip-code recognition. It seems likely that the SHE complex recognizes a precise three-dimensional zip-code structure. However, a tertiary structure of a zip-code element from yeast is missing to date.

### 1.2.3 The RNA-binding protein She2p

She2p is an RNA-binding protein without a canonical RNA-binding domain. Its crystal structure revealed that She2p is entirely  $\alpha$ -helical and forms dimers in the crystal lattice (Figure 1.7 A) (Niessing et al. 2004). A positively charged surface patch, termed basic helical hairpin, is responsible for RNA binding. In addition, the C-terminus and helix E, which protrudes at right angle from the core of the structure, contribute to RNA recognition (Müller 2009).

Small-angle X-ray scattering combined with mutational studies showed that two She2p dimers can assemble head-to-head to form a tetrameric assembly in solution (Figure 1.7 B) (Müller 2009; Müller et al. 2009). Formation of She2p tetramers is required for mRNA binding, SHE-complex assembly, and mRNA localization (Müller 2009; Müller et al. 2009; Chung and Takizawa 2010). The modeled structure of tetrameric She2p reveals two large RNA-binding surfaces on opposite sites (Figure 1.7 B) (Müller 2009; Müller et al. 2009). Since different stoichiometric ratios have been proposed for the RNA:She2p interaction (Niessing et al. 2004; Olivier et al. 2005), it remains unclear if two or four zip-code elements interact with one She2p tetramer. Alternatively, different stoichiometries might apply for different types of zip-code elements.

She2p binds zip-code RNAs with sub-micromolar affinities (Du et al. 2008; Müller 2009; Müller et al. 2009). However, the affinity to unrelated stem-loop RNAs is only two to ten-fold weaker. This low *in vitro* specificity is in contrast to

the situation *in vivo*, where only few mRNAs are bound and transported by the SHE machinery (Takizawa et al. 2000; Shepard et al. 2003; Oeffinger et al. 2007).

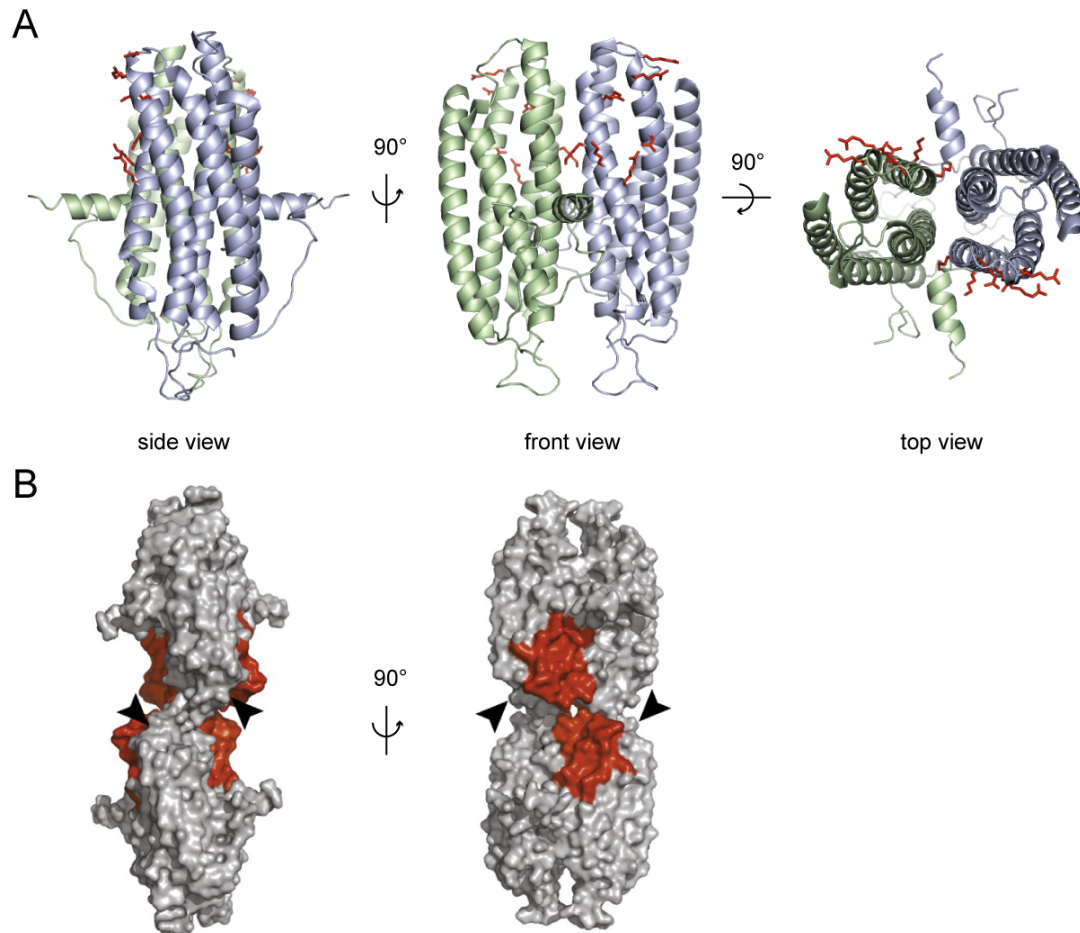


**Figure 1.7: Structure of the RNA-binding protein She2p. A)** Cartoon of the She2p crystal structure (PDB ID: 1XLY) in side, front, and top view. The two chains of the She2p dimer (in ribbon representation) are colored green and blue. Side chains of the basic helical hairpin motif (in stick representation) involved in RNA binding are shown in red. The figure was prepared with PyMol (<http://pymol.org>). **B)** Surface representation of the modeled She2p tetramer in side and front view. The basic helical hairpin regions are colored red. Two dimers interact in head-to-head orientation and form a large RNA-binding surface on each side of the tetramer. Arrowheads indicate the positions of the C-termini that are not resolved in the She2p crystal structure. Figure B was taken from Müller et al. 2009.

A non-classical nuclear localization sequence mediates import of She2p into the nucleus (Shen et al. 2009). There, co-transcriptional recruitment of She2p and its passage through the nucleolus are crucial for localization and translational silencing of *ASH1* mRNA (Du et al. 2008; Shen et al. 2009; Shen et al. 2010). Co-transcriptional recruitment of She2p only showed a weak preference for genes encoding localizing transcripts (Shen et al. 2010). However, RNase treatment specifically reduced the recruitment of She2p to these genes, suggesting that She2p preferentially binds to nascent localizing mRNAs.

### 1.2.4 The adapter protein She3p

She3p functions as an adapter protein between She2p and the motor Myo4p (Böhl et al. 2000; Long et al. 2000; Takizawa and Vale 2000). The N-terminus of She3p is predicted to be  $\alpha$ -helical and has the propensity to form coiled-coils (Figure S2). It binds tightly to Myo4p probably by forming a heterocoiled-coil (Böhl et al. 2000; Long et al. 2000; Hodges et al. 2008). The C-terminus has a high degree of disorder (Figure S2) and interacts with She2p (Böhl et al. 2000; Long et al. 2000). Several phosphorylation sites have been identified in She3p (Landers et al. 2009). Phospho-mimicking mutations of three residues in the C-terminus of She3p abolished *ASH1* mRNA localization, suggesting that phosphorylation might negatively regulate the function of She3p. Interestingly, She3p is conserved in the fungal pathogen *C. albicans* (Figure S3), where it is an essential component of the mRNA transport machinery (Elson et al. 2009).

### 1.2.5 The type V myosin Myo4p

Myo4p belongs to the type V myosin motors and shares their typical domain structure (Section 1.1.7 and Figure 1.4 C) (Reck-Peterson et al. 2000). In contrast to myosin V from higher eukaryotes, Myo4p does not form a stable coiled-coil and is thus monomeric (Dunn et al. 2007; Heuck et al. 2007; Hodges et al. 2008). Consequently, Myo4p does not act as a processive motor *in vitro* (Reck-Peterson et al. 2001; Dunn et al. 2007; Hodges et al. 2008).

The crystal structure of the Myo4p globular tail domain (GTD) revealed two  $\alpha$ -helical sub-domains (Heuck et al. 2010). The sub-domains are very similar to Myo2p (the other myosin V in *S. cerevisiae*) but they are oriented in a different angle relative to each other (Pashkova et al. 2006; Heuck et al. 2010). In addition to the GTD, the more N-terminal coiled-coil and linker regions are required for efficient interaction with the N-terminus of She3p (Heuck et al. 2007; Heuck et al. 2010).

## INTRODUCTION

Deletion of the GTD resulted in increased actin-activated ATPase activity, suggesting possible auto-inhibition of Myo4p (Hodges et al. 2008). However, the actin-activated ATPase activity of Myo4p was not stimulated by addition of  $\text{Ca}^{2+}$  or binding of the adapter protein She3p (Hodges et al. 2008). This is in contrast to the findings on MyoVa auto-inhibition (Section 1.1.8) (Li et al. 2005; Lu et al. 2006). In addition, residues involved in auto-inhibition of MyoVa are not conserved in Myo4p (Heuck et al. 2010). Therefore, it seems unlikely that Myo4p activity is regulated by auto-inhibition.

The co-complex of She3p and a chimeric myosin (consisting of the motor domain and neck of mouse MyoVa joined to the rod and globular tail of Myo4p) contained only one monomer of the chimeric myosin (Hodges et al. 2008). In contrast, artificial dimerization of Myo4p stabilized the interaction with She3p, suggesting that Myo4p might dimerize in the co-complex (Heuck et al. 2007). Purification of SHE-transport complexes from yeast revealed that at least two Myo4p copies are present in one complex (Chung and Takizawa 2010). In single-molecule experiments, at least three Myo4p motors were necessary for sustained movement of particles purified from yeast (Dunn et al. 2007). Similarly, multiple Myo4p motors coupled to a quantum dot supported continuous movement *in vitro* (Hodges et al. 2008). Artificial tethering of Myo4p motors to one RNA revealed that the efficiency of RNA localization *in vivo* rises with increasing motor number (Chung and Takizawa 2010). In summary, multiple Myo4p motors seem to be required for mRNP transport. How many Myo4p copies are incorporated into one SHE complex and how complex assembly regulates motility is still unclear.

UCS (UNC-45/CRO1/She4p) proteins have been proposed to enhance the folding, stability, and actin binding of myosins (Barral et al. 2002; Lord et al. 2008). The UCS protein She4p is required for the localization of Myo4p (Toi et al. 2003; Wesche et al. 2003). The crystal structure of She4p reveals an elongated dimer that binds to the motor domain of Myo4p (Shi and Blobel 2010). Therefore, it has been speculated that She4p might link two motor domains and thereby influence processivity and step-size of Myo4p.

### 1.2.6 Translational regulation of localizing transcripts

Translation of localizing mRNAs needs to be repressed during their transport to achieve efficient protein localization. In addition, translational silencing is required for efficient mRNA transport itself since it might prevent the ribosome from stripping off transport complexes (Irie et al. 2002; Gu et al. 2004). The proteins Puf6p and Khd1p function as translational repressors of *ASH1* mRNA (Irie et al. 2002; Gu et al. 2004).

Khd1p contains three KH domains and binds to the *ASH1*-E1 zip-code element (Irie et al. 2002; Paquin et al. 2007). Another study suggested binding of Khd1p to CNN repeats that lie 5' of the *ASH1*-E1 element (Hasegawa et al. 2008). Khd1p interacts directly with the translation initiation factor eIF4G1 (Paquin et al. 2007) possibly preventing recruitment of the pre-initiation complex to the mRNA (Besse and Ephrussi 2008). The membrane-anchored yeast casein kinase 1 (Yck1p) phosphorylates Khd1p at the bud tip (Paquin et al. 2007). Upon phosphorylation the affinity of Khd1p for the *ASH1*-E1 element decreases and local translation is initiated .

Translational control by Puf6p is regulated by a similar mechanism. Puf6p has seven pumilio-like repeats and binds to the pumilio family (PUF) recognition sequence UUGU (Gu et al. 2004). The *ASH1* 3' UTR contains two UUGU tetranucleotides, at least one of which overlaps with the E3 zip-code element. Binding of Puf6p to the translation initiation factor eIF5B blocks recruitment of the 60S ribosomal subunit (Deng et al. 2008). This translational repression is relieved upon phosphorylation by casein kinase 2 (Ck2) at the bud tip.

Interestingly, recruitment of Puf6p to the *ASH1* mRNA depends on the presence of She2p in the nucleus (Du et al. 2008; Shen et al. 2009). Thus, nuclear pre-assembly seems to be crucial for efficient translational repression during mRNA transport.

### 1.3 Active transport of endoplasmic reticulum in yeast

In addition to mRNA localization, the SHE machinery is also involved in the transport of cortical endoplasmic reticulum (ER) to the bud (Estrada et al. 2003). ER transport takes place at an early stage of the cell cycle, shortly after the appearance of the bud. Myo4p and the N-terminus of She3p but not She2p are required for active transport of ER (Estrada et al. 2003). It is not known how the She3p:Myo4p complex binds to the ER. She2p associates with the ER independently of She3p and Myo4p, thereby coupling the transport of *ASH1* mRNA and ER (Schmid et al. 2006; Aronov et al. 2007).

### 1.4 Objectives

Although many insights into the process of mRNA localization in yeast have been gained during the last years, important issues remain unresolved: How are localizing mRNAs specifically recognized for transport? What is the molecular mechanism of mRNP assembly? And how does mRNP assembly regulate motor activity? *ASH1*-mRNA transport has been studied extensively *in vivo*. However, detailed biochemical and structural studies *in vitro* are often required to draw mechanistic conclusions. So far, such analyses have focused mainly on individual factors, like She2p and Myo4p (Heuck 2009; Müller 2009). A comprehensive analysis of the SHE complex and its assembly is missing. Therefore, the aim of this study was to reconstitute the SHE complex *in vitro* and assess the role of individual factors in RNA recognition, complex assembly, and regulation of transport.

So far, *in vitro* reconstitution of the SHE complex has been hampered mainly by the lack of stable, recombinant She3p. Thus, the first aim of this thesis was to express and purify She3p protein and use it to reconstitute the SHE complex *in vitro* (Section 2.1).

Previous studies on She2p revealed a relatively low specificity for zip-code RNAs (Du et al. 2008; Müller 2009; Müller et al. 2009), although only few transcripts

## INTRODUCTION

are selected for transport in the cell (Takizawa et al. 2000; Shepard et al. 2003; Oeffinger et al. 2007). This discrepancy suggests that other proteins might be required for specific recognition of localizing mRNAs. An important goal was to investigate at which step of assembly specific mRNA recognition is achieved, which proteins contribute to recognition, and how they interact with the RNA (Section 2.2).

To date, there is only one high resolution structure of a zip-code element (Bullock et al. 2010). Structural information on a zip-code element in complex with an RNA-binding protein that mediates localization is missing. Such a structure would greatly enhance the understanding of mRNA recognition and transport. Therefore, an aim of this thesis was to obtain structural information on the *ASH1-E3* zip-code element in complex with She2p and She3p by X-ray crystallography or cryo-electron microscopy (cryo-EM) (Section 2.3).

Assembly of the SHE complex is still poorly understood: How many copies of each component are present in one transport unit? What is the size of this unit? Can several units assemble into a larger mRNP? How does assembly affect oligomerization and activity of the motor Myo4p? To address these questions, the size, stoichiometry, and actin-activated ATPase activity of different SHE sub-complexes were investigated (Section 2.4).

## 2 RESULTS

### 2.1 *In vitro* reconstitution of the SHE complex

#### 2.1.1 Expression and purification of SHE components

To perform *in vitro* biochemical studies on the SHE complex, all proteins except for full-length Myo4p were purified to homogeneity (Figure 2.1 A). She2p and the C-terminal part of Myo4p were purified from *E. coli* as described before (Heuck 2009; Müller 2009).

To obtain stable full-length She3p protein, it was necessary to co-express C-terminally 6x His-tagged She3p (She3p-His) together with She2p in insect cells. By a three-step purification, about 3 mg of pure She3p protein were isolated from 0.5 l culture of High Five insect cell (Figure 2.1 A). In contrast, co-expression of She3p-His and She2p in *E. coli* did not yield stable protein. Similarly, expression in insect cells failed when She3p-His was expressed in isolation or together with the Myo4p C-terminus. When N-terminally 6x His-tagged She3p was co-expressed with She2p in insect cells only little amounts of full-length She3p were detected. During expression tests of She3p, a stable C-terminal fragment starting with amino acid 354 was identified. It could be extended to amino acid 274 or 334 (Figure 2.1 A), but residues N-terminal to position 354 were susceptible to degradation. All C-terminal She3p constructs were expressed in *E. coli*.

Full-length N-terminally FLAG-tagged Myo4p was co-expressed with She3p, She4p, and CaM in insect cells. Although some degradation was observed (Figure 2.1 A), the purified full-length Myo4p was stable. The Myo4p preparation showed filamentous actin (F-actin) dependent ATPase activity (Section 2.4.6) and supported movement of actin filaments in gliding assays (personal communication from Dennis Zimmermann and Dr. Zeynep Ötken). Actin was purified from rabbit muscle by ultra-centrifugation as previously described (Spudich and Watt 1971).

## RESULTS

Zip-code RNAs (Figure S1) were either prepared by *in vitro* transcription or expressed in *E. coli* in fusion with a transfer RNA (tRNA)-tag (Ponchon and Dardel 2007; Ponchon et al. 2009) (Figure 2.1 B). Expression as tRNA-fusion constructs yielded milligram quantities of RNA required for many reconstitution experiments.

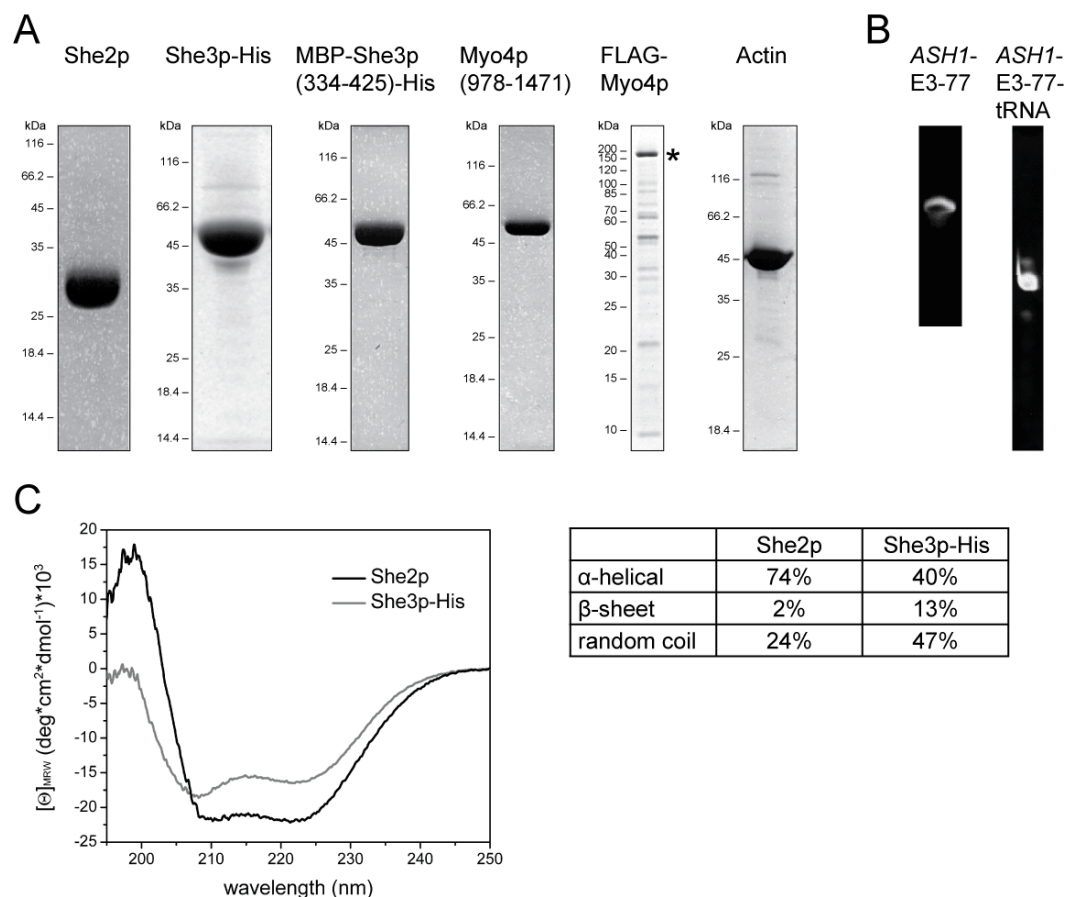


**Figure 2.1: Purification and characterization of proteins and RNAs used in this study.** **A)** SDS-PAGE shows that proteins were purified to homogeneity. In the case of FLAG-Myo4p, the preparation contained additional proteins. Some of them might be due to co-purification of She3p, She4p and CaM. The purified full-length FLAG-Myo4p (marked by asterisk) was stable and did not show substantial degradation. **B)** Urea-PAGE of purified RNAs. *ASH1-E3-77* was produced by *in vitro* transcription and purified by native PAGE. *ASH1-E3-77-tRNA* was expressed in *E. coli* and purified by ion-exchange chromatography. **C)** CD spectra of She2p and She3p. Table summarizes the secondary structure content as determined from the spectra with the program K2d (Andrade et al. 1993).

The secondary structure of She2p and She3p was assessed by circular dichroism (CD) spectroscopy (Figure 2.1 C). This analysis revealed a helical content of 74% for She2p, which is in perfect agreement with its crystal structure (Niessing et al. 2004). Secondary structure prediction algorithms predict the N-terminal half of She3p to be largely  $\alpha$ -helical, whereas the C-terminal half has a high degree of

disorder (Figure S2). The prediction is supported by the CD analysis of full-length She3p, suggesting 40% helices and 47% random coil (Figure 2.1 C).

### 2.1.2 Reconstitution of the SHE-core complex *in vitro*

To assess whether the purified proteins and RNA were able to form an intact complex, size-exclusion chromatography (SEC) was performed. *ASH1-E3-77*-tRNA co-eluted with She2p, She3p, and the Myo4p C-terminus in a single peak (Figure 2.2). I will refer to this complex as the SHE-core complex in this thesis. Dynamic light scattering (DLS) analysis revealed that the reconstituted complex is monodisperse and has a hydrodynamic radius of 15.2 nm (Section 2.4.5). Reconstitution of the SHE-core complex by SEC was also achieved with the shorter *ASH1-E3-51* RNA and the *IST2*-tRNA (Section 2.4.4). These experiments demonstrate that the recombinant proteins and RNAs are functional and can be used for *in vitro* reconstitution of SHE complexes.

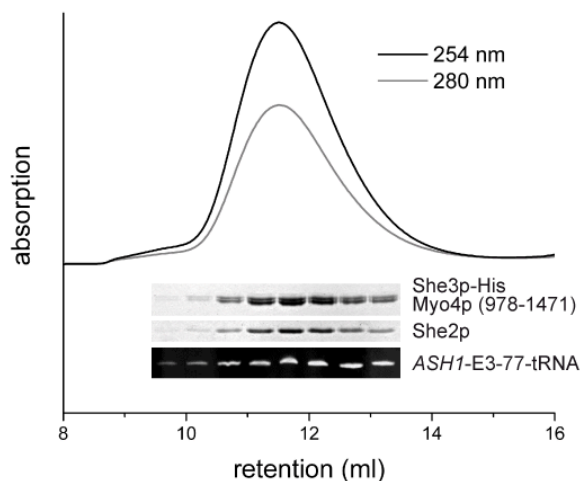


**Figure 2.2: Reconstitution of the SHE-core complex *in vitro*.** Proteins and RNA were mixed and the reconstituted complex was separated by SEC. 10  $\mu$ M *ASH1-E3-77*-tRNA, 20  $\mu$ M She2p, 30  $\mu$ M She3p and 15  $\mu$ M Myo4p were loaded on a Superose 6 10/300 GL column (GE Healthcare). SDS-PAGE (proteins) and Urea-PAGE (RNA) of corresponding fractions are shown below the chromatogram. Note that She3p-His and Myo4p (978-1471) migrate at similar height in SDS-PAGE and appear as a double-band.

## 2.2 Analysis of zip-code RNA recognition by She2p and She3p

### 2.2.1 She2p and She3p form a complex

After nuclear export, the RNA:She2p complex binds to the myosin adapter protein She3p. Since it is assumed that this interaction is mainly based on protein-protein interactions (Böhl et al. 2000; Long et al. 2000; Gonsalvez et al. 2003), the binary interaction between She2p and She3p was investigated. She2p co-purified with His-tagged She3p in a pull-down experiment (Figure 2.3 A). Additionally, the proteins eluted as a co-complex in SEC (Figure 2.3 B). She2p bound to surface-coupled She3p with a  $K_d$  of  $1.6 \pm 0.2 \mu\text{M}$  in steady-state surface plasmon resonance (SPR) experiments (Figure 2.3 C). SPR also revealed fast complex dissociation (Figure 2.3 C). These experiments show that She2p forms a complex with She3p, but affinity and stability of the interaction are not very high.

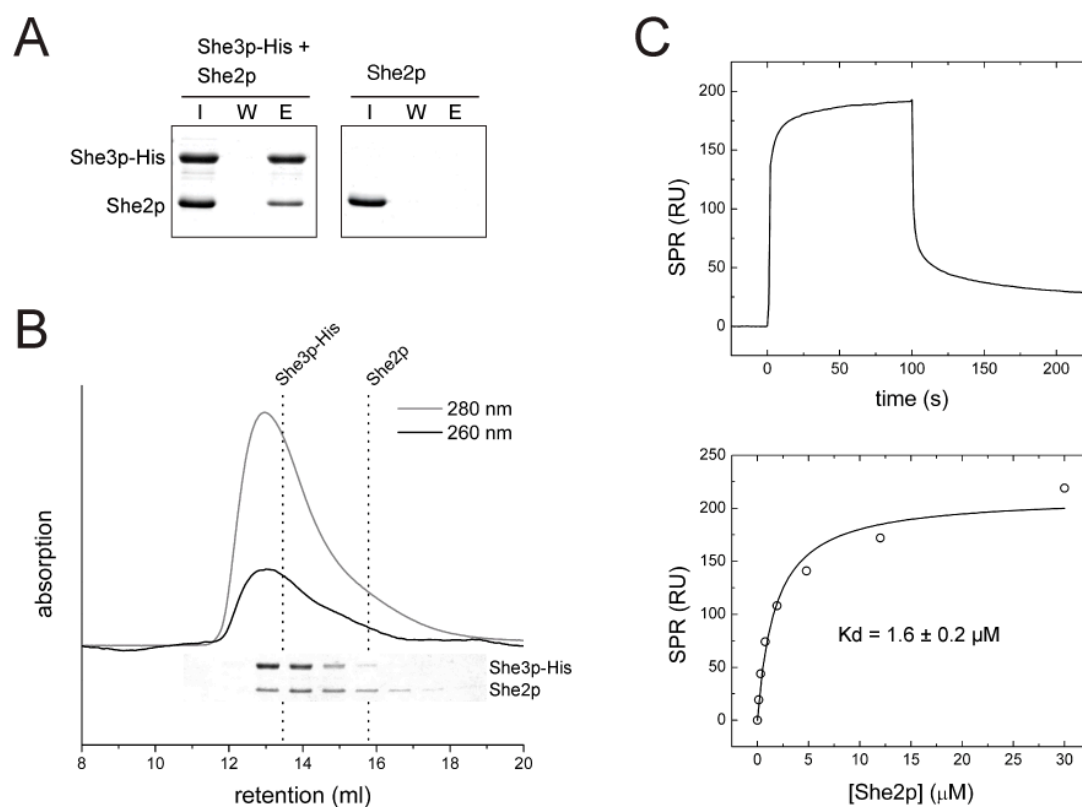


**Figure 2.3: She2p and She3p interact directly.** **A**) In pull-down experiments, She2p co-purified with immobilized His-tagged She3p (I: input, W: final wash, E: elution). **B**) In SEC, She2p and His-She3p formed a complex.  $20 \mu\text{M}$  She2p and  $30 \mu\text{M}$  She3p were loaded on a Superose 6 10/300 GL column (GE Healthcare). SDS-PAGE of corresponding fractions is shown below the chromatogram. Dotted lines indicate the peak retention volumes of the individual components. **C**) In SPR experiments, She2p bound to surface-coupled His-She3p. Upper panel: Binding kinetics reveals fast on- and off-rates.  $10 \mu\text{M}$  She2p was used. Lower panel: In steady-state measurements, the  $K_d$  of the interaction was  $1.6 \pm 0.2 \mu\text{M}$  (mean and deviation of two independent experiments).

### 2.2.2 She3p binds RNA unspecifically

The affinity of She2p to zip-code RNAs is only two to ten-fold higher than to unrelated RNA stem-loops, like the HIV-1 TAR RNA (Du et al. 2008; Müller 2009; Müller et al. 2009). In contrast, only few mRNAs are bound and transported by the SHE machinery *in vivo* (Takizawa et al. 2000; Shepard et al. 2003; Oeffinger et al. 2007). Thus, another protein of the SHE machinery might contribute to specific recognition of localizing mRNAs.

In an electrophoretic mobility shift assay (EMSA), She3p itself bound to *ASH1*-E3 RNA with sub-micromolar affinity (Figure 2.4 A). Similar affinity to zip-code RNAs has been reported for She2p (Du et al. 2008; Müller 2009; Müller et al. 2009). Thus, She3p is a previously undetected RNA-binding protein. However, no sequence similarity between She3p and known RNA-binding domains could be detected by database searches.

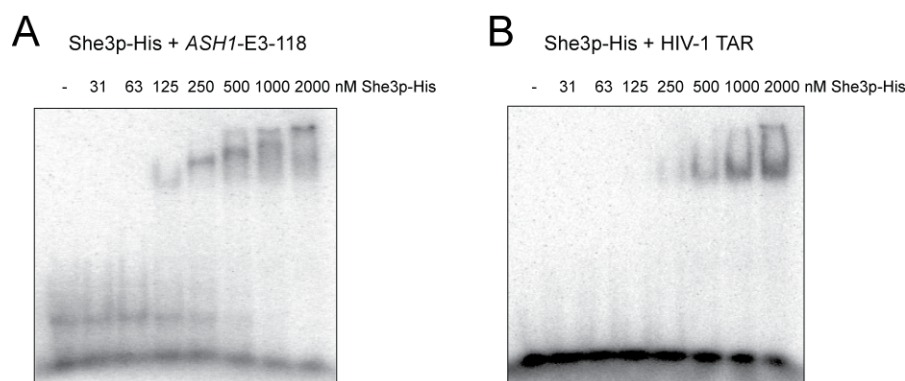


**Figure 2.4: She3p is an unspecific RNA-binding protein.** In EMSAs, She3p bound to the *ASH1*-E3 zip-code element (A) and the HIV-1 TAR stem-loop (B) with similar affinity. The size of shifted complexes increased in a concentration-dependent manner indicating several She3p binding sites on one RNA.

To assess the RNA-binding specificity of She3p, the HIV-1 TAR stem-loop (Figure S1) was used as a structured control RNA without a function in mRNA localization. She3p bound to the HIV-1 TAR stem-loop and to *ASH1*-E3 RNA with similar affinity (Figure 2.4 A, B). The size of the shifted complexes increased in a concentration-dependent manner, indicating that several She3p molecules can bind to one RNA. These observations suggest that She3p binds zip-code RNAs rather unspecifically.

### 2.2.3 She2p and She3p synergistically recognize *ASH1*-E3 zip-code RNA

She3p showed only weak specificity for zip-code RNAs *in vitro* (Section 2.2.2). In the cell, She3p interacts with RNAs already bound by She2p. Therefore, conjoint RNA-binding by She2p and She3p was investigated by SEC. She2p and She3p eluted as a high molecular weight complex with full-length *ASH1*-E3 RNA in fusion with a tRNA-tag (*ASH1*-E3-118-tRNA) (Figure 2.5 A). A shortened version of *ASH1*-E3 zip-code RNA (*ASH1*-E3-33-tRNA), unable to associate with She2p (Table 2.3), was used as control. This shortened RNA did not form a complex with She2p and She3p (Figure 2.5 A), suggesting that only functional zip-code RNAs join the She2p:She3p complex.

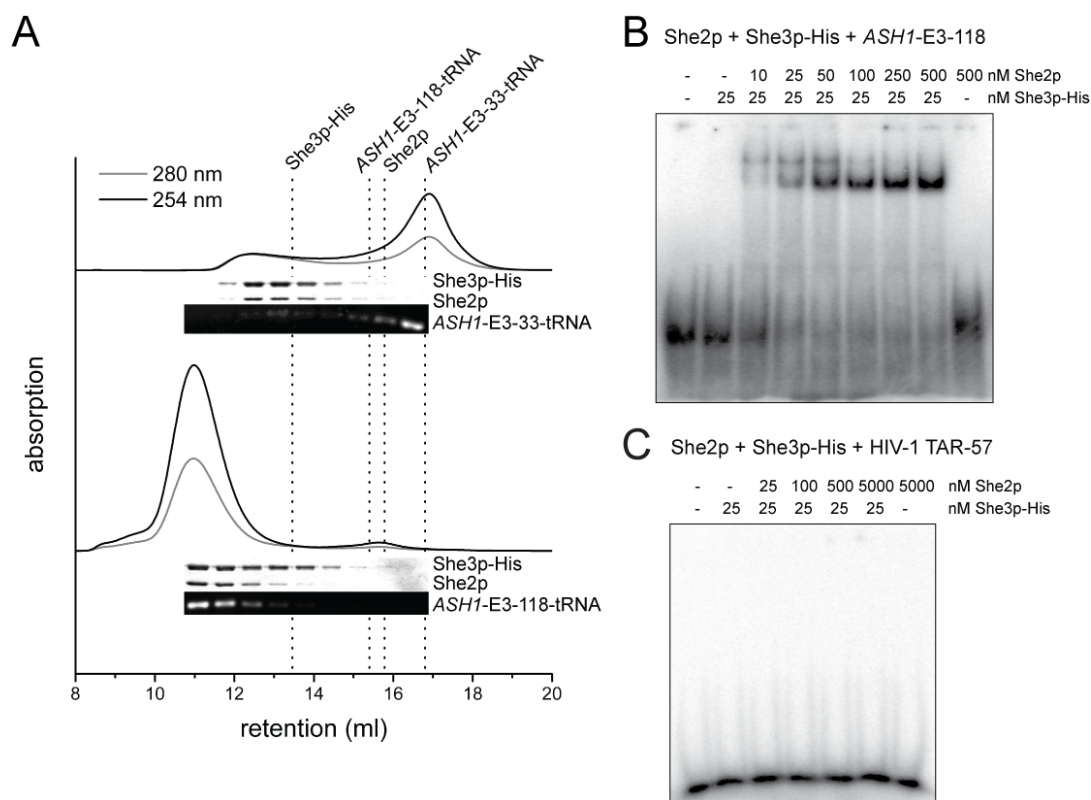


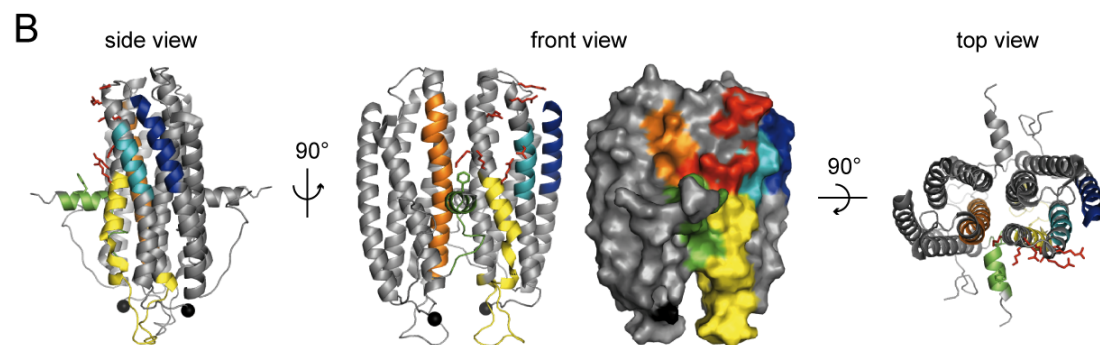
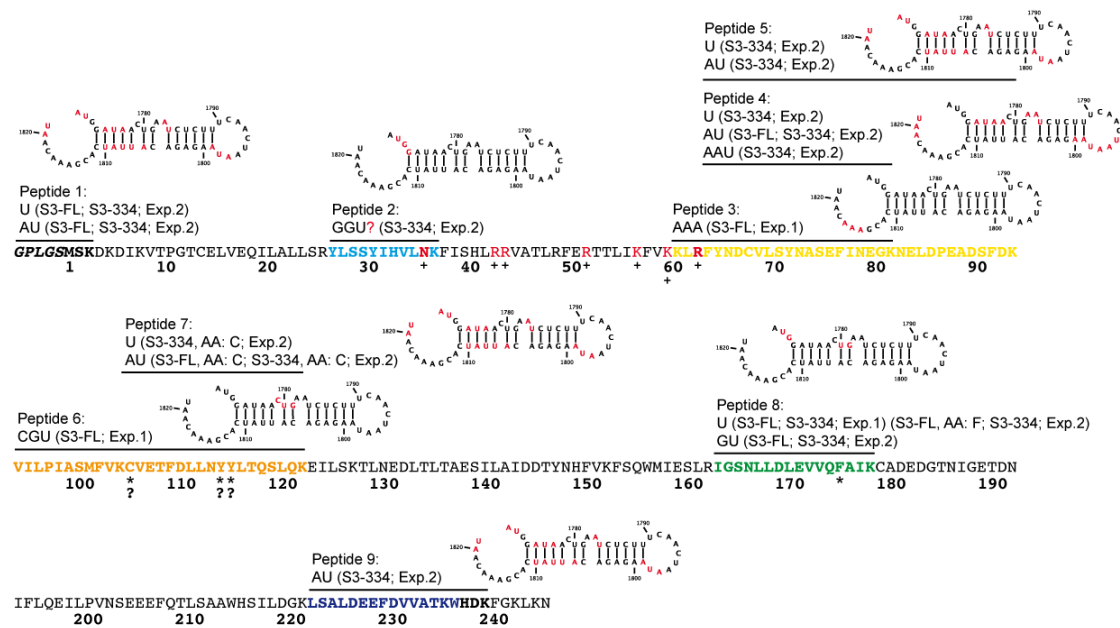
**Figure 2.5: She2p and She3p form specific ternary complexes with zip-code RNAs.** **A)** In SEC, She2p and She3p eluted as a ternary complex with *ASH1*-E3-118-tRNA (lower chromatogram) but not with the non-functional *ASH1*-E3-33-tRNA (upper chromatogram). SDS-PAGE and agarose gel electrophoresis of corresponding fractions are shown below the chromatograms. Dotted lines indicate the peak retention volumes of the individual components. **B)** EMSA with a constant She3p concentration (25 nM) and varying She2p concentrations shows strong complex formation with the *ASH1*-E3 zip-code element. Note that only one distinct band was observed at She2p concentrations above 100 nM indicating the formation of a homogeneous complex **C)** No ternary complex was formed with the HIV-1 TAR stem-loop, even if a She2p concentration of 5  $\mu$ M was used.

The results from SEC suggested that the She2p:She3p complex might have a higher specificity for zip-code RNAs than the individual proteins. To detect

potential synergistic binding by She2p and She3p, an EMSA with a constant concentration of 25 nM She3p was performed. At this concentration, She3p did not bind to *ASH1*-E3 RNA (Figure 2.5 B). In addition, She2p binding to *ASH1*-E3 RNA was not detectable in EMSAs, even at a concentration of 500 nM (Figure 2.5 B). However, if both proteins were present, strong binding to *ASH1*-E3 RNA was observed (Figure 2.5 B) suggesting that She2p and She3p act synergistically to bind *ASH1*-E3 RNA. The defined size of the band shift at high She2p concentrations indicates that a homogeneous ternary complex was formed. The affinity of this ternary interaction can be estimated to 25-50 nM. No binding of She2p and She3p to the HIV-1 TAR stem-loop was detected, even at She2p concentrations of 5 $\mu$ M (Figure 2.5 C). Thus, the She2p:She3p complex has at least 100-fold higher affinity for a zip-code RNA, compared to a non-localizing control. Although this is only a rough estimate, it indicates that the She2p:She3p complex recognizes zip-code RNA with high specificity.

#### **2.2.4 Mapping of RNA-protein binding sites in the ternary complex of *ASH1*-E3 RNA, She2p, and She3p**

She2p and She3p act synergistically to recognize zip-code RNAs and to incorporate them into high affinity ternary complexes (Section 2.2.3). Since the molecular basis of RNA recognition by She2p and She3p is unclear, the RNA-protein interaction sites in the ternary complex were determined. The complex was reconstituted and purified by SEC and subjected to UV cross-linking. Treatment by UV light induces covalent cross-links only at sites, where RNA and protein are in close contact (Urlaub et al. 2008). After digestion with RNase and trypsin, cross-linked peptides were identified by mass spectrometry. Katharina Kramer and Prof. Henning Urlaub carried out all experimental steps following purification of the complexes including the analysis of mass spectrometry data.

A She2p cross-links to *ASH1*-E3-51 RNA

**Figure 2.6: Mapping of RNA-She2p binding sites in the *ASH1*-E3:She2p:She3p complex by UV-cross-linking and mass spectrometry.** After UV cross-linking of the ternary complexes, peptide-RNA cross-links were identified by mass spectrometry. Two kinds of complexes were investigated: “S3-FL” means complex of *ASH1*-E3-51, She2p and She3p-His. “S3-334” means complex of *ASH1*-E3-51, She2p, She3p(334-425)-His. The experiment was performed twice (labeled Exp. 1 and 2). **A)** She2p peptides cross-linked to *ASH1*-E3-51 RNA are printed in bold and marked by black bars. Cross-linked nucleotides are indicated above the respective peptide. Type of complex, cross-linked amino acid (if detected), and experiment that identified the cross-link are given in brackets. Secondary structure prediction of the *ASH1*-E3-51 RNA is shown next to the peptides with possible cross-linking sites printed in red. Note that only the type of nucleotides but not their order can be deduced from the data. An N-terminal linker sequence in She2p that is not part of the native protein is indicated in italics. “+” marks amino acids of the basic helical hairpin motif described in Niessing et al. 2004. “\*” marks amino acids that were cross-linked to RNA. “?” means that no clear identification of nucleotides or amino acids was possible. **B)** Cartoon of the She2p crystal structure (PDB ID: 1XLY) in side, front, and top view. A surface representation of the front view is also shown. RNA cross-linked peptides (in ribbon representation) and side chains of the basic helical hairpin motif (in stick representation) are color-coded as in A. The side chain of phenylalanine 176 is shown in stick representation (green). For simplicity, the described features are only highlighted on one side of the She2p dimer. Both N-termini of the She2p dimer (aspartate 6) are represented as black spheres. The figure was prepared with PyMol (<http://pymol.org>).

Ternary complexes were either reconstituted with full-length She3p or with a C-terminal She3p construct comprising amino acids 334-425. The experiment was performed twice for each complex. Most peptides were detected in both

experiments (Figure 2.6 A and Figure 2.7). However, the She2p peptides 1, 2, and 9 only appeared in the second experiment (Figure 2.6 A), most likely because a mass spectrometer with higher sensitivity was used. The She2p peptides 2 and 9 as well as the She3p peptide 3 were only detected in complexes containing the She3p C-terminus (Figure 2.6 A and Figure 2.7). This might reflect conformational differences between the different ternary complexes. In case of the She3p peptide, the N-terminal linker sequence of the C-terminal She3p construct might have promoted cross-linking.

#### She3p cross-links to *ASH1*-E3-51 RNA

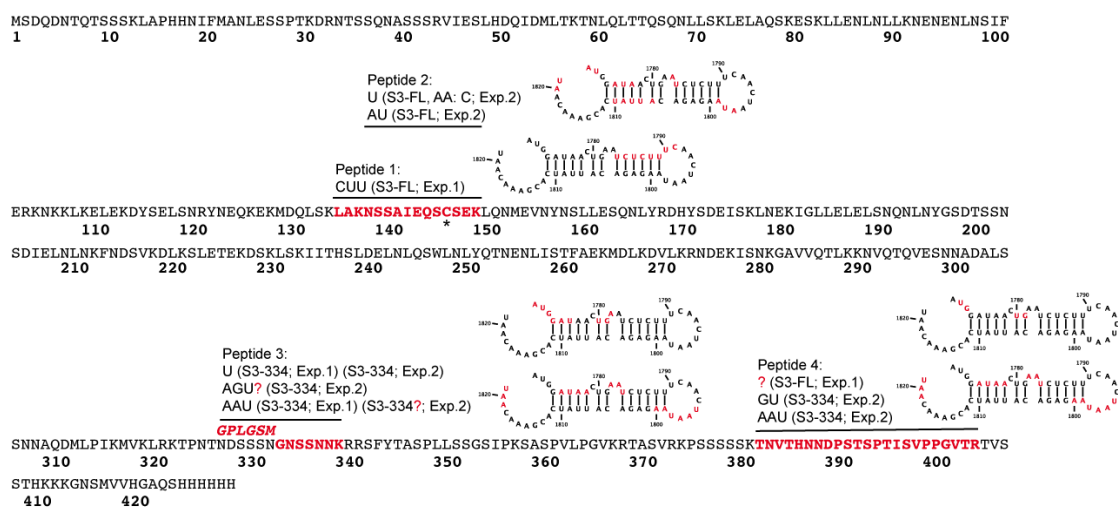


**Figure 2.7: Mapping of RNA-She3p binding sites in the *ASH1*-E3:She2p:She3p complex by UV-cross-linking and mass spectrometry.** She3p peptides cross-linked to *ASH1*-E3-51 RNA are printed in bold red letters and marked by black bars. The N-terminal linker sequence of She3p(334-425)-His is indicated in italics above the She3p sequence. Layout and labeling as described in Figure 2.6.

Cross-links to the *ASH1*-E3-51 RNA were identified in six distinct regions of She2p (Figure 2.6 A). Interestingly, two of these regions (Figure 2.6, cyan and yellow) overlap with the basic helical hairpin motif (Figure 2.6, red), previously identified to be involved in RNA-binding (Niessing et al. 2004). In addition, three regions in the vicinity of the basic helical hairpin motif cross-linked to RNA (Figure 2.6, orange, green, and blue). Together, these five regions form an extended RNA-binding surface including the protruding helix E and the C-terminus (Figure 2.6 B, green and blue). Interestingly, deletion of helix E or the C-terminus of She2p leads to decreased RNA-binding (Table 2.2) (Müller 2009). The cross-linked amino acid in helix E (peptide 8) was phenylalanine 176, which is in a good position at the upper side of helix E to contact the RNA (Figure 2.6 B).

The N-terminus of She2p was also identified to cross-link to RNA (Figure 2.6 A). However, it is distant from the extended RNA-binding surface in the crystal structure (Figure 2.6 B, black spheres) and its deletion has only a minor effect on RNA binding (Müller 2009).

Three regions of She3p cross-link to *ASH1*-E3 RNA (Figure 2.7). This experiment demonstrates for the first time that She3p binds directly to the RNA in the ternary complex. Two of the cross-linked regions are located in the C-terminal half of She3p that is interacting with She2p (Böhl et al. 2000). Surprisingly, one region lies in the N-terminal half of She3p that is responsible for the RNA-independent interaction with Myo4p (Böhl et al. 2000). The cross-link of this N-terminal region is established via cysteine 147.

The mass spectrometry analysis provides information about the type of nucleotide(s) that are cross-linked to a certain peptide (Figure 2.6 A and Figure 2.7). In case of the She2p peptides 2, 3, and 6, this information is sufficient to unambiguously identify the binding site on the *ASH1*-E3-51 RNA. Interestingly, two of these binding sites overlap with a conserved RNA motif required for She2p binding and mRNA localization *in vivo* (Olivier et al. 2005).

### **2.2.5 The C-terminus of She3p mediates synergistic RNA binding with She2p**

The N-terminus of She3p binds to Myo4p, whereas its C-terminus interacts with She2p (Böhl et al. 2000; Long et al. 2000). It is thus likely that the C-terminus of She3p also mediates synergistic RNA binding with She2p. Indeed, a C-terminal construct of She3p starting with residue 334 supported synergistic RNA-binding with She2p in an EMSA (Figure 2.8 A, C and Table 2.1). However, if 20 amino acids from the N-terminus of this construct were deleted (She3p (354-425)), synergistic RNA binding was markedly decreased (Figure 2.8 A, D and Table 2.1). In SEC, ternary complex formation was only observed with She3p (334-425) but not with She3p (354-425) (Figure 2.8 B). These results confirm the UV cross-linking data that implicated residues 334-340 in RNA binding (Figure 2.7).

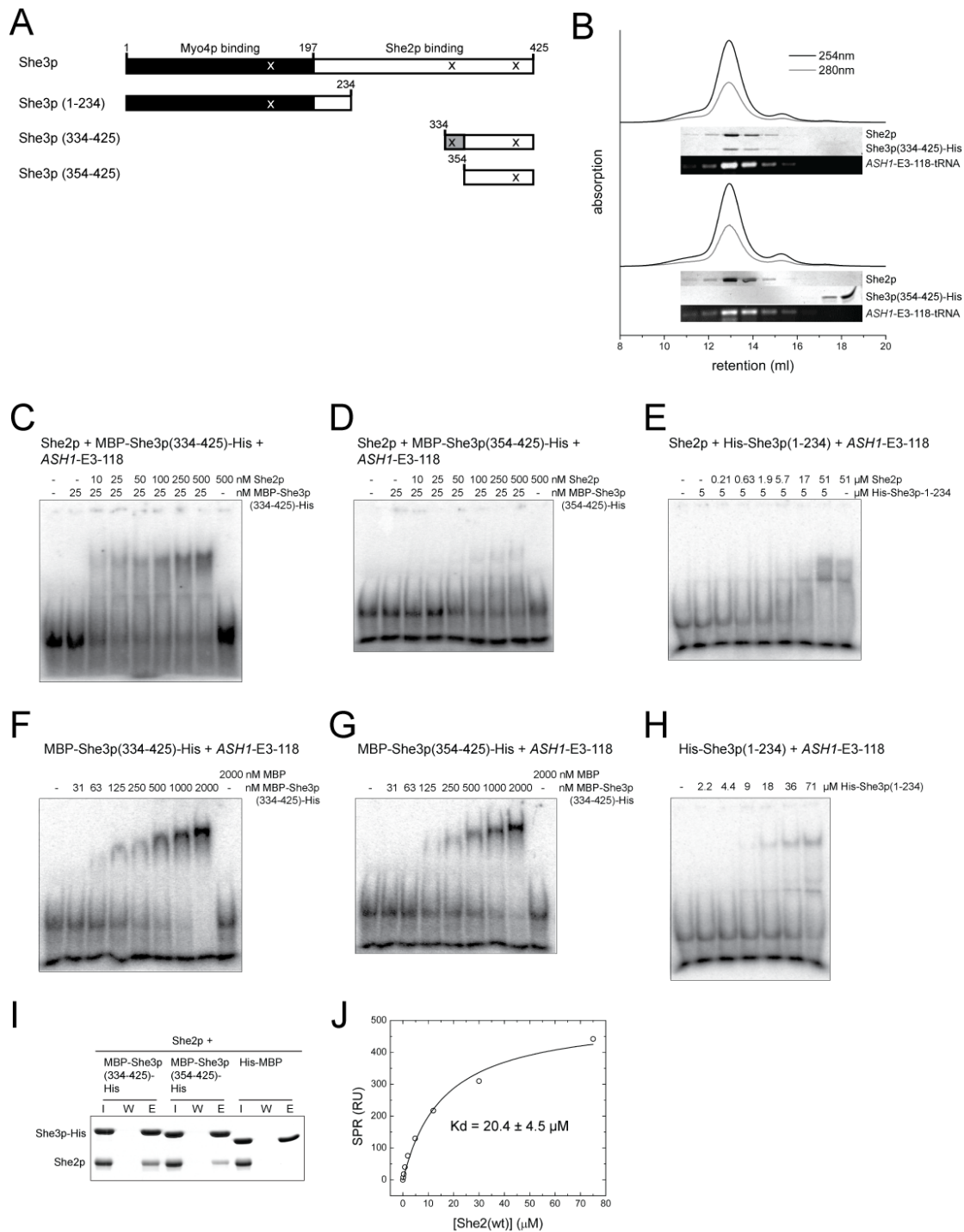


**Figure 2.8: A C-terminal fragment of She3p mediates synergistic RNA interaction with She2p.** **A)** Schematic drawing of tested She3p fragments. “X” marks sites of UV cross-linking to RNA (Figure 2.7). **B)** In SEC, only She3p(334-425)-His (upper chromatogram) but not She3p(354-425)-His (lower chromatogram) supported stable ternary complex formation. SDS-PAGE and agarose gel electrophoresis of corresponding fractions are shown below the chromatograms. Please note, that the C-terminal She3p constructs do not show any absorption at 280 nm or 254 nm. **C-E)** In EMSAs, only MBP-She3p(334-425)-His (C), but not MBP-She3p(354-425)-His (D) or His-She3p(1-234) (E) supported synergistic RNA binding with She2p. **F-H)** In EMSAs, both C-terminal She3p fragments bound to *ASH1-E3* RNA with nanomolar affinity. However, RNA binding of MBP-She3p(354-425)-His (G) was slightly weaker than of MBP-She3p(334-425)-His (F). The N-terminal construct His-She3p(1-234) (H) bound to *ASH1-E3* RNA with micromolar affinity. **I)** In a pull-down assay, She2p co-purified more efficiently with MBP-She3p(334-425)-His than with MBP-She3p(354-425)-His (I: input, W: final wash, E: elution). **J)** In steady-state SPR, She2p bound to surface-coupled She3p(354-425)-His with a  $K_d$  of  $20.4 \pm 4.5 \mu\text{M}$  (mean and deviation of two independent experiments).

Impaired complex formation with She3p (354-425) could be due to a defect in RNA binding or in the She2p:She3p interaction. In an EMSA, She3p (354-425) showed slightly decreased binding to *ASH1*-E3 RNA compared to She3p (334-425) (Figure 2.8 F, G and Table 2.1). Both She3p constructs bound She2p in a pull-down assay (Figure 2.8 I and Table 2.1). However, when She3p (354-425) was used, co-purification of She2p was less efficient. In steady-state SPR, She2p bound to surface-coupled She3p (354-425) with a  $K_d$  of  $20.4 \pm 4.5 \mu\text{M}$  (Figure 2.8 J). This interaction is about ten-times weaker than with full-length She3p (compare with Figure 2.3 C). In summary, these analyses show that the strong defect of She3p (354-425) in ternary complex formation results from mild defects in the binary interactions with RNA and She2p.

The N-terminus of She3p cross-linked to *ASH1*-E3 RNA (Figure 2.7). Indeed, an N-terminal construct of She3p bound to *ASH1*-E3 RNA in an EMSA (Figure 2.8 A, H). However, the RNA-binding affinity of the She3p N-terminus was about two orders of magnitude lower than for the She3p C-terminus (Figure 2.8 F-H). Since the N-terminus of She3p does not interact with She2p (Böhl et al. 2000), it also did not support synergistic RNA binding with She2p (Figure 2.8 E).

### **2.2.6 Point mutations in the C-terminus of She3p impair synergistic RNA binding with She2p**

Residues 334-353 of She3p are crucial for synergistic RNA-binding with She2p (Section 2.2.5). Two point mutations in that region have already been described to disrupt *ASH1*-mRNA localization *in vivo* (Landers et al. 2009). It seems likely, that the described mutations affect synergistic RNA binding with She2p. Whereas She3p (S343E S361E) supported synergistic RNA binding in a similar manner as the wild-type, She3p (S348E) weakly impaired the synergism (Figure 2.9 A, B and Table 2.1). Both mutants retained the ability to bind *ASH1*-E3 RNA and She2p like wild-type She3p (Figure 2.9 E-G, I and Table 2.1). The rather weak defects in synergistic RNA binding suggest that the mutations might mainly affect a different step in mRNA localization.

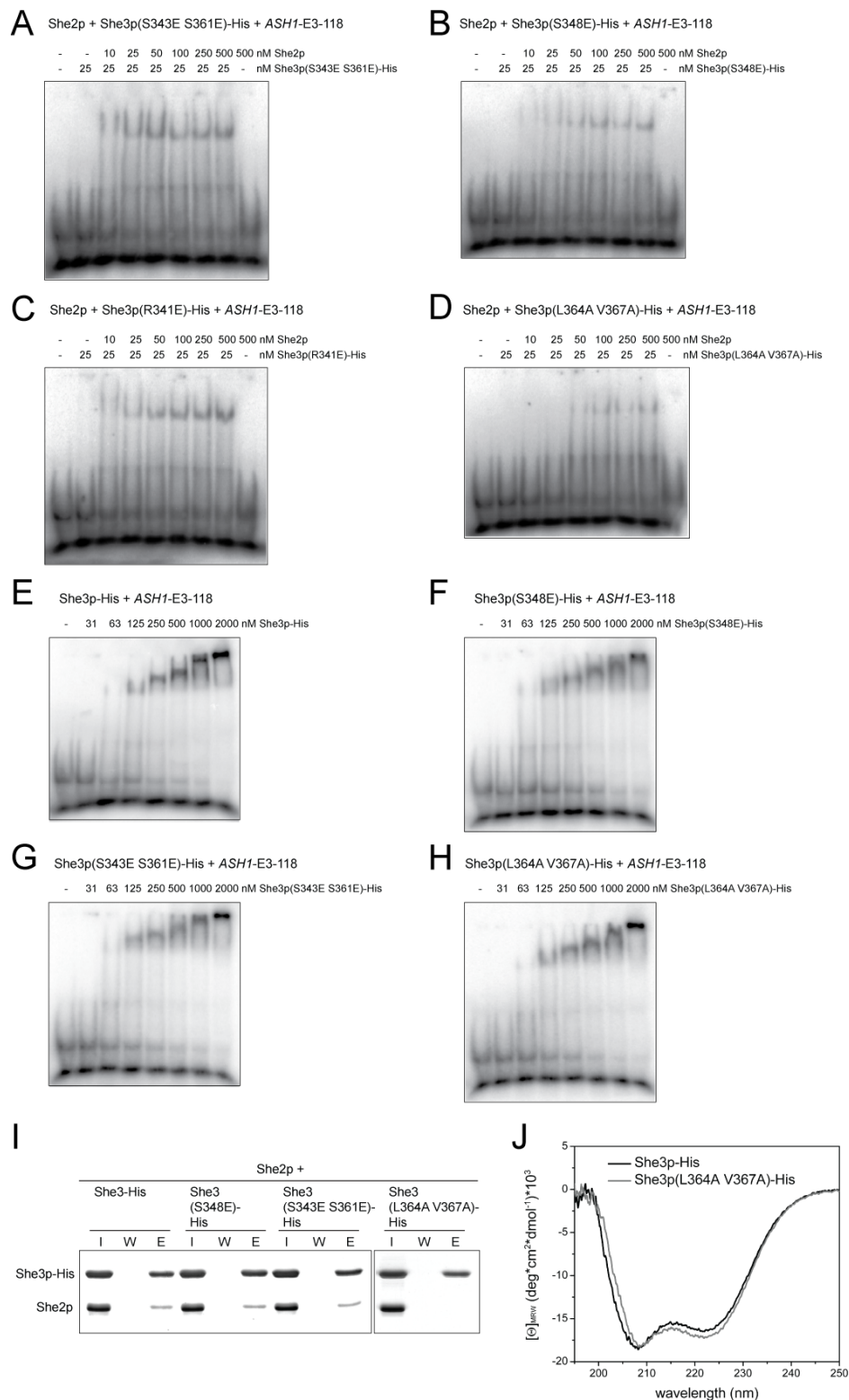


**Figure 2.9: Analysis of She3p point mutants. A-D)** In EMSAs, synergistic *ASH1*-E3 RNA binding with She2p was not significantly reduced for She3p (S343E S361E) (A) and She3p (R341E) (C) as compared to the wild-type (Figure 2.5 B). She3p (R348E) (B) showed a slightly reduced and She3p (L364A V367A) (D) a strongly reduced synergistic RNA binding. **E-H)** In EMSAs, *ASH1*-E3 RNA binding of She3p (R348E) (F), She3p (S343E S361E) (G), and She3p (L364A V367A) (H) was comparable to wild-type She3p (E). **I)** Interactions between immobilized His-tagged She3p mutants and wild-type She2p were analyzed by pull-down assays (I: input, W: final wash, E: elution). She2p binding to She3p (S348E) and She3p (S343E S361E) was comparable to wild-type She3p. In contrast, She3p (L364A V367A) did not interact with She2p. **J)** CD spectroscopy confirmed that the mutant She3p (L364A V367A) was properly folded.

Additional point mutations were generated at conserved positions of the She3p C-terminus (Figure S3). She3p (R341E) did not affect synergistic RNA binding with She2p (Figure 2.9 C and Table 2.1). In contrast, the mutant She3p (L364A V367A) significantly impaired the synergism (Figure 2.9 D and Table 2.1). CD spectroscopy demonstrated that She3p (L364A V367A) was correctly folded (Figure 2.9 J). Further analyses showed that this mutant still bound *ASH1*-E3 RNA like the wild-type, but its interaction with She2p was completely abolished (Figure 2.9 E, H, I and Table 2.1). Thus, synergistic RNA binding by She2p and She3p does not only require proper RNA binding by the individual proteins but also their interaction with each other.

**Table 2.1: Summary of the defects observed upon mutations in She3p.**

Protein	Synergistic RNA binding with She2p	RNA binding	She2p:She3p interaction
She3p (wt)	+++	+++	+++
She3p (1-234)	-	+	- (*)
She3p (334-425)	+++	+++	++ (x)
She3p (354-425)	+	++	+
She3p (R341E)	+++	n.d.	n.d.
She3p (S343E S361E) (Landers et al. 2009)	+++	+++	+++
She3p (S348E) (Landers et al. 2009)	++	+++	+++
She3p (L364A V367A)	+	+++	-

“Synergistic RNA binding with She2p” and “RNA binding” were assessed by EMSAs with *ASH1*-E3-118 RNA. “She2p:She3p interaction” was investigated by pull-down experiments. (\*) marks that the experiment was done by Böhl et al. 2000. (x) indicates that binding was wild-type-like in pull-down assays but reduced in SEC.

+++ wt-like binding  
 ++ moderately reduced binding  
 + reduced binding  
 - abrogated binding  
 n.d. not determined

### 2.2.7 Helix E of She2p mediates synergistic RNA binding with She3p

The protruding helix E and the very C-terminus of She2p are highly conserved (Niessing et al. 2004). Deletion mutants of helix E and of the C-terminal six amino acids have already been described (Müller 2009) and are illustrated in Figure 2.10. Previous analyses of these mutants demonstrated that both regions are

important for the full RNA-binding affinity and specificity of She2p (Table 2.2) (Müller 2009).

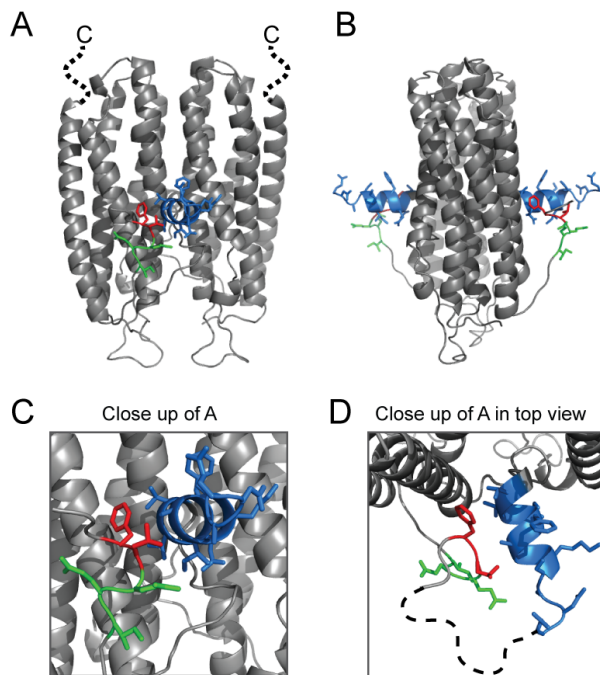


**Figure 2.10: She2p mutations affecting synergistic RNA binding with She3p.** **A)** Cartoon of the She2p crystal structure (PDB ID: 1XLY) in front view. Mutated features are colored and side-chains are shown in stick representation. The dotted line represents the C-terminal six residues not part of the crystal structure that were deleted in She2p ( $\Delta$ C). The protruding helix E deleted in She2p ( $\Delta$ hE) is shown in blue. Red and green regions close to helix E represent residues mutated in She2p (F195A L196A) and She2p (Q197A E198A I199A), respectively. **B)** Side view of the structure shown in A, rotated by 90° around the vertical axis. **C)** Close-up of A. **D)** Close-up shown in C, rotated by 90° around the horizontal axis. The dashed line indicates a loop region not resolved in the crystal structure that was mutated in She2p (F183A D184A G185A) and She2p (T191A D192A). The figure was taken from Müller et al. 2011.

Deletion of helix E (She2p ( $\Delta$ hE)) completely abolished synergistic RNA binding with She3p, whereas deletion of the C-terminus (She2p ( $\Delta$ C)) only had a weak effect on the synergism (Figure 2.11 A and Table 2.2). In SEC, She2p ( $\Delta$ C) formed a high-molecular weight complex with She3p and *ASH1*-E3-118-tRNA, but not with the non-functional *ASH1*-E3-33-tRNA (Figure 2.11 B). In contrast, She2p ( $\Delta$ hE) completely failed to form a ternary complex (Figure 2.11 B). Subsequent pull-down experiments revealed that helix E is essential for the interaction with She3p, whereas the C-terminus is dispensable (Figure 2.11 C). Also in SPR experiments, no interaction of She2p ( $\Delta$ hE) with surface-coupled She3p was detected (Figure 2.11 D), even at a concentration of 150  $\mu$ M. In contrast, She2p ( $\Delta$ C) bound to She3p with a  $K_d$  of  $2.0 \pm 0.2 \mu$ M (Figure 2.11 D), which is comparable to the affinity of wild-type She2p (Figure 2.3 C).

In summary, these analyses define the protruding helix E of She2p as a key functional element. On the one hand, it serves as an interaction platform for She3p. On the other hand, it is involved in the recognition of zip-code RNAs. Therefore, helix E recruits She3p and RNA for synergistic binding. In contrast,

deletion of the She2p C-terminus has a selective effect on RNA binding without affecting She3p interaction.

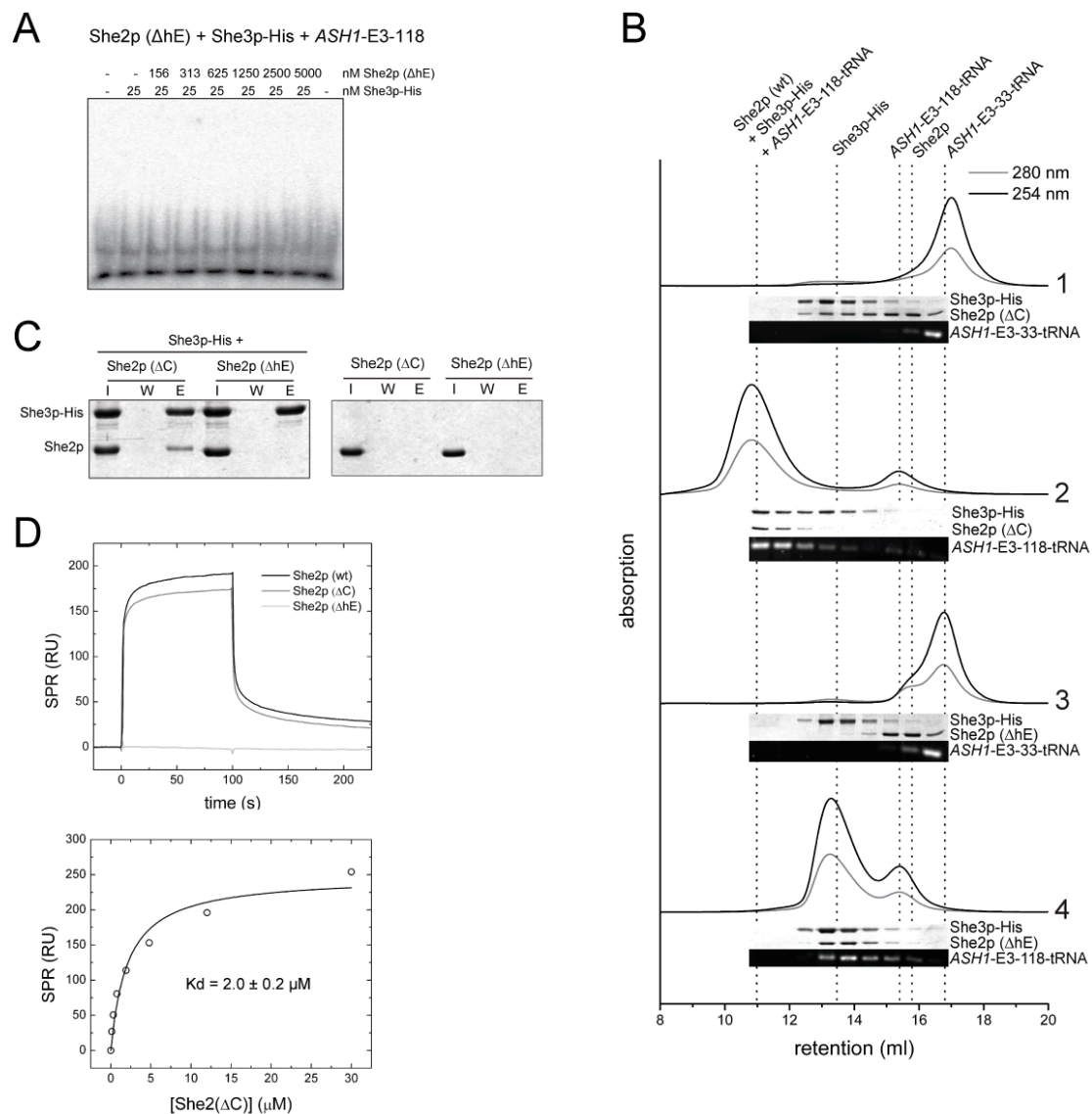


**Figure 2.11: The helix E of She2p is required for the interaction with She3p and synergistic RNA binding.** **A)** She2p ( $\Delta$ hE) did not form a ternary complex with *ASH1*-E3 RNA and She3p in an EMSA. **B)** In SEC, She2p ( $\Delta$ C) (chromatogram 2) but not She2p ( $\Delta$ hE) (chromatogram 4) eluted as high-molecular weight complex with She3p and *ASH1*-E3-118-tRNA. Please note that She3p co-migrates with the She2p ( $\Delta$ hE):*ASH1*-E3-118-tRNA co-complex, but no ternary complex is formed. No ternary complexes were detected with *ASH1*-E3-33-tRNA (chromatogram 1 and 3). SDS-PAGE and agarose gel electrophoresis of corresponding fractions are shown below the chromatograms. Dotted lines mark the peak retention volumes of the indicated components. **C)** In pull-down experiments, She2p ( $\Delta$ C) but not She2p ( $\Delta$ hE) copurified with immobilized His-tagged She3p (I: input, W: final wash, E: elution). **D)** SPR experiments. Upper panel: She2p ( $\Delta$ C) but not She2p ( $\Delta$ hE) bound to surface-coupled She3p. 10  $\mu$ M of each She2p variant was used. Lower panel: In steady-state measurements, the  $K_d$  of the She2p( $\Delta$ C):She3p interaction was  $2.0 \pm 0.2 \mu\text{M}$  (mean and deviation of two independent experiments).

### 2.2.8 Point Mutations around helix E of She2p impair synergistic RNA binding with She3p

To investigate the role of She2p's helix E in ternary complex formation in more detail, four sets of point mutations at conserved sites in the vicinity of helix E were designed (Figure 2.10). The point mutations She2p (E183A D184A G185A) and She2p (T191A D192A) located in the flexible loop region at the distal end of helix E (Figure 2.10 D, dashed line) had no significant effect on synergistic RNA binding with She3p (Figure 2.12 A, B and Table 2.2). In contrast, the mutants She2p (F195A L196A) and She2p (Q197A E198A I199A) that affect amino acids supporting helix E (Figure 2.10 C) strongly affected the synergism (Figure 2.12 C, D and Table 2.2). Subsequent pull-down experiments revealed that both mutants did not interact with She3p (Figure 2.12 E and Table 2.2). In addition, their RNA-binding affinity was reduced to about 40% of the wild-type (Table 2.2). CD spectroscopy confirmed that both mutants were correctly folded (Figure 2.12 F).

**Table 2.2: Summary of the defects observed upon mutations in She2p.**

Protein	Synergistic RNA binding with She3p	RNA binding (*)	She2p:She3p interaction
She2p (wt)	+++	+++	+++
She2p ( $\Delta$ hE) (Müller 2009)	-	+	-
She2p ( $\Delta$ C) (Müller 2009)	++ (*)	+	+++
She2p (E183A D184A G185A)	+++	n.d.	n.d.
She2p (T191A D192A)	+++	n.d.	n.d.
She2p (F195A L196A)	+	++	-
She2p (Q197A E198A I199A)	+	++	-
She2p (L130Y)	n.d.	n.d.	+

"Synergistic RNA binding with She3p" was assessed by EMSAs, She2p "RNA binding" by filter-binding assays, and "She2p:She3p interaction" by pull-down experiments. All RNA-binding experiments were performed with *ASH1-E3-118* RNA. (\*) marks experiments performed by Dr. Marisa Müller (Müller 2009; Müller et al. 2011).

+++ wt-like binding  
 ++ moderately reduced binding  
 + reduced binding  
 - abrogated binding  
 n.d. not determined

In summary, mutations in the loop supporting helix E (residues 195-199) have a similar effect as deletion of helix E. Since this loop is in direct contact with helix E (Figure 2.10 C, D), it cannot be excluded that deletion of helix E affects the

conformation of the adjacent loop or vice versa. However, it seems likely that helix E and the adjacent loop provide a joint interaction site for ternary complex formation with She3p and RNA.

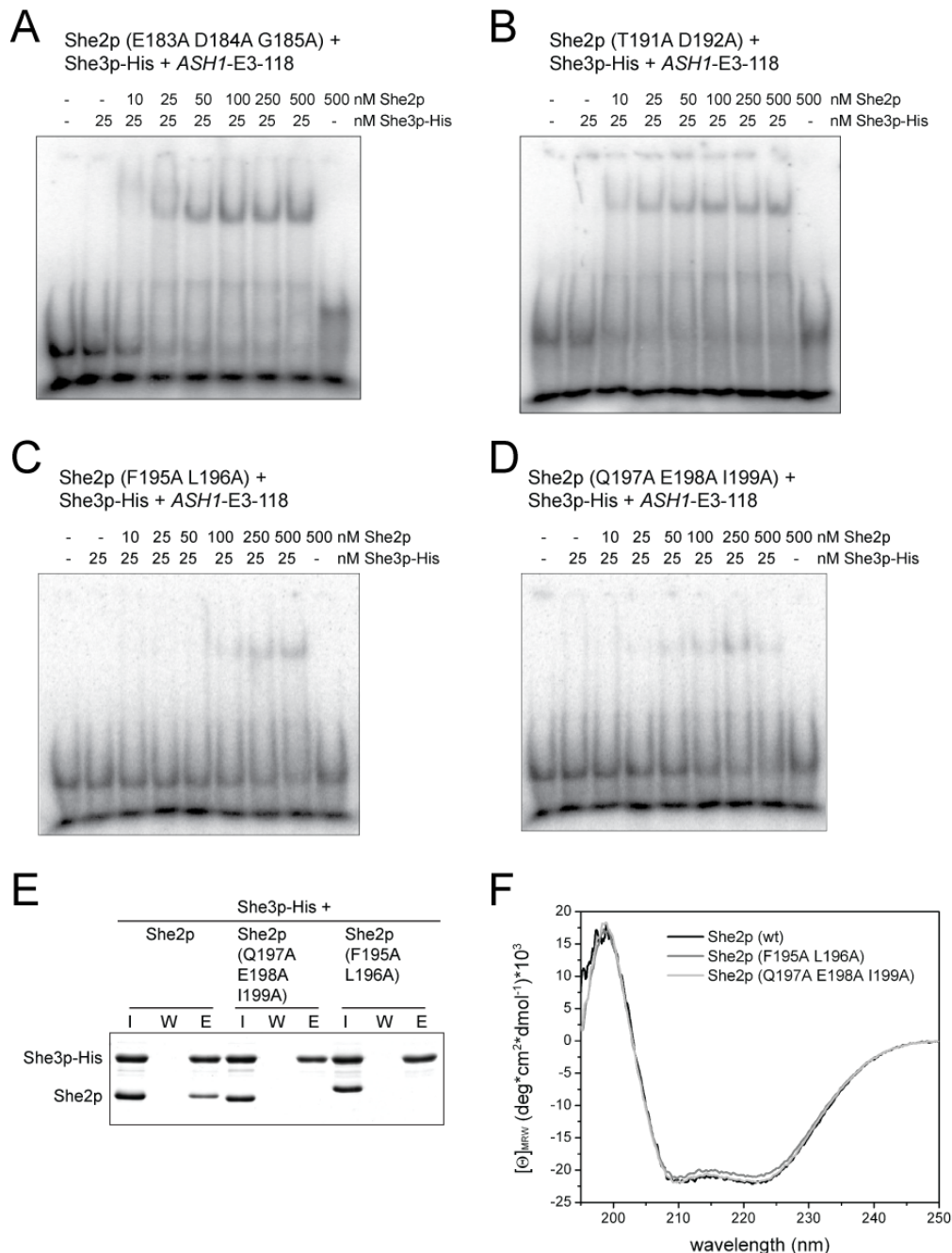


**Figure 2.12: Analysis of She2p point mutants. A-D)** She2p constructs with point mutations around helix E were tested by EMSAs. She2p (E183A D184A G185A) (A) and She2p (T191A D192A) (B) showed wild-type like synergistic RNA binding with She3p. In contrast, She2p (F195A L196A) (C) and She2p (Q197A E198A I199A) (D) had strong defects in the synergism. **E)** In pull-down experiments, She2p (Q197A E198A I199A) and She2p (F195A L196A) did not co-purify with immobilized His-tagged She3p (I: input, W: final wash, E: elution). Please note that She2p (F195A L196A) migrated slightly slower than the wild type in SDS-PAGE. However, the expected mass of both point mutants was confirmed by mass spectrometry. **F)** CD spectroscopy of She2p (Q197A E198A I199A), She2p (F195A L196A), and wild-type She2p confirmed that the mutants were properly folded.

## 2.3 Structural studies on SHE sub-complexes

### 2.3.1 Identification of a core-binding region in the *ASH1*-E3 zip-code element

For structural studies it is required to identify protein and RNA constructs that are structurally well defined. The *ASH1*-E3 zip-code element has been narrowed down to a stem-loop of 77 nucleotides that is functional *in vivo* (Figure S1) (Gonzalez et al. 1999). *In vitro*, the *ASH1*-E3 RNA has the highest affinity to She2p among all tested zip-code elements (Müller 2009). Thus, the *ASH1*-E3 zip-code element seems to be well suited for structural studies.

To narrow down the binding site of the She2p:She3p co-complex on the *ASH1*-E3 RNA, a range of RNA deletion constructs with 118, 77, 51, 38, and 33 nucleotides were designed (Figure S1). The 51 nucleotides-long version still bound to She2p and to the She2p:She3p co-complex in SEC (Table 2.3). It also supported synergistic binding in an EMSA (Figure 2.13 A). Further shortening to 38 or 33 nucleotides resulted in a complete loss of binding in SEC (Table 2.3). Thus, at least one of the single-stranded regions at the 5' and 3' end of the stem-loop (Figure S1) seems to be required for efficient binding by She2p and She3p.

**Table 2.3: Analysis of *ASH1*-E3 RNA deletion mutants for complex formation with She2p and She3p.**

RNA	Synergistic binding by She2p and She3p (EMSA)	Complex formation with She2p (SEC)	Complex formation with She2p and She3p (SEC)
<i>ASH1</i> -E3-118	+	n.d.	+ (*)
<i>ASH1</i> -E3-77	+	+ (*)	+ (*)
<i>ASH1</i> -E3-51	+	+ (*)	+
<i>ASH1</i> -E3-51 ( $\Delta$ 1786-1802)	+	n.d.	+
<i>ASH1</i> -E3-51 ( $\Delta$ 1782-1804)	-	n.d.	n.d.
<i>ASH1</i> -E3-38	n.d.	- (*)	n.d.
<i>ASH1</i> -E3-33	n.d.	- (*)	- (*)

"Synergistic binding" was assessed by EMSAs, whereas "complex formation" was investigated by SEC. (\*) marks that RNAs were tested in fusion with tRNA. Note that tRNA alone did not bind to She2p in SEC.

+ efficient binding or complex formation  
 - abrogated binding or complex formation  
 n.d. not determined

To investigate the importance of the *ASH1*-E3 upper stem and hairpin loop, nucleotides 1786-1802 or 1782-1804 were replaced by a GAAA tetraloop (Leontis and Westhof 2003; Bevilacqua and Blose 2008) (Figure 2.13 B, C).

Analysis by EMSA revealed that part of the upper stem and the hairpin loop (nucleotides 1786-1802) were not essential for synergistic binding of *ASH1*-E3 RNA by She2p and She3p *in vitro* (Figure 2.13 B). However, further deletion including also the bulged dinucleotide AA (nucleotides 1782-1804) resulted in strongly decreased binding (Figure 2.13 C). The dinucleotide AA was also part of several potential cross-linking sites to She2p and She3p (Figure 2.6 A and Figure 2.7) and is thus likely to be in direct contact with the proteins of the ternary complex.

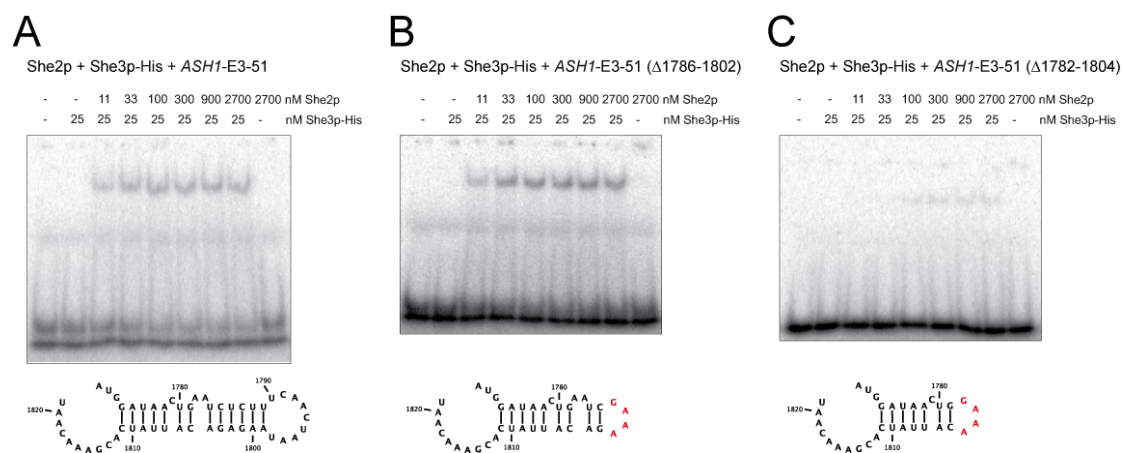


**Figure 2.13: Identification of a core-binding region in the *ASH1*-E3 zip-code element.** Synergistic RNA binding of She2p and She3p was tested by EMSAs. **A)** She2p and She3p efficiently bound a 51 nucleotides-long version of the *ASH1*-E3 zip-code element. **B)** When the upper stem and the hairpin loop of *ASH1* E3 were replaced by a GAAA tetraloop (*ASH1*-E3-51 (Δ1786-1802)), full binding was maintained. **C)** Replacement of the bulged AA dinucleotide, the upper stem, and the hairpin loop of *ASH1* E3 by a GAAA tetraloop (*ASH1*-E3-51 (Δ1782-1804)) strongly reduced binding of She2p and She3p. Secondary structure predictions of the tested RNAs are shown below the EMSAs. The GAAA tetraloop is indicated in red.

In summary, a core-binding region in the *ASH1*-E3 zip-code element was identified. It comprises 5' and 3' single-stranded regions and a stem with two bulges (Figure 2.13 B). This finding is fully consistent with the UV cross-linking analysis (Section 2.2.4). At least one of the potential RNA cross-linking sites of each peptide overlaps with the core RNA binding region described here.

### 2.3.2 Crystallization trials with She2p, She3p, and *ASH1*-E3 RNA

To date, no high resolution structure of She2p in complex with She3p and/or zip-code RNA is available. Thus, crystallization trials were performed with sub-complexes of She2p, She3p, and *ASH1*-E3 RNA.

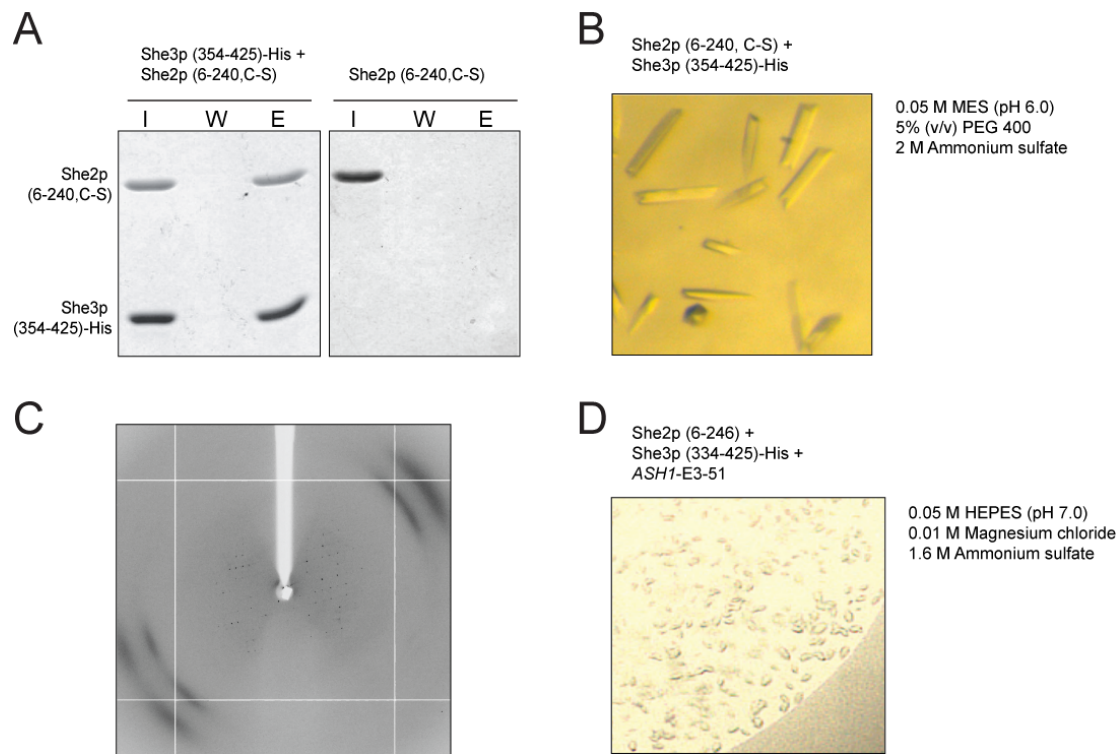


**Figure 2.14: Crystallization trials with She2p, She3p, and ASH1-E3 RNA.** **A)** She2p (6-240, C-S) bound to immobilized She3p(354-425)-His in a pull-down assay. Note that She2p (6-240, C-S) alone did not bind to nickel sepharose. **B)** Refined crystals of She2p (6-240, C-S) and She3p (354-425)-His. The proteins were mixed in approximately equimolar amounts prior to crystallization. The drop was set up with 1  $\mu$ l of protein solution and 1  $\mu$ l of precipitant solution in hanging drop format. The final concentration of She2p (6-240, C-S) in the drop was 2.3 mg/ml. **C)** X-ray diffraction of one of the crystals shown in B. **D)** Initial crystals of a complex of She2p (6-246), She3p(334-425)-His, and ASH1-E3-51. The complex was purified by SEC prior to crystallization. The drop was set up with 100 nl protein and 100 nl precipitant solution in sitting drop format. The final concentration of the complex in the drop was approximately 1.1 mg/ml.

Initially, needle-shaped crystals were obtained for a complex of wild-type She2p and She3p(354-425)-His. The crystal morphology could be improved by replacing wild-type She2p with a construct that contains residues 6-240 with all four cyteines mutated to serines (She2p (6-240, C-S)) (Niessing et al. 2004). Like wild-type She2p (Figure 2.8 I), She2p (6-240, C-S) co-purified with She3p(354-425)-His in a pull-down assay (Figure 2.14 A), but the interaction was not strong enough to purify the complex by SEC prior to crystallization. After refinement of the conditions, rod-shaped crystals with a dimension of approximately 20 x 80  $\mu$ m were obtained at 4  $^{\circ}$ C and 20  $^{\circ}$ C in 50 mM MES (pH 6.0), 1.7-2 M  $\text{NH}_4\text{SO}_4$ , and 5% (v/v) PEG 400 (Figure 2.14 B). These crystals diffracted up to 8  $\text{\AA}$  and the diffraction pattern was anisotropic, regardless if glycerol or ethylene glycol was used as cryoprotectant (Figure 2.14 C).

Zip-code RNA stabilized the interaction between She2p and She3p (Section 2.2.1 and 2.2.3). Therefore, addition of the RNA to the She2p:She3p complex might improve crystallization. However, initial crystallization trials with a purified complex of *ASH1*-E3-51 RNA, She2p (6-246), and She3p (334-425)-His only resulted in very small crystals in few conditions (Figure 2.14 D). Similar crystals were obtained when *ASH1*-E3-51 ( $\Delta$ 1786-1802) RNA was used. Attempts to improve the crystals of the ternary complex were so far not successful.

### 2.3.3 The ribosome as a structural scaffold for cryo-EM analysis of small RNA-protein complexes

Crystallization of the complex between RNA, She2p (and She3p) proved to be difficult (Section 2.3.2) (Müller 2009). The aim of this project was to develop a system based on single-particle cryo-EM to determine the structure of RNA-protein complexes that are otherwise too small for cryo-EM. The ribosome is well suited for single-particle cryo-EM (Frank 2001). Furthermore, the ribosome is able to accommodate heterologous RNA elements in certain positions and systems for genetic modification of ribosomal RNAs (rRNAs) are available (Spahn et al. 1999; Matadeen et al. 2001; Slagter-Jager et al. 2006; Hobbie et al. 2007; Yokoyama and Suzuki 2008).

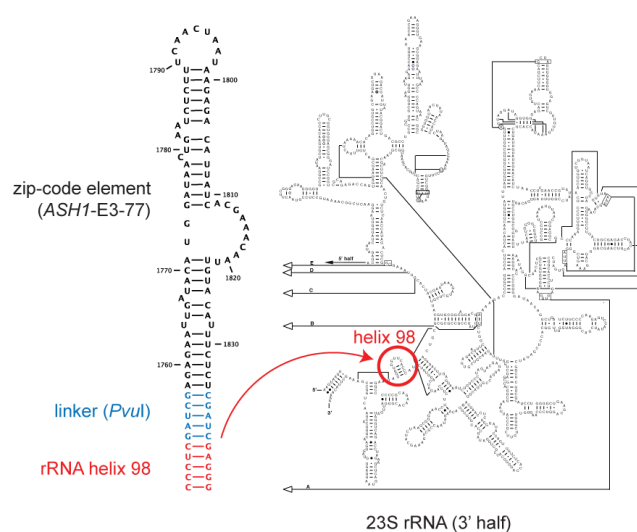


**Figure 2.15: Strategy for the construction of zip-code ribosomes.** Zip-code elements from the *ASH1* mRNA were fused to helix 98 (red) of *Mycobacterium smegmatis* 23S rRNA via a linker sequence containing a PvuI restriction site (blue) for cloning. Left side: Secondary structure prediction of *ASH1*-E3-77 fused to linker and helix 98. Right side: Secondary structure map of the 3' half of *Mycobacterium leprae* 23S rRNA (Cannone et al. 2002). Red circle marks the position of helix 98. The rRNA sequence of *Mycobacterium leprae* is highly homologous to *Mycobacterium smegmatis*.

Here, the ribosome from *Mycobacterium smegmatis* (Hobbie et al. 2007) was used to insert zip-code elements from the *ASH1* mRNA. The zip-code elements were genetically fused to helix 98 of the 23S ribosomal DNA via a PvuI restriction site, thereby producing engineered ribosomes, which were termed "zip-code ribosomes" (Figure 2.15). In eukaryotes, helix 98 harbors expansion segment 39 and thus provides enough space for heterologous RNA insertions (Spahn et al. 1999; Matadeen et al. 2001; Slagter-Jager et al. 2006; Yokoyama and Suzuki 2008).

#### 2.3.4 She2p and She3p bind to zip-code containing ribosomes

Each of the four *ASH1* zip-code elements (Figure S1) was inserted into the *M. smegmatis* ribosome. To test the functionality of the inserted stem-loops, binding of She2p was tested by a ribosome-pelleting assay (Figure 2.16). She2p co-purified with *ASH1*-E3 and *ASH1*-E1 zip-code ribosomes, whereas no binding to wild-type ribosomes was detected (Figure 2.16 A). Surprisingly, *ASH1*-E2A and *ASH1*-E2B zip-code ribosomes did not bind She2p. This might be due to the weaker affinity of these elements to She2p (Müller 2009). Alternatively, misfolding or steric hindrance could occur in the context of ribosome fusion. *ASH1*-E3 zip-code ribosomes showed strongest binding to She2p (Figure 2.16 A) and were used for all further analyses. In addition, *ASH1*-E3 zip-code ribosomes also formed a co-complex with She2p and She3p (Figure 2.16 B).

To determine the stoichiometry of binding, increasing amounts of She2p were mixed with a constant amount of *ASH1*-E3 zip-code ribosomes. Subsequent pelleting of the ribosomes revealed saturation of the complex at a ratio of two She2p molecules to one zip-code ribosome (Figure 2.16 C). This is in agreement with the stoichiometric ratio determined in a previous experiment (Niessing et al. 2004) and demonstrates that fusion of *ASH1* E3 with the ribosome does not change the stoichiometry of She2p binding.

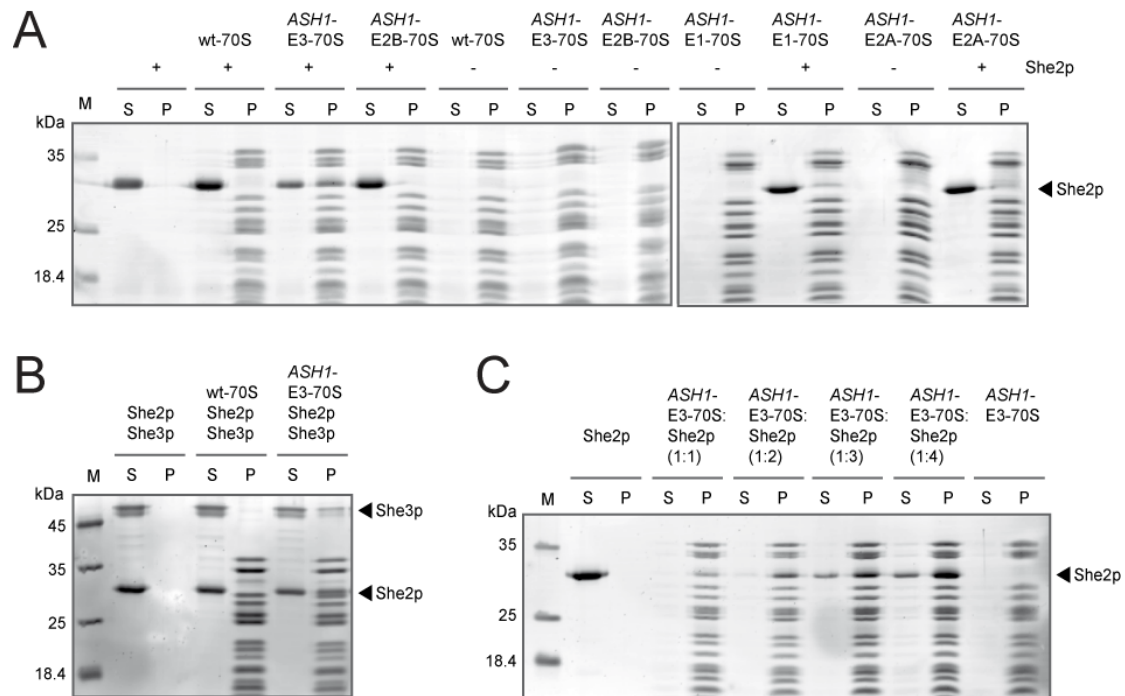


**Figure 2.16: She2p and She3p bind to zip-code ribosomes. A)** In ribosome pelleting assays, She2p bound efficiently to *ASH1*-E3 zip-code ribosomes and weakly to *ASH1*-E1 zip-code ribosomes. In contrast, no binding to *ASH1*-E2A and *ASH1*-E2B zip-code ribosomes as well as to wild-type ribosomes was detected. In the pelleting assay, bound proteins co-migrate with ribosomes in the pellet fraction (P), whereas unbound proteins remain in the supernatant (S). SDS-polyacrylamide gels were stained with SYPRO Orange (Sigma-Aldrich). **B)** She2p and She3p efficiently bound to *ASH1*-E3 zip-code ribosomes but not to wild-type ribosomes in a pelleting assay. **C)** She2p binds to *ASH1*-E3 zip-code ribosomes with 2:1 stoichiometry. Increasing amounts of She2p were incubated with a constant amount of ribosomes and subsequently fractionated by centrifugation. Excess She2p in the supernatant indicates saturation of the complex.

### 2.3.5 Cryo-EM reconstruction of *ASH1*-E3 zip-code ribosomes in complex with She2p

Preparation of cryo-EM grids and image collection were performed by Charlotte Ungewickell, Dr. Otto Berninghausen, and Dr. Thomas Becker in the laboratory of Prof. Roland Beckmann. Based on this data, single-particle cryo-EM reconstructions of wild-type and *ASH1*-E3 zip-code ribosomes were calculated at 25 Å resolution. Comparison of both structures revealed an additional electron density in *ASH1*-E3 zip-code ribosomes (Figure 2.17 A). Docking of the crystal structure of the *E. coli* ribosome (Borovinskaya et al. 2007) suggests that the additional electron density protrudes from helix 98 and thus corresponds to the inserted *ASH1*-E3 zip-code element (Figure 2.17 A). A three-dimensional model of the *ASH1*-E3 element was prepared with the program iFoldRNA (Sharma et al.

2008) and manually placed into the protruding electron density (Figure 2.17 A). However, the electron density accommodates only half of the modeled stem-loop. This might indicate that the stem-loop has a high degree of flexibility. Interestingly, the electron density vanishes in a region, where a large internal loop is predicted in the secondary structure of the *ASH1-E3* element (Figure 2.17 A). Deletion of this internal loop to obtain a more rigid stem-loop was not possible since it is essential for She2p binding (Section 2.3.1).

Binding of She2p to the *ASH1-E3* zip-code element might stabilize a distinct conformation and improve the quality of the reconstruction. Therefore, an excess of She2p was added to *ASH1-E3* zip-code ribosomes and a single-particle cryo-EM reconstruction was calculated at 25 Å resolution. Compared to unbound *ASH1-E3* zip-code ribosomes, the additional electron density was more pronounced (Figure 2.17 B). It is big enough to accommodate one She2p dimer but not a tetramer. This result might be explained by the selection of single ribosomal particles during image processing. Since the She2p tetramer has two distinct RNA binding sites (Figure 1.7 B) (Müller et al. 2009), it likely binds two zip-code ribosomes simultaneously. However, such dimeric ribosomes were excluded from the image analysis.

A reconstruction of the *ASH1-E3* zip-code ribosome in complex with She2p at 10 Å resolution was calculated from about 60 000 single ribosomal particles. Although helical features of the rRNA started to appear, the electron density corresponding to the *ASH1-E3*:She2p complex was blurred and did not improve during refinement (Figure 2.17 C). Its behavior was very similar to the highly flexible L7/L12 stalk of the ribosome (Diaconu et al. 2005) suggesting that the *ASH1-E3* stem-loop itself and/or its linkage to rRNA are flexible.

In summary, the *ASH1-E3* zip-code element was visualized in fusion with the ribosome by cryo-EM. Additional electron density corresponding to bound She2p was also observed. However, flexibility of the inserted zip-code element prevented further refinement and interpretation of the electron density.

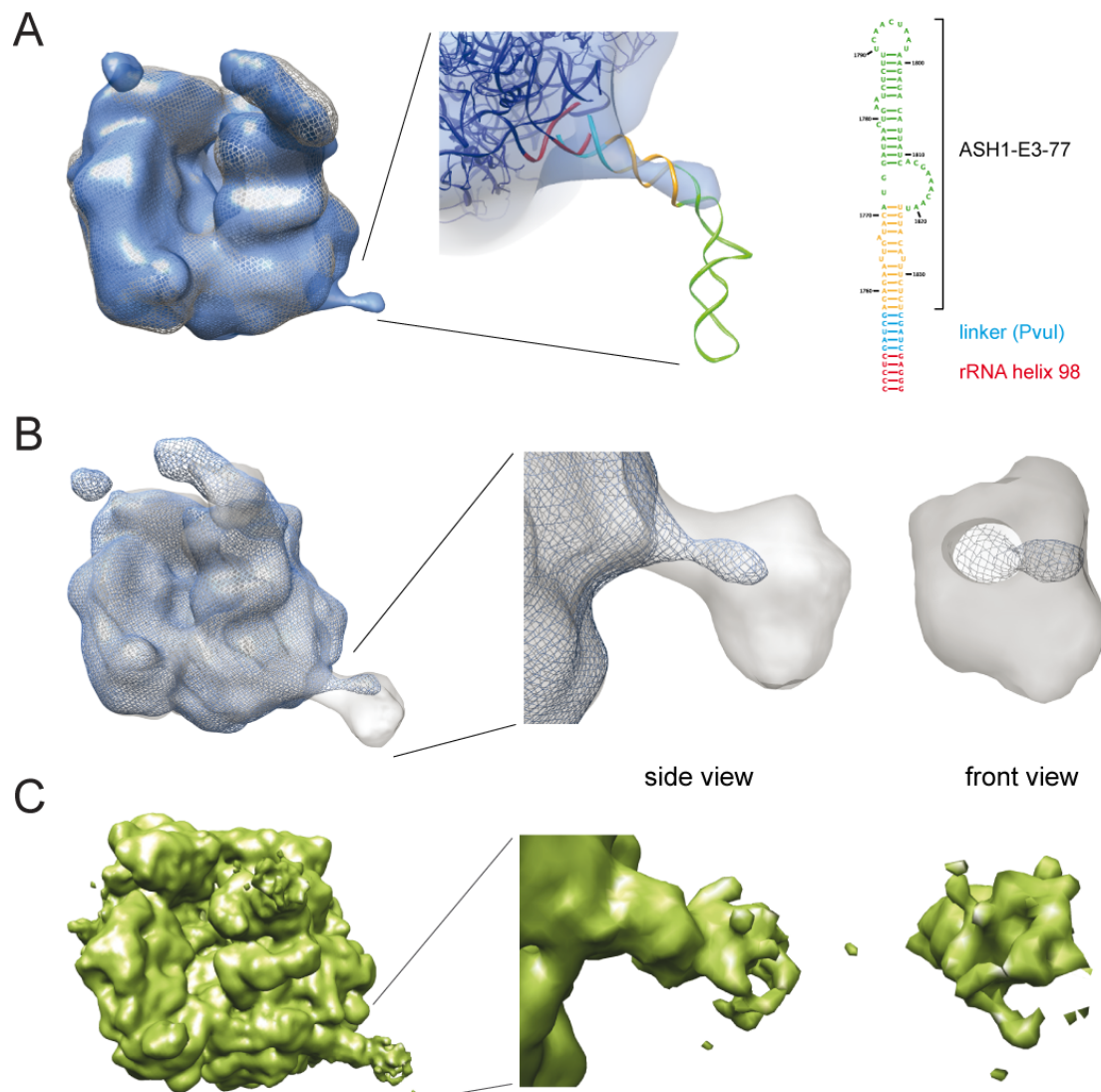


**Figure 2.17: The *ASH1-E3* zip-code element and bound *She2p* can be visualized by cryo-EM using the ribosome scaffold. **A**) Overlay of single-particle cryo-EM reconstructions of wild-type ribosomes (grey mesh) with *ASH1-E3* zip-code ribosomes (blue envelope) at 25 Å resolution. Inset shows a magnification of the electron density corresponding to the inserted *ASH1-E3* zip-code element. The crystal structure of the *E. coli* ribosome (PDB ID: 2QAM) (Borovinskaya et al. 2007) was docked into the electron density and is shown in blue ribbon representation with helix 98 indicated in red. A three-dimensional structure prediction of the *ASH1-E3* zip-code element was prepared with iFoldRNA (Sharma et al. 2008) and manually placed into the electron density. The modeled *ASH1-E3* RNA structure is color-coded as in the secondary structure prediction shown on the right. **B**) Overlay of single-particle cryo-EM reconstructions of *ASH1-E3* zip-code ribosomes without (blue mesh) and with bound *She2p* (grey envelope) at 25 Å resolution. Insets show magnifications of the insertion site in side and front view. When *She2p* was bound to the zip-code element, a more pronounced electron density was observed. **C**) Single-particle cryo-EM reconstruction of the *ASH1-E3* zip-code ribosome in complex with *She2p* at 10 Å resolution. Insets show magnifications of the insertion site in side and front view. Figures were prepared with UCSF CHIMERA (Pettersen et al. 2004).**

## 2.4 Size and stoichiometry analysis of SHE-complex assembly

### 2.4.1 She3p oligomerizes via its N-terminus

The oligomeric state of She3p is not known. Chemical cross-linking with 1-Ethyl-3-[3-dimethylaminopropyl]carbodiimide (EDC) and N-Hydroxysuccinimide (NHS) revealed oligomerization of She3p via its N-terminus (amino acids 1-234) (Figure 2.18). In contrast, the monomeric Myo4p or the C-terminus of She3p (amino acids 274-425) alone were not efficiently cross-linked. The molecular weight of the observed cross-linking products is consistent with the formation of a She3p dimer (Figure 2.18). The tendency of She3p to form higher oligomers prevented unambiguous molecular weight analysis by SLS. However, the co-complex of She3p and Myo4p was amenable to SLS and the measured molecular weight suggests the existence of a She3p dimer in the co-complex (Section 2.4.2).

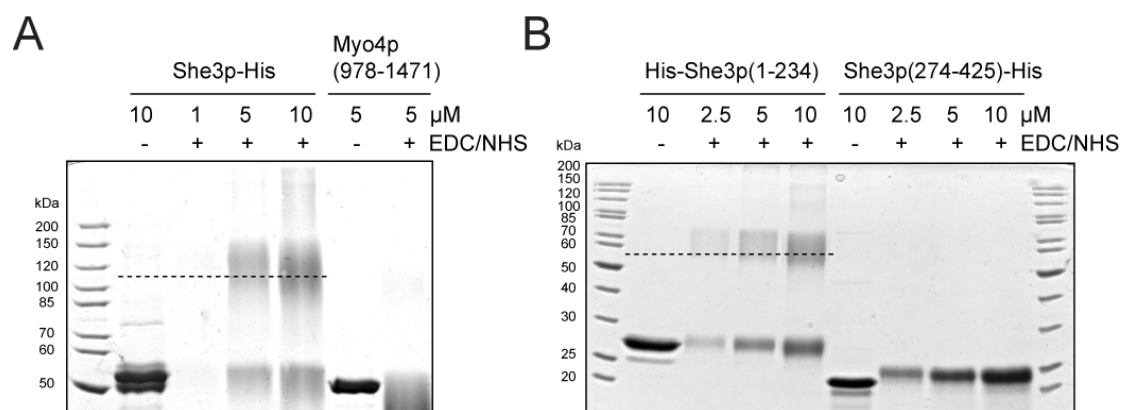


**Figure 2.18: She3p oligomerizes via its N-terminus.** **A)** Chemical cross-linking with EDC and NHS revealed oligomerization of full-length She3p. The monomeric Myo4p (978-1471) was not cross-linked. Dotted line indicates the expected migration of a She3p dimer. **B)** Chemical cross-linking of the She3p N-terminus (His-She3p(1-234)) and C-terminus (She3p(274-425)-His) demonstrated that the N-terminus is responsible for oligomerization. Dotted line indicates the expected migration of the dimeric She3p N-terminus.

### 2.4.2 A She3p dimer and a Myo4p monomer form a constitutive co-complex

To perform efficient transport of its cargoes the monomeric Myo4p has to form oligomers (Section 1.2.5). It is not known how oligomerization of Myo4p is achieved, how many Myo4p molecules are incorporated into one transport

complex, and how this assembly regulates transport activity. Therefore, different SHE sub-complexes were analyzed for their size and stoichiometry to determine the mechanism of mRNP assembly.

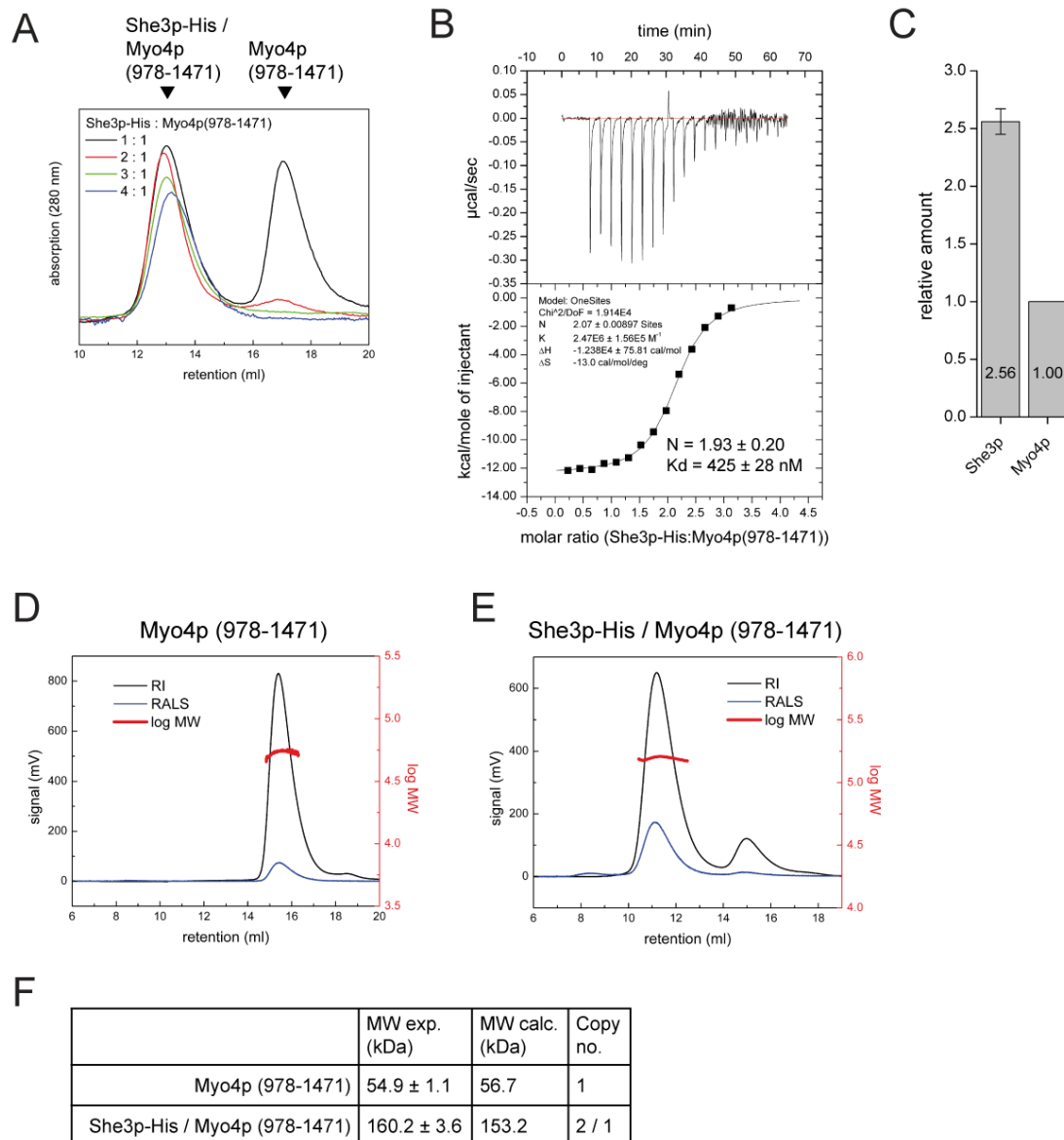


**Figure 2.19: One She3p dimer forms a complex with one Myo4p monomer.** **A)** The stoichiometry of the She3p:Myo4p complex was determined by SEC. Increasing amounts of Myo4p (3-12  $\mu$ M) were mixed with a constant amount of She3p (12  $\mu$ M) and excess Myo4p was separated from the complex by SEC. The complex was saturated at a ratio of two molecules She3p to one molecule Myo4p. **B)** ITC revealed a stoichiometry of  $1.93 \pm 0.20$  (mean and standard deviation of two experiments) for the She3p:Myo4p complex. She3p was titrated into Myo4p. **C)** Quantitative mass spectrometry with heavy-isotope labeled peptides showed a stoichiometry of  $2.56 \pm 0.11$  (mean and standard deviation of two independent experiments) for the She3p:Myo4p complex. The amount of She3p was normalized with respect to Myo4p. **D)** SLS profile of Myo4p. RI: refractive index, RALS: right angle light scattering, MW: fitted molecular weight. **E)** SLS profile of the She3p:Myo4p complex. Note that a slight excess of Myo4p was used to saturate the complex. **F)** Comparison of molecular weights determined by SLS (MW exp.) and calculated from sequence (MW calc.). Shown are the mean and standard deviation of three experiments with varying sample concentrations.

In the cytoplasm, Myo4p forms a constitutive co-complex with She3p (Heuck et al. 2007; Hodges et al. 2008). Isothermal titration calorimetry (ITC), quantitative mass spectrometry with heavy-isotope labeled peptides, and titrations by SEC were performed to determine the stoichiometry of this complex (Figure 2.19 A-C). Quantitative mass spectrometry was carried out by Dr. Lars Israel in the laboratory of Prof. Axel Imhof. Analyses by SEC and ITC clearly indicated a stoichiometric ratio of two She3p molecules to one Myo4p monomer (Figure 2.19 A, B). Quantitative mass spectrometry yielded a slightly divergent stoichiometry ratio of  $2.56 \pm 0.11$  for She3p:Myo4p (Figure 2.19 C). In summary, these experiments indicate a stoichiometric ratio of 2:1 for the She3p:Myo4p complex. This finding is in agreement with the existence of a She3p dimer (Section 2.4.1).

In line with previous studies (Dunn et al. 2007; Heuck et al. 2007; Hodges et al. 2008), molecular-weight determination by SLS confirmed that Myo4p is a monomer in isolation (Figure 2.19 D, F). SLS with the complex of She3p and Myo4p yielded a molecular weight of  $160.2 \pm 3.6$  kDa (Figure 2.19 E, F). This result is in agreement with the 2:1 stoichiometry and suggests a complex of one She3p dimer and one Myo4p monomer. Thus, oligomerization of Myo4p does not occur at this step of assembly, suggesting a transport incompetent motor complex in the absence of cargo.

### 2.4.3 A She2p tetramer binds two zip-code RNAs

In the nucleus, She2p pre-assembles with *ASH1* mRNA (Shen et al. 2010). Efficient mRNA binding and localization requires the formation of She2p tetramers (Müller et al. 2009; Chung and Takizawa 2010). However, it is unclear how many zip-code elements bind to one She2p tetramer.

To address this question, the size of She2p in complex with *ASH1*-E3 RNA was determined by SLS. The measured molecular weight implies that one She2p tetramer bound two *ASH1*-E3 RNAs (Figure 2.20 A, B, D). This result is in agreement with a previous filter-binding experiment that indicated binding of

## RESULTS

one *ASH1*-E3 element per She2p dimer (Niessing et al. 2004). Complex formation between two zip-code RNAs and a She2p tetramer was consistently observed for a 51 nucleotides-long *ASH1*-E3 RNA (*ASH1*-E3-51), a 77 nucleotides-long *ASH1*-E3 RNA fused to tRNA (*ASH1*-E3-77-tRNA), and *IST2* RNA fused to tRNA (*IST2*-tRNA) (Figure 2.20). This analysis shows that the tRNA-tag does not change the stoichiometry of She2p binding. Furthermore, it suggests that zip-code RNAs from different localizing transcripts bind the She2p tetramer in a similar manner.

The modeled tetrameric She2p structure shows two continuous RNA-binding surfaces on opposite sides (Figure 1.7 B) (Müller et al. 2009). Therefore, one zip-code RNA might bind on each side of the tetramer.

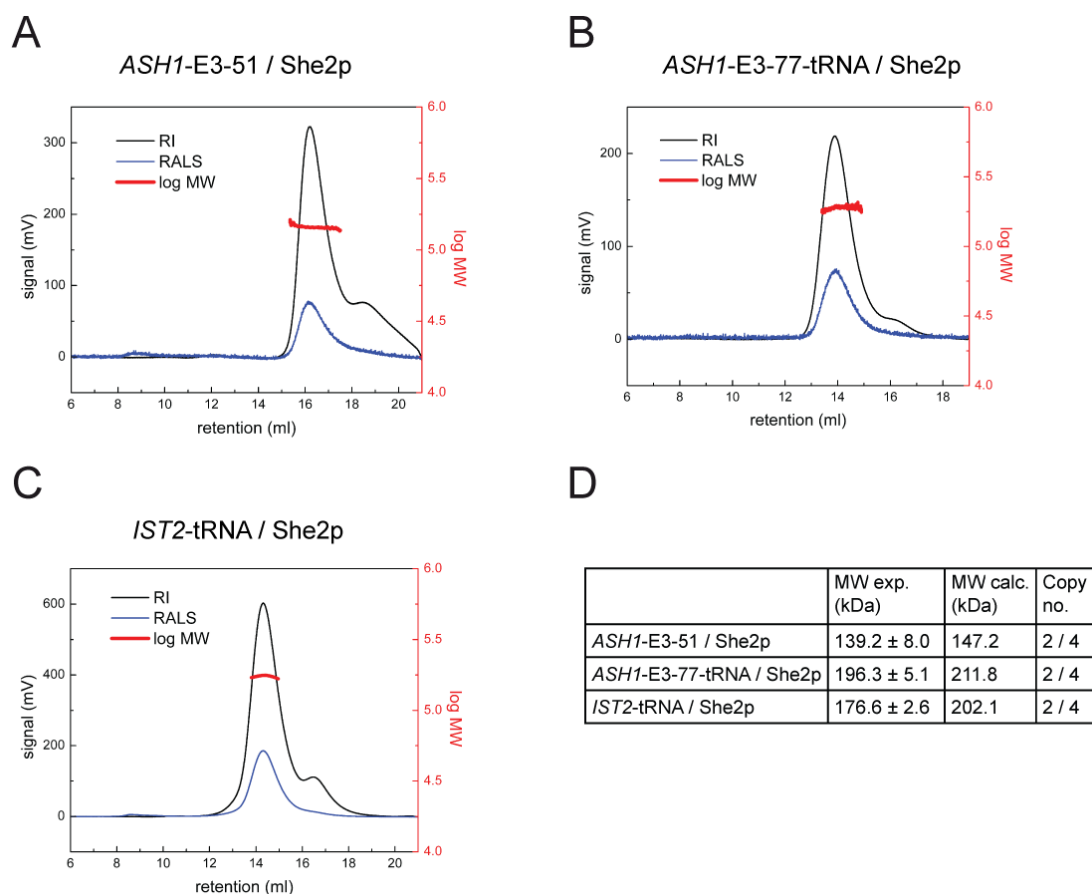


**Figure 2.20: One She2p tetramer binds two zip-code elements.** A-C) SLS profiles of the *ASH1*-E3-51:She2p complex (A), the *ASH1*-E3-77-tRNA:She2p complex (B), and the *IST2*-tRNA:She2p complex (C). Note that a slight excess of *ASH1*-E3-51 was used to saturate the complex. RI: refractive index, RALS: right angle light scattering, MW: fitted molecular weight. D) Comparison of molecular weights determined by SLS (MW exp.) and calculated from sequence (MW calc.). Shown are the mean and standard deviation of at least three experiments with varying sample concentrations.

#### 2.4.4 Assembly of the SHE-core complex induces Myo4p dimerization

When the RNA:She2p complex reaches the cytoplasm, it assembles with She3p and Myo4p to form the mature mRNP (Section 1.2.1). Efficient mRNA transport requires oligomeric Myo4p (Section 1.2.5), but the She3p:Myo4p complex contains only one Myo4p monomer (Section 2.4.2). Thus, it might be that Myo4p oligomerization occurs during the final step of mRNP assembly.

SHE-core complexes were either reconstituted with *ASH1*-E3-51 RNA or with *ASH1*-E3-77-tRNA and the protein stoichiometries in these complexes were determined by quantitative mass spectrometry with heavy-isotope labeled peptides. The stoichiometric ratio between She3p and Myo4p was 2.12 in the *ASH1*-E3-51 RNA complex and 2.23 in the *ASH1*-E3-77-tRNA complex (Figure 2.21 A). Thus, the stoichiometry between She3p and Myo4p in the SHE-core complex is the same as in the She3p:Myo4p complex (Section 2.4.2). The results were less clear for She2p and She3p. The stoichiometric ratio between She2p and She3p in both SHE-core complexes varied between 0.34 and 1.00 depending on the heavy-isotope labeled She2p peptide used for quantification (Figure 2.21 A).

To clarify the stoichiometry of the She2p:She3p interaction in the SHE-core complex, a series of EMSA experiments were performed (Figure 2.21 B-F). A constant amount of 125 nM *ASH1*-E3-77 RNA and 250 nM She2p (equals 63 nM of a 2:4 complex) was titrated with increasing amounts of She3p:Myo4p complex (Figure 2.21 B). At a ratio of two She3p:Myo4p (2:1) complexes to one RNA-bound She2p tetramer, a single band appeared indicating the formation of a homogeneous, stoichiometric complex (Figure 2.21 B, lane 6). When *ASH1*-E3-77:She2p was not saturated by She3p:Myo4p, an additional band emerged indicating formation of a second complex with lower molecular weight (Figure 2.21 B, lane 3-5). In contrast, when She3p:Myo4p was in excess, a band with higher molecular weight appeared (Figure 2.21 B, lane 7). A control EMSA showed that formation of this high-molecular weight band was not simply due to concentration-dependent aggregation of She3p:Myo4p bound to RNA (Figure 2.21 E) but rather due to excess amounts of She3p:Myo4p in relation to *ASH1*-E3-

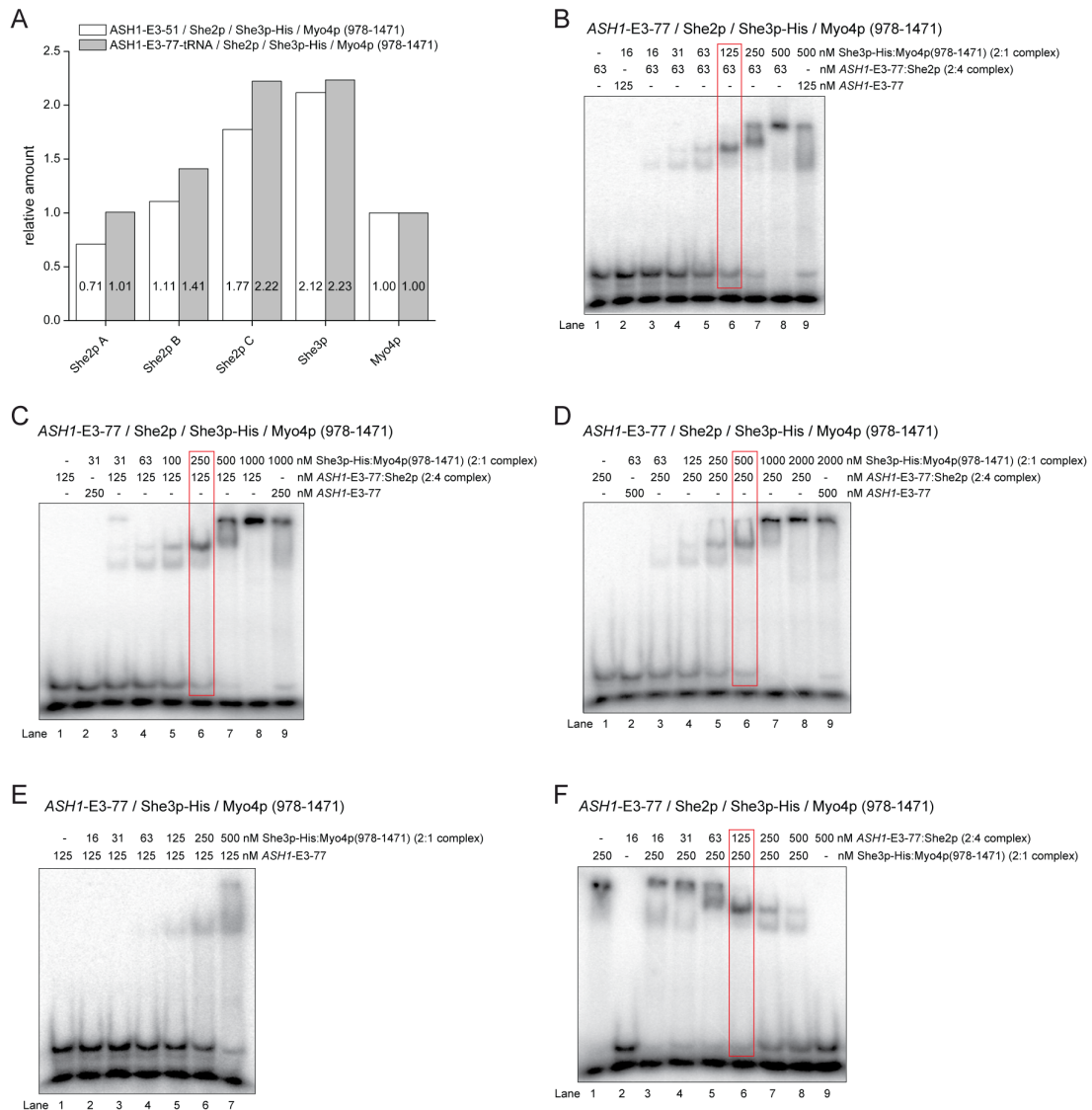


**Figure 2.21: Determination of the protein stoichiometries in the SHE-core complex.** **A)** Quantitative mass spectrometry of the SHE-core complex reconstituted with *ASH1-E3-51* (white bars) or *ASH1-E3-77-tRNA* (grey bars). Heavy-isotope labeled peptides of She2p, She3p, and Myo4p were used for quantification. The stoichiometry of the She3p:Myo4p interaction was 2.12 (*ASH1-E3-51* complex) or 2.23 (*ASH1-E3-77-tRNA* complex). For the She2p:She3p stoichiometry, inconsistent results were obtained with the She2p peptides A, B, and C. The amount of She2p and She3p was normalized with respect to Myo4p. **B-D)** The stoichiometry of the SHE-core complex was determined by EMSAs. A constant concentration of *ASH1-E3:She2p* was used and increasing concentrations of She3p:Myo4p were titrated. The distinct band observed in lane 6 (red box) indicates binding of two She3p:Myo4p complexes to one RNA-bound She2p tetramer. Given concentrations relate to a 2:1 complex of She3p:Myo4p and a 2:4 complex of *ASH1-E3:She2p*. The experiment was performed with 63 nM (B), 125 nM (C) and 250 nM (D) *ASH1-E3:She2p* (2:4 complex) to rule out a concentration-dependent aggregation of the complex. Instead, the increase in size of the shifted bands (lane 7 and 8) is rather due to excess She3p:Myo4p bound to RNA. **E)** Control EMSA with She3p:Myo4p and *ASH1-E3* RNA. No significant aggregation was observed below 500 nM She3p:Myo4p (2:1 complex). **F)** Inversion of the experiment shown in C. A constant concentration of She3p:Myo4p was used and increasing concentrations of *ASH1-E3:She2p* were titrated. The distinct band observed in lane 6 (red box) indicates binding of two She3p:Myo4p complexes to one RNA-bound She2p tetramer.

77:She2p. To further exclude a concentration dependency of the observed effects, the EMSA titration was repeated with higher sample concentrations (Figure 2.21 C, D). Regardless of the concentrations used in these EMSAs,

## RESULTS

saturation of the complex always occurred at the same stoichiometric ratio. Inversion of the experiment by using a constant amount of She3p:Myo4p and increasing amounts of *ASH1-E3-77*:She2p yielded the same result (Figure 2.21 F). This experiment further confirms that the different size of the observed band shifts was not due to varying concentrations of She3p:Myo4p, but rather reflects the formation of complexes with different stoichiometry. In summary, the EMSA analyses suggest that two She3p:Myo4p (2:1) complexes associate with one RNA-bound She2p tetramer to form a SHE-core complex with defined size.

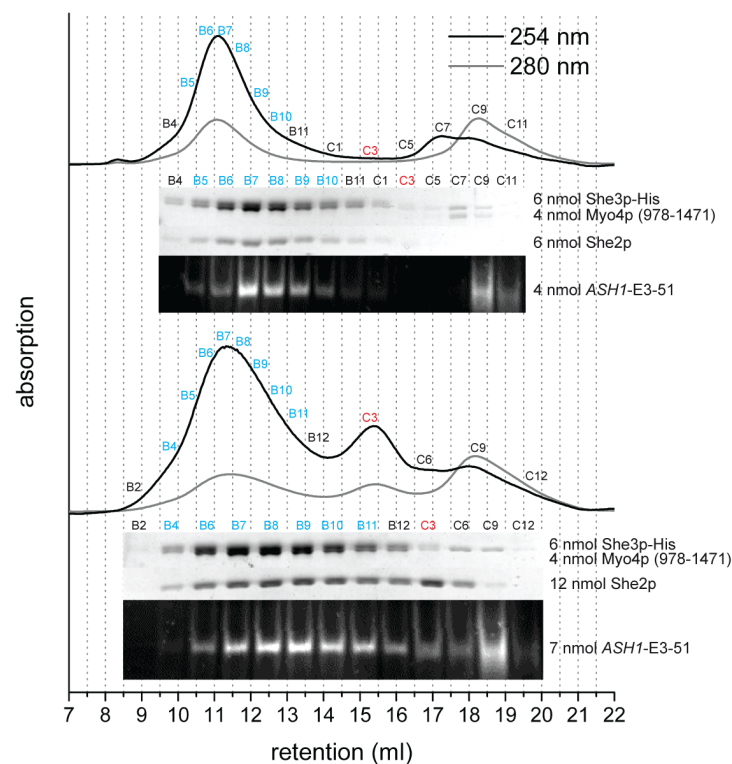


**Figure 2.22: SEC to determine the protein stoichiometries in the SHE-core complex.** When equimolar amounts of She2p and She3p were used, a homogeneous SHE-core complex (cyan) but no excess of *ASH1-E3*:She2p (red) was detected (upper chromatogram). In contrast, a two-fold molar excess of She2p over She3p led to an excess of *ASH1-E3*:She2p (red) that was not in complex with She3p:Myo4p (lower chromatogram). These experiments indicate a 1:1 ratio between She2p and She3p in the SHE-core complex. Amounts used for reconstitution are given. A slight excess of *ASH1-E3* and Myo4p over She2p and She3p, respectively, was used to ensure saturation. Samples were separated on a Superose 6 10/300 GL column (GE Healthcare). Indicated fractions were analyzed by SDS-PAGE (proteins) and PAGE (RNA). Note that She3p-His and Myo4p (978-1471) migrate at similar height in SDS-PAGE and appear as a double-band.

To validate the EMSA titration, two SEC experiments were performed. In the first experiment, equimolar amounts of She2p and She3p were incubated with a slight excess of *ASH1-E3-51* RNA and Myo4p. After SEC a homogeneous complex of all the components but no excess of *ASH1-E3*:She2p was present (Figure 2.22,

## RESULTS

upper chromatogram). In contrast, if a two-fold molar excess of She2p over She3p was used, a large amount of *ASH1-E3:She2p* was separated from the quaternary SHE-core complex (Figure 2.22, lower chromatogram). These experiments indicate that the SHE-core complex is saturated at equimolar amounts of She2p and She3p. This is in agreement with the stoichiometry determined by EMSAs.

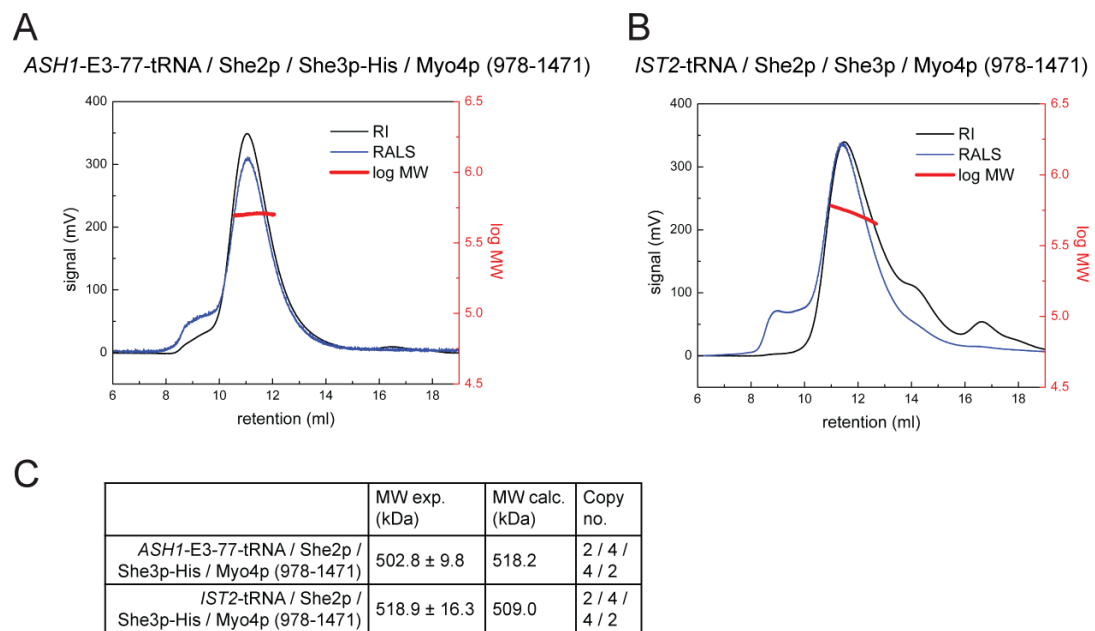


**Figure 2.23: Molecular weight analysis of the SHE-core complex. A-B)** SLS profile of the *ASH1-E3-tRNA:She2p:She3p:Myo4p* complex (A) and the *IST2-tRNA:She2p:She3p:Myo4p* complex (B). In case of the *IST2-tRNA* (B), the complex was not entirely stable during chromatography. RI: refractive index, RALS: right angle light scattering, MW: fitted molecular weight. **C)** Comparison of molecular weights determined by SLS (MW exp.) and calculated from sequence (MW calc.). Shown are the mean and standard deviation of at least three experiments with varying sample concentrations.

In order to confirm these results by a different approach, the absolute molecular weight of the SHE-core complex was determined by SLS. The reconstituted complexes were only stable enough for SLS analysis when tRNA-tagged zip-code RNAs were used. This might be due to stabilization of the stem-loop structure by the attachment of tRNA. Interestingly, stabilization of the interaction between an RNA-binding protein and zip-code RNA by fusion with an RNA aptamer has already been described for RNAs from *Drosophila* (Dienstbier et al. 2009). For a SHE-core complex consisting of *ASH1-E3-77-tRNA*, She2p, She3p, and Myo4p a molecular weight of  $502.8 \pm 9.8$  kDa was measured (Figure 2.23 A, C). This result is consistent with binding of two She3p:Myo4p complexes to one RNA-bound She2p tetramer, as suggested by the stoichiometry determination. A similar

molecular weight was observed for a SHE-core complex reconstituted with *IST2*-tRNA (Figure 2.23 B, C). However, this complex partially dissociated during SLS and the molecular weight distribution was not completely homogeneous over the complex peak (Figure 2.23 B).

In summary, stoichiometry and molecular weight analyses indicate that the She2p tetramer provides a platform for binding of two zip-code RNAs and two She3p:Myo4p (2:1) complexes. The components of a single SHE-transport unit assemble into a complex of ca. 500 kDa (ca. 880 kDa, if *ASH1*-E3-77 RNA, She2p, She3p, and full-length Myo4p including six light chains per Myo4p neck are taken into account).

The large size of the SHE-core complex might allow for structural characterization by EM. Charlotte Ungewickell from the laboratory of Prof. Roland Beckmann prepared electron micrographs of the SHE-core complex negatively stained with uranyl acetate, methylamine vanadate, or phosphotungstic acid. However, only small and inhomogeneous particles were visible. This observation might be due to dissociation of the complex at the low concentrations used for EM or because of incompatibility with the staining conditions.

#### **2.4.5 RNAs with two zip-code elements induce clustering of SHE-core complexes**

One SHE-core complex is able to bind two zip-code RNAs (Section 2.4.3 and 2.4.4). On the other hand, transported mRNAs, like *ASH1* mRNA or *WSC2* mRNA, contain more than one zip-code element (Chartrand et al. 1999; Gonzalez et al. 1999; Jambhekar et al. 2005). Assembly of bivalent complexes with bi- or multivalent RNAs should enable the formation of multimers with variable size.

## RESULTS

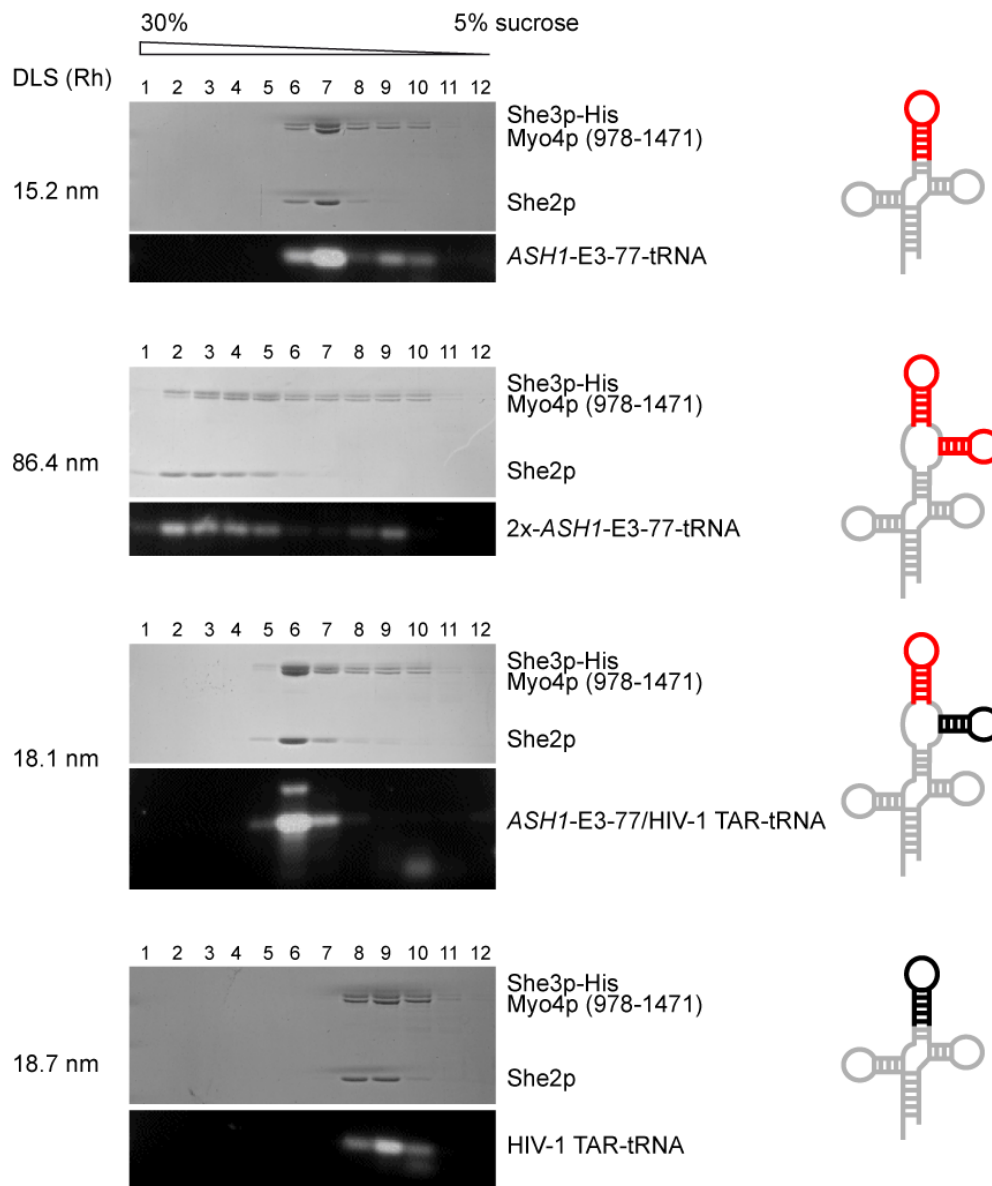


**Figure 2.24: An RNA with two zip-code elements induces multimerization of SHE-core complexes.** DLS analysis and sucrose density gradient centrifugation of SHE-core complexes with different RNA constructs. Fractions were analyzed by SDS-PAGE (proteins) and agarose gel electrophoresis (RNA). An RNA containing two zip-code elements (*2x-ASH1-E3-77-tRNA*) induced the formation of much bigger complexes than an RNA with only one zip-code element (*ASH1-E3-77-tRNA* or *ASH1-E3-77/HIV-1 TAR-tRNA*). The increased hydrodynamic radius (Rh) and the faster sedimentation indicate multimerization of SHE-core complexes in the presence of *2x-ASH1-E3-77-tRNA*. Furthermore, the broad distribution of complexes in the gradient suggests that a range of complex sizes was formed. No stable complex formation was detected with HIV-1 TAR-tRNA. However, smaller sub-complexes co-migrated in the sucrose gradient. Schematics of the RNA constructs are shown on the right. Distinct features are color-coded: *ASH1-E3-77* (red), HIV-1 TAR (black), three-way junction and tRNA (grey).

To verify this conclusion, an RNA construct with two zip-code elements was designed. Therefore, two *ASH1-E3* elements were fused to the tRNA-tag via a three-way junction from the Twort intron (Lescoute and Westhof 2006) (Figure 2.24, *2x-ASH1-E3-77-tRNA*, and Figure S1). This RNA was reconstituted with SHE-core complexes and analyzed by DLS and sucrose density gradient

centrifugation. The respective complex showed a marked increase in the hydrodynamic radius as well as faster sedimentation compared to a SHE-core complex with a single *ASH1*-E3 zip-code element (*ASH1*-E3-77-tRNA) (Figure 2.24). The almost six-fold increase in the hydrodynamic radius suggests the formation of multimers containing several SHE-core complexes. The broad distribution of the complex in the sucrose gradient (Figure 2.24, 2x-*ASH1*-E3-77-tRNA, fractions 2-5) indicates that a range of multimers with variable size was formed. This behavior is well explained by the association of two bivalent interaction partners. As a control, an RNA with one *ASH1*-E3 zip-code and one HIV-1 TAR stem-loop fused to tRNA via a three-way junction (*ASH1*-E3-77/TAR-tRNA) was used. This RNA behaved similar to *ASH1*-E3-tRNA (Figure 2.24), demonstrating that neither the HIV-1 TAR RNA nor the three-way junction bound to the SHE-core complex. The HIV-1 TAR stem-loop fused to tRNA did also not induce complex formation (Figure 2.24, TAR-tRNA). In summary, these experiments demonstrate that an RNA containing at least two zip-code elements is able to multimerize SHE-core complexes. Thereby, clustering of several mRNAs and multiple motor molecules can be achieved.

#### **2.4.6 Assembly of SHE-core complexes does not influence the actin-activated ATPase activity of Myo4p**

The type V myosin MyoVa prevents unnecessary ATP consumption by auto-inhibition of its motor domain (Section 1.1.8) (Li et al. 2006; Liu et al. 2006; Li et al. 2008). Binding of the adapter protein melanophilin likely relieves auto-inhibition (Li et al. 2005). It is under debate, if Myo4p is regulated by a similar or even by a very different mechanism (Section 1.2.5) (Hodges et al. 2008; Heuck et al. 2010).

Purified full-length Myo4p from insect cells (Section 2.1.1) was active in ATPase assays with saturating concentrations of F-actin and ATP (Figure 2.25). The ATPase activity depended on the concentration of F-actin and salt in the assay.

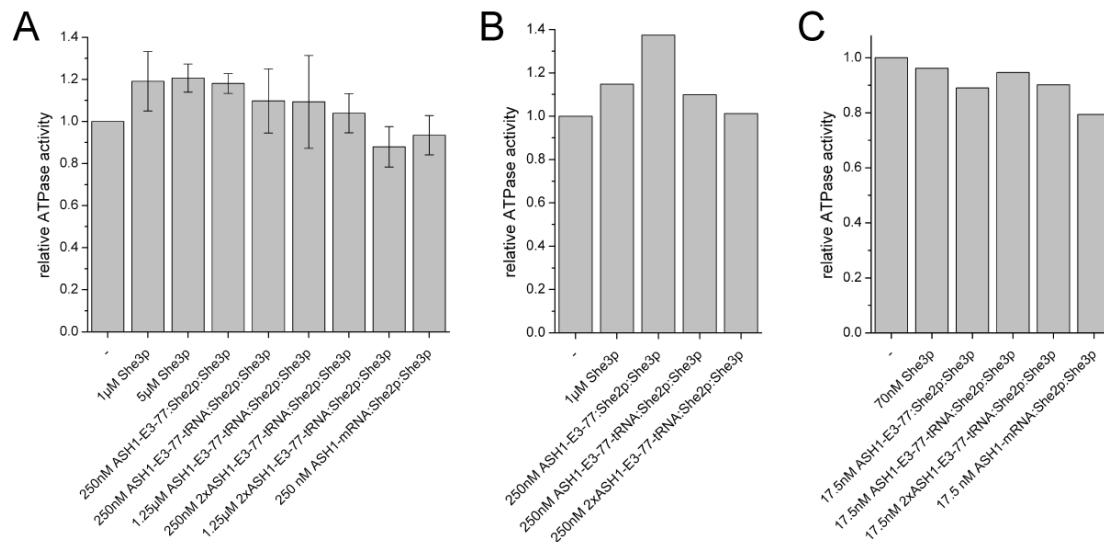


**Figure 2.25: SHE complex assembly does not influence the ATPase activity of Myo4p. A)** Regenerative ATPase assay with saturating concentrations of F-actin and ATP. The actin-activated ATPase activity was similar for the She3p:Myo4p complex and SHE-core complexes with different zip-code containing RNAs. In this assay, hydrolyzed ATP is regenerated by an enzymatic system. This reaction is coupled to NADH consumption, which was measured by absorption at 340 nm. The speed of NADH consumption provides a measure of the ATPase activity and was normalized with respect to Myo4p alone yielding the relative ATPase activity. Shown are the mean and standard deviation of at least three experiments. **B)** Radioactive ATPase assay confirms the results shown in A. **C)** Regenerative ATPase assay with stoichiometric concentrations to ensure that two Myo4p molecules were bound per SHE-core complex. Only minor differences in the actin-activated ATPase activity were detected. In all experiments, She3p concentrations relate to the monomer, whereas concentrations for zip-code RNA:She2p:She3p relate to a 2:4:4 complex. 15  $\mu$ M F-actin, 1 mM ATP and ca. 35 nM monomeric Myo4p were used in all assay.

The effects of complex assembly on the actin-activated ATPase activity of Myo4p were rather small (Figure 2.25). In regenerative ATPase assays a slight stimulation was observed upon addition of exogenous She3p (Figure 2.25 A). This effect might be underestimated, since a certain amount of She3p was likely present also in the Myo4p preparation (Section 2.1.1). Compared to the She3p:Myo4p complex, assembly of SHE-core complexes with *ASH1*-E3 zip-code RNAs barely changed the actin-activated ATPase activity of Myo4p (Figure 2.25 A). When RNAs with two *ASH1*-E3 zip-code elements or full-length *ASH1* mRNA with four zip-code elements were used, even a slight decrease in the actin-activated ATPase activity was observed. Similar results were obtained with a radioactive ATPase assay (Figure 2.25 B). Please note, that the complex of *ASH1*-E3-tRNA, She2p, and She3p was stable during SEC also under salt concentrations that were identical to the ATPase assay.

To assure that two Myo4p molecules were bound per SHE-core complex, the regenerative ATPase assay was repeated with stoichiometric concentrations of

## RESULTS

RNA and proteins. The concentrations were above the estimated  $K_d$  of the RNA:She2p:She3p complex (Section 2.2.3) and should therefore allow for complex formation. However, no pronounced effect on the ATPase activity was observed (Figure 2.25 C). Taken together, assembly of SHE-core complexes did not affect the ATPase activity of Myo4p in a significant way.

### 3 DISCUSSION

#### 3.1 Specific recognition of zip-code RNA is mediated by the co-complex of She2p and She3p

*The nuclear RNA-binding proteins She2p and Puf6p show modest specificity for localizing mRNAs*

The current model of *ASH1* mRNA localization in yeast suggests that She2p recognizes the RNA already in the nucleus (Section 1.2.1). However, She2p has only two to ten-fold higher affinity for zip-code RNAs, when compared to non-localizing stem-loop RNAs (Müller 2009; Müller et al. 2011). Such low specificity is unlikely to explain the selective incorporation of localizing transcripts into mRNPs and their subsequent transport *in vivo*. In addition to She2p, the translational repressor Puf6p binds to *ASH1* mRNA in the nucleus (Gu et al. 2004; Du et al. 2008). Since Puf6p has only modest specificity for the *ASH1*-E3 element with two PUF-consensus sites *in vitro*, it is unlikely to contribute to the specific recognition of localizing mRNAs (Müller et al. 2011). Moreover, She2p and Puf6p do not cooperate to achieve higher specificity for zip-code RNAs (Müller et al. 2011). In summary, the modest RNA-binding specificity of the nuclear proteins She2p and Puf6p *in vitro* does not sufficiently explain the high selectivity for localizing transcripts *in vivo*.

*She2p and She3p interact directly with modest affinity*

To date, the described role of She3p is to act as an adapter protein between the RNA-binding protein She2p and the motor protein Myo4p (Böhl et al. 2000; Long et al. 2000; Gonsalvez et al. 2003). Purified recombinant She3p indeed bound to She2p directly with a  $K_d$  of 1.6  $\mu\text{M}$  (Section 2.2.1). This affinity is sufficient to explain co-immunoprecipitation of She3p with a She2p mutant that lacks RNA-binding activity (Gonsalvez et al. 2003). However, the modest affinity and rapid dissociation of the co-complex suggest that additional components might be necessary to stabilize the She2p:She3p interaction for efficient transport *in vivo*.

*She3p is an unspecific RNA-binding protein*

A previous study showed that She3p induced a supershift in an EMSA with She2p and *ASH1-E3* RNA (Böhl et al. 2000). However, it remained ambiguous if this supershift is mediated exclusively by protein-protein interaction or if She3p also binds to the RNA. In an EMSA, purified recombinant She3p indeed bound to the *ASH1-E3* zip-code element with nanomolar affinity, similar to She2p and Puf6p (Section 2.2.2). Binding to the non-localizing HIV-1 TAR stem-loop was only slightly weaker, suggesting that RNA-binding by She3p is rather unspecific. Database searches did not reveal any known RNA-binding domains in She3p. In addition, CD analysis revealed that a large part of She3p might be unstructured (Section 2.1.1). In agreement with this result, the highly basic C-terminus of She3p that mediates RNA binding is predicted to be unfolded (Figure S2). A recent study described She3p mutants that were defective for mRNA localization although they retained the ability to associate with She2p and Myo4p (Landers et al. 2009). The finding that She3p binds to RNA provides a likely explanation for the observed effects.

*She2p and She3p synergistically recognize zip-code RNA*

She3p has the ability to bind zip-code RNAs and She2p. Thus, She3p might cooperate with She2p to achieve specific recognition of zip-code RNAs. In EMSAs, the co-complex of She2p and She3p bound to *ASH1-E3* RNA with an apparent  $K_d$  in the range of 25-50 nM (Section 2.2.3). The individual proteins did not show any detectable interaction at this concentration. Thus, She2p and She3p act synergistically to bind *ASH1-E3* RNA. Similarly, all other *ASH1* zip-code elements as well as the *EAR1* zip-code element showed synergistic complex formation with She2p and She3p in a similar affinity range (Müller et al. 2011). The finding that She2p and She3p cooperate to bind zip-code RNAs with high affinity is in agreement with several previous studies. Two groups independently reported that the She3p C-terminus is required to detect interaction between She2p and zip-code RNAs in a yeast three-hybrid assay (Jambhekar et al. 2005; Olivier et al. 2005). In addition, synergistic binding by She2p and She3p explains the

supershift induced by Shep3p in an EMSA with She2p and *ASH1*-E3 RNA (Böhl et al. 2000).

The She2p:She3p co-complex did not bind to the HIV-1 TAR stem-loop in an EMSA, even at a She2p concentration of 5  $\mu$ M (Section 2.2.3). This observation suggests that the She2p:She3p co-complex has at least 100-fold higher affinity for zip-code elements than for non-localizing structured RNAs. Such high specificity for localizing transcript has not been reported before. Since many mRNPs contain multiple RNA-binding proteins, it might well be that other transport complexes also use cooperative binding to achieve high specificity for localizing RNAs. Interestingly, many RNA-binding proteins are composed of several domains that cooperate to recognize RNA. For example, two RRM domains form a positively charged cleft for the specific binding of single-stranded RNAs in the proteins Sex lethal, HuD, and Hrp1 (Handa et al. 1999; Wang and Tanaka Hall 2001; Perez-Canadillas 2006).

The protein-protein interaction between She2p and She3p was rather weak with a  $K_d$  of 1.6  $\mu$ M (Section 2.2.1). In the presence of *ASH1*-E3 RNA, a ternary complex with an apparent  $K_d$  of 25-50 nM was formed (Section 2.2.3). Thus, the RNA itself stabilizes the interaction between She2p and She3p. In agreement with this finding, UV cross-linking analysis revealed that She2p and She3p contact *ASH1*-E3 RNA directly in the ternary complex (Section 2.2.4).

#### *Detailed analyses of interactions in the ternary complex*

All three components of the specific ternary complex were subjected to mutational analyses and UV cross-linking. These experiments offered a detailed picture of the molecular interactions in the ternary complex. Successive deletion of the *ASH1*-E3 RNA revealed that at least one of the single-stranded regions at the termini and a double-stranded stem with the bulged nucleotides C and AA are the minimal requirements for efficient binding by She2p and She3p *in vitro* (Section 2.3.1). In contrast, the terminal loop is not required. These results are in agreement with previous mutational analyses of the *ASH1*-E3 stem-loop (Chartrand et al. 1999; Gonzalez et al. 1999; Jambhekar et al. 2005; Olivier et al.

2005). However, an additional stem (nucleotides 1758-1771 and 1822-1834) included in the construct *ASH1-E3-77* (Figure S1) seems to be important for mRNA localization *in vivo*, whereas it is dispensable for binding by She2p and She3p *in vitro* (Chartrand et al. 1999; Gonzalez et al. 1999).

UV cross-linking combined with mass-spectrometric analyses unambiguously identified two sites in the *ASH1-E3* RNA that are in contact with She2p in the ternary complex (Section 2.2.4). Strikingly, these sites overlap with a conserved sequence motif implicated in zip-code recognition (Olivier et al. 2005). The UV cross-linking analysis assigns distinct regions of She2p (i.e. the basic helical hairpin motif and helix C) to interact with the bipartite motif (Section 2.2.4). Many other potential sites of contact with She2p and She3p were spread around this RNA sequence motif. For each cross-linked peptide, at least one of the potential interaction sites of the RNA overlaps with the minimal *ASH1-E3* element described above.

Previous studies implicated three regions of She2p in RNA binding: the basic helical hairpin motif, the protruding helix E, and the C-terminal six amino acids (Niessing et al. 2004; Müller 2009). Of the six regions that cross-linked to *ASH1-E3* RNA, two overlap with the basic helical hairpin motif, one with helix E, and one borders on the C-terminal six residues (Figure 2.6 B and Figure 3.1). The other two regions comprise helix C in the vicinity of the basic helical hairpin motif and the very N-terminus of She2p. Thus, the cross-linking analysis confirms and extends the previously determined RNA-binding motif of She2p.

Mutational analyses of She2p showed that the helix E region has a key function in the assembly of ternary complexes (Table 2.2). On one hand helix E is involved in zip-code RNA binding, on the other hand it provides the main interaction site for She3p (Figure 3.1). In addition, amino acids 195-199 that form a loop supporting helix E (Figure 2.10) are crucial for She3p binding. Deletion of helix E completely disrupted ternary complex formation with She3p and RNA. In contrast, deletion of the C-terminal six amino acids of She2p predominantly affected RNA binding but only slightly the She3p interaction (Table 2.2).

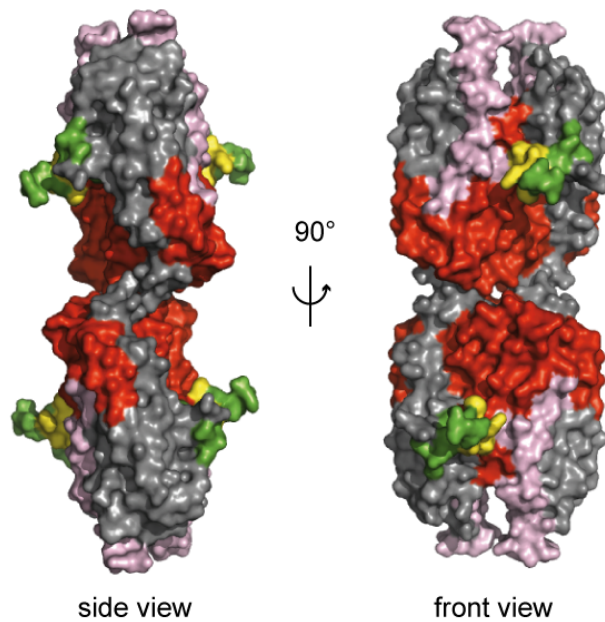


**Figure 3.1: Surface features of the She2p tetramer involved in RNA and She3p interaction.** Model of the She2p tetramer in side and front view (Müller et al. 2009). Regions exclusively involved in RNA-binding are shown in red. This includes the basic helical hairpin motif (aa 36-63) (Niessing et al. 2004) and peptides that UV cross-linked to RNA (aa 95-123, 164-173, and 223-237, Figure 2.6). Peptides from the UV cross-linking analysis that overlap with the basic helical hairpin motif are colored in light pink (aa 27-35 and 64-94, Figure 2.6). Regions that mediate interaction with She3p are shown in green (aa 180-183 and 195-199, Table 2.2). Features implicated in RNA as well as She3p binding are indicated in yellow (aa 174-179). Note that only parts of the colored regions may actually contribute to binding.

Previous studies showed that the She3p C-terminus mediates the interaction with She2p (Böhl et al. 2000; Long et al. 2000). Mutational analyses identified two She2p interaction sites in the She3p C-terminus: amino acids 334-353 and 364/367 (Figure 3.2). Especially, leucine 364 and valine 367 were crucial for She2p binding since their mutation completely abolished the interaction (Table 2.1). UV cross-linking identified two regions in the C-terminus of She3p (amino acids 334-340 and 383-405) that bind directly to *ASH1*-E3 RNA in the ternary complex (Figure 3.2). EMSAs revealed that the C-terminus of She3p is sufficient to mediate synergistic RNA binding with She2p (Table 2.1). This observation is consistent with the previous finding that the She3p C-terminus is required for efficient interaction between She2p and zip-code RNAs in yeast three-hybrid screens (Jambhekar et al. 2005; Olivier et al. 2005). Residues 334-353 were involved in binding to *ASH1*-E3 RNA as well as She2p and their deletion strongly impaired synergistic RNA binding (Table 2.1). Similar to helix E of She2p, this region represents an important interaction site for the assembly of the ternary complex.

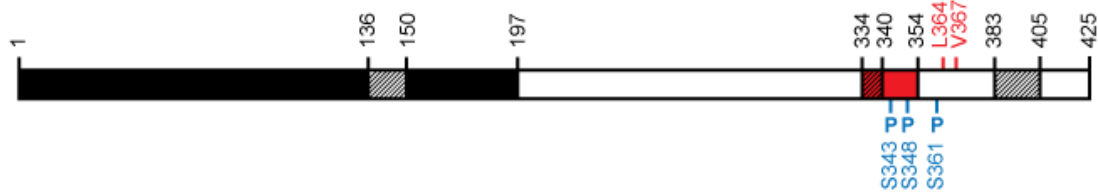


**Figure 3.2: Schematic representation of She3p.** The N-terminus (black) interacts with Myo4p, whereas the C-terminus (white) mediates binding to She2p and RNA (Böhl et al. 2000). Sites that were UV cross-linked to RNA are hatched. Regions and residues involved in synergistic RNA binding with She2p are indicated in red. Phosphorylation sites with an effect on *ASH1* mRNA localization are shown in blue (Landers et al. 2009). Numbers indicate amino acid positions.

Unexpectedly, one region in the N-terminus of She3p (amino acids 136-150) also cross-linked to *ASH1*-E3 RNA (Figure 3.2) and an N-terminal fragment showed weak affinity for *ASH1*-E3 RNA (Table 2.1). Since the C-terminus is sufficient to mediate synergistic RNA-binding with She2p, this interaction does not seem to make an important contribution to ternary complex formation.

A total of 12 mutations in She2p and She3p were investigated (Table 2.1 and Table 2.2). Seven of them showed impaired ternary complex formation and four of these also had a defect in both binary interactions, RNA and protein binding. It seems that both interactions are spatially intertwined to achieve synergistic binding.

#### *Disruption of synergistic binding by She2p and She3p impairs localization in vivo*

Upon deletion of helix E or the C-terminus, She2p fails to co-immunoprecipitate She3p from yeast cells (Müller 2009; Müller et al. 2011). These results suggest that the *in vitro* assays used in this thesis adequately recapitulate the interactions in the cell. Furthermore, *ASH1* mRNA and She2p delocalize *in vivo* when helix E of She2p is deleted (Müller 2009; Müller et al. 2011) confirming the crucial role of the helix E in the ternary complex assembly. Deletion of the C-terminus also causes She2p delocalization *in vivo* (Müller 2009; Müller et al. 2011). Thus, slightly reduced synergistic RNA-binding *in vitro* is already sufficient to completely disrupt She2p localization *in vivo*.

*Specific RNA recognition by She2p and She3p takes place in the cytoplasm*

In this study, the co-complex of She2p and She3p was identified to mediate specific recognition and incorporation of zip-code containing mRNAs into transport complexes. Whereas She2p shuttles between the nucleus and the cytoplasm (Böhl et al. 2000; Kruse et al. 2002; Du et al. 2008; Shen et al. 2009), nuclear localization of She3p has not been described so far. Prof. Ralf-Peter Jansen showed by immunofluorescence microscopy that She3p does not accumulate in the nucleus of a yeast strain deficient for nuclear export (Müller et al. 2011). Andreas Mayer from Prof. Patrick Cramer's laboratory demonstrated by chromatin immunoprecipitation that co-transcriptional recruitment of She2p is not significantly affected in a  $\Delta she3$  yeast strain (Müller et al. 2011). These observations strongly argue against a role of She3p in the nucleus. The previous finding that She3p is a tightly associated subunit of the cytoplasmic motor Myo4p supports this notion (Heuck et al. 2007; Hodges et al. 2008). In summary, these experiments suggest that specific recognition of localizing mRNAs by the She2p:She3p co-complex is restricted to the cytoplasm.

Experiments in *Drosophila* embryos and oligodendrocytes showed that several mRNAs are efficiently localized upon injection into the cytoplasm (Ainger et al. 1993; Ferrandon et al. 1994; Bullock and Ish-Horowicz 2001; Wilkie and Davis 2001; MacDougall et al. 2003). These results demonstrate that localization of mRNAs can occur without nuclear history. Thus, specific mRNA recognition and transport-complex assembly in the cytoplasm seems to be a conserved theme in different organisms and cell types.

*Specificity of mRNA recognition in the nucleus*

It has been shown that nuclear mRNP assembly is crucial for translational control and efficient transport of *ASH1* mRNA (Du et al. 2008; Shen et al. 2009; Shen et al. 2010). Since She3p does not enter the cytoplasm and She2p alone has only weak specificity for zip-code RNAs (Müller 2009; Müller et al. 2011), it remains unclear how specific RNA recognition in the nucleus might be achieved.

One possibility would be that another cofactor contributes to RNA recognition in the nucleus. Puf6p is unlikely to fulfill this function since it has only modest specificity for zip-code RNAs and does not interact with She2p directly (Müller et al. 2011). Other nuclear RNA-binding proteins with a role in mRNA localization are Khd1p and Loc1p. Whether these proteins contribute to specific RNA recognition in the nucleus or if other, yet unknown proteins are involved, has to be clarified by future studies.

Alternatively, the modest specificity of these RNA-binding proteins might be sufficient for the assembly of nuclear mRNPs. The formation of translationally silenced complexes in the nucleus appears to be a prerequisite for efficient cytoplasmic mRNA transport since it likely prevents the ribosome from stripping off transport complexes from the mRNA during premature translation (Irie et al. 2002; Gu et al. 2004). In the cytoplasm, assembly of the SHE transport complex provides an independent step to assure specific transport of zip-code containing transcripts.

#### *Phosphorylation of She3p might regulate its function*

A recent study reported phosphorylation of She3p at several sites (Landers et al. 2009). The phospho-mimicking mutants She3p (S348E) and She3p (S343E S361E) impaired *ASH1* mRNA localization *in vivo*. Interestingly, all three sites are located in regions of She3p that are crucial for synergistic RNA-binding with She2p (Figure 3.2). When the phospho-mimicking mutants were characterized by EMSA, only She3p (S348E) showed a slightly impaired synergism (Table 2.1). Nevertheless, such a mild defect was sufficient to disrupt localization of She2p ( $\Delta C$ ) *in vivo* (Müller 2009; Müller et al. 2011). Simultaneous phosphorylation of all three sites in She3p (S343, S348, and S361) might even have a stronger effect. Therefore, phosphorylation of She3p might provide a mechanism to disassemble SHE complexes after successful localization. It is tempting to speculate that such phosphorylation happens at the plasma membrane of the bud tip, as it has been described for the translational repressors Khd1p and Puf6p (Paquin et al. 2007; Deng et al. 2008). However, it

cannot be ruled out that phosphorylation of She3p affects a different step of *ASH1*-mRNA localization.

#### *Model of ASH1 mRNA recognition and mRNP assembly*

On the basis of this work, a revised model of *ASH1*-mRNA transport can be proposed (Figure 3.3). In the nucleus, She2p is associated with the RNA polymerase II elongation complex and binds to nascent mRNAs (Figure 3.3 A) (Shen et al. 2010). In addition, Puf6p binds to PUF-consensus sites in the *ASH1* 3' UTR, but it does not interact with She2p directly (Figure 3.3 B) (Gu et al. 2004; Müller et al. 2011). Both proteins show modest specificity for zip-code RNAs (Müller et al. 2011).

In the cytoplasm, She3p and Myo4p form a constitutive co-complex with nanomolar affinity (Heuck et al. 2007; Hodges et al. 2008). In the absence of RNA, She3p interacts only weakly with She2p (Figure 3.3 C). The co-complex has a Kd of 1.6  $\mu$ M and shows fast dissociation.

When zip-code RNA and She2p are exported from the nucleus and meet the She3p:Myo4p co-complex in the cytoplasm, a stable complex with an apparent Kd of 25-50 nM is formed (Figure 3.3 D). This mature complex has more than 100-fold higher affinity for zip-code RNAs compared to non-localizing stem-loops. She2p and She3p act synergistically to mediate this highly specific RNA binding. Both proteins are in direct contact with the RNA and with each other in the ternary complex.

The affinity of the She2p:She3p interaction is at least 30-fold increased in the presence of zip-code RNA. Thus, the RNA itself triggers the assembly of mature mRNPs. Since She3p is tightly associated with Myo4p (Heuck et al. 2007; Hodges et al. 2008), this interaction also incorporates the motor into the mRNP. In summary, cytoplasmic assembly of the SHE-core complex directly couples specific recognition of zip-code containing mRNAs to transport via the motor Myo4p. This process likely represents a quality control step to ensure that only target mRNAs are transported.

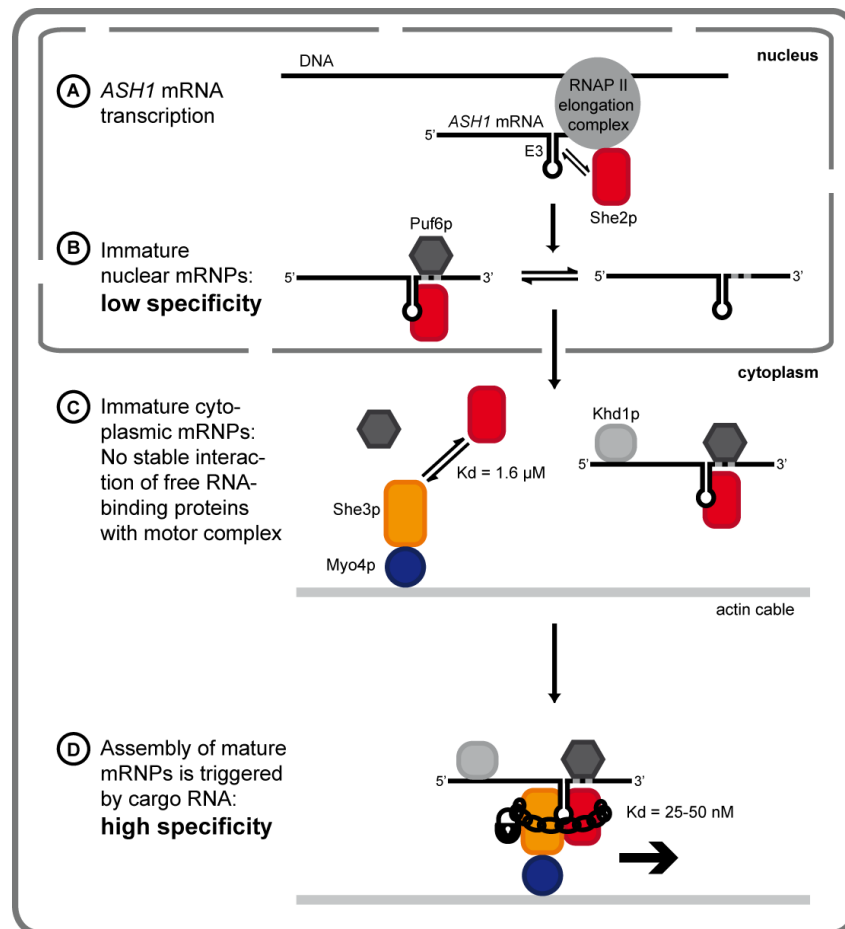


**Figure 3.3: Model of *ASH1*-mRNA recognition and mRNP assembly.** **A**) In the nucleus, She2p (red) binds co-transcriptionally to zip-code elements of the *ASH1* mRNA. **B**) The translational repressor Puf6p (dark grey) binds to PUF-consensus sites (grey patches) in the 3' UTR of *ASH1* mRNA (Gu et al. 2004). Note that Puf6p does not bind to She2p directly (Müller et al. 2011). She2p and Puf6p do not show highly specific binding to zip-code RNAs (Müller 2009; Müller et al. 2011). **C**) In the cytoplasm, She3p (orange) and Myo4p (blue) form a constitutive co-complex (Heuck et al. 2007; Hodges et al. 2008). She2p only weakly interacts with She3p in the absence of RNA ( $K_d$  of 1.6  $\mu$ M). The translational repressor Khd1p (light grey) associates with the E1 element of the *ASH1* mRNA (Irie et al. 2002; Paquin et al. 2007). **D**) After nuclear export, the co-complex of *ASH1* mRNA and She2p binds to She3p with an apparent  $K_d$  in the range of 25-50 nM. She2p and She3p interact directly with the RNA and with each other to synergistically recognize zip-code RNAs with high specificity. At the same time, She3p-bound Myo4p is incorporated into the complex. Thus, this final step of assembly couples specific mRNA recognition to directional transport by Myo4p. This figure has been adapted from Müller et al. 2011 .

### *Implications for mRNA localization in other organisms*

In the fungal pathogen *C. albicans* a set of 40 mRNAs is localized in a She3p-dependent manner (Elson et al. 2009). Since no clear homolog of She2p is present in the *C. albicans* genome, the question arises how mRNA recognition in *C. albicans* is achieved. As shown in this thesis, *S. cerevisiae* She3p binds to zip-code RNA with low specificity and simultaneously interacts with She2p. The C-terminus of She3p mediates both interactions. A sequence alignment of She3p

shows that the C-terminus varies considerably between species with and without a She2p homolog in their genome (Figure S3). This raises the possibility that in She2p-lacking species the C-terminus of She3p might either have evolved to bind zip-code RNAs with higher specificity or to interact with another RNA-binding protein.

A complex containing the RNA-binding protein Egl, the adapter protein BicD, and the motor protein dynein mediates the localization of pair-rule transcripts in *Drosophila* embryos. Egl shares some general similarities with She2p. It has no canonical RNA-binding motif and shows only three to six-fold higher affinity for functional zip-code elements, than for mutated, non-functional RNA constructs (Dienstbier et al. 2009). Nevertheless, transcripts from pair-rule genes and *wingless* mRNA injected into the cytoplasm of *Drosophila* embryos localize apically, whereas control transcripts diffuse away from the site of injection (Bullock and Ish-Horowicz 2001; Wilkie and Davis 2001). Thus, synergistic RNA binding, as described for She2p and She3p, might also be required for highly specific RNA recognition in *Drosophila*. Interestingly, Egl only showed selectivity for functional RNA zip-code elements when the adapter protein BicD was co-expressed (Dienstbier et al. 2009). Unlike She3p, BicD does not bind the RNA directly but rather seems to enhance folding of Egl. Other co-factors might further enhance the RNA-binding specificity of the Egl:BicD co-complex.

In *Drosophila*, the RNA-binding protein Staufen is involved in the localization of *bicoid* mRNA. A single double-stranded RNA-binding domain of Staufen binds indiscriminately to double-stranded RNA *in vitro* (St Johnston et al. 1992). In contrast, RNA injection experiments into embryos demonstrated that Staufen specifically associates with its target RNA (the *bicoid* 3' UTR) but not with control RNAs *in vivo* (Ferrandon et al. 1994). The interaction with the *bicoid* 3' UTR is also required for the efficient localization of Staufen-containing RNPs. These observations are remarkably similar to the situation in yeast, where the specific incorporation of *ASH1* mRNA into the mRNP triggers its localization. A similar mechanism might be in place to ensure efficient mRNA transport also in other eukaryotes.

### 3.2 Structural studies on the SHE-core complex

To date, crystal structures of She2p and the globular tail domain of Myo4p are available (Niessing et al. 2004; Heuck et al. 2010). Since structure determination of SHE sub-complexes failed so far, a co-structure that explains cargo recognition or motor activation is missing (Heuck 2009; Müller 2009).

In this thesis, a cryo-EM based approach to visualize RNA:protein complexes that are otherwise too small for cryo-EM was developed. To this end, the *ASH1-E3* zip-code element was fused to rRNA from the *M. smegmatis* ribosome (Section 2.3.3). A single-particle cryo-EM reconstruction of this “zip-code ribosome” in complex with She2p was obtained (Section 2.3.5). However, intrinsic flexibility of the *ASH1-E3* RNA or its flexible linkage to the ribosome prevented high resolution and complicated the interpretation of the reconstruction. For more rigid RNAs, fusion to the ribosome might provide a fast and standardized way to obtain a three-dimensional cryo-EM structure. Similar approaches have been applied successfully to visualize tRNA and a group II intron by cryo-EM (Spahn et al. 1999; Slagter-Jager et al. 2006).

The reconstituted SHE-core complex has a size of about 500 kDa and is therefore amenable to EM. However, negative-stained electron micrographs of the SHE-core complex only showed small and inhomogeneous particles (Section 2.4.4). In this thesis, expression and purification of full-length Myo4p was established. Rotary shadowing EM of full-length Myo4p has already been performed (Dunn et al. 2007; Kremntsova et al. 2011). Similar analyses of reconstituted SHE complexes containing full-length Myo4p might help to understand the architecture of these assemblies. Moreover, higher-order assembly of SHE complexes on *ASH1* mRNA could be investigated.

Low quality crystals of She2p and She3p in the presence and absence of *ASH1-E3* RNA were obtained (Section 2.3.2). For X-ray structure determination, these crystals need further improvement. The biochemical studies presented in this thesis have yielded detailed insights on the molecular interactions and the assembly of the SHE complex (Section 3.1 and 3.3). For instance, a minimal

binding region in the *ASH1*-E3 zip-code element and C-terminal constructs of She3p that still interact with RNA and She2p have been identified. Moreover, interaction sites in the SHE complex have been mapped and the sub-unit stoichiometries have been determined. These analyses provide valuable information to further optimize protein and RNA constructs for crystallization. Since full-length She3p contains extended coiled-coils as well as unstructured regions (Section 2.1.1), it is unlikely to promote crystallization. However, the She3p C-terminus might adopt a rigid conformation in complex with RNA and She2p. Thus, minimal She3p constructs that still bind to RNA and She2p might enhance crystallization of the RNA:She2p:She3p complex.

The components of the SHE complex are partially conserved among different yeast species (Figure S3). Therefore, homologs especially from thermophilic yeast strains should be considered for structural studies in future. *ASH1* mRNA from *C. albicans* was shown to be transported in *S. cerevisiae* (Münchow et al. 2002). Thus, even a combination of SHE components from different yeast species might be used to assemble a complex that allows for structure determination by X-ray crystallography.

### 3.3 SHE-core complex assembly induces motor multimerization

Unlike other type V myosins, Myo4p is monomeric and does not support processive movement on its own (Dunn et al. 2007; Heuck et al. 2007; Hodges et al. 2008). However, multiple Myo4p molecules seem to be required for sustained transport *in vivo* (Chung and Takizawa 2010). Here, I investigated how transport complex assembly affects oligomerization and activity of Myo4p.

#### *A She3p dimer and a Myo4p monomer form a constitutive co-complex*

The oligomeric state of She3p has not been addressed so far. Chemical cross-linking showed that She3p oligomerizes via its N-terminus (Section 2.4.1). The size of the cross-linking product indicated formation of a She3p dimer. Secondary structure predictions suggest that coiled-coil regions in the N-terminus of She3p might mediate dimerization (Figure S2). Similarly, many organelle adapter proteins of type V myosins contain coiled coils and dimerize (Li and Nebenfuhr 2008).

In the cytoplasm, Myo4p forms a constitutive co-complex with She3p (Heuck et al. 2007; Hodges et al. 2008). Whereas one study suggested that this co-complex contains only one myosin (Hodges et al. 2008), another study showed that artificial dimerization of Myo4p stabilizes its interaction with She3p indicating that Myo4p dimerization might occur in the co-complex (Heuck et al. 2007). In agreement with Hodges et al. 2008, the size and stoichiometry analyses presented in this thesis clearly showed that one She3p dimer assembles with one Myo4p monomer to form a single-headed motor complex (Section 2.4.2 and Figure 3.4 B). An important consequence of this finding is that the She3p:Myo4p co-complex is not able to support processive movement on its own. In agreement with this conclusion, previous actin gilding assays and *in vitro* single molecule studies demonstrated that the She3p:Myo4p co-complex is indeed non-processive (Dunn et al. 2007; Hodges et al. 2008).

*A She2p tetramer binds two zip-code elements*

She2p forms tetrameric assemblies with two large, continuous RNA-binding surfaces on opposite sides (Figure 3.1) (Müller et al. 2009). Since different stoichiometric ratios for RNA:She2p co-complexes have been proposed for different zip-code elements (Niessing et al. 2004; Olivier et al. 2005), it remained unclear how many zip-code RNAs are bound per She2p tetramer. In this thesis, the molecular weight of She2p in complex with the *ASH1-E3* or the *IST2* zip-code RNA was determined by SLS (Section 2.4.3). For both RNAs, this analysis suggests binding of two zip-code elements to one She2p tetramer. This observation is consistent with the previously determined stoichiometric ratio of one *ASH1-E3* RNA per She2p dimer (Niessing et al. 2004). By binding two zip-code elements simultaneously, the She2p tetramer is able to incorporate two transcripts into one transport complex (Figure 3.4 A). Live-cell imaging indeed revealed co-transport of two different mRNAs in one particle (Lange et al. 2008).

*SHE-core complex assembly induces dimerization of Myo4p*

When the co-complex of *ASH1* mRNA and She2p reaches the cytoplasm, it interacts with the pre-assembled motor complex to form the mature transport complex. Analyses by EMSA, SEC, and SLS suggest that one RNA-bound She2p tetramer accommodates two motor complexes, each built up of a She3p dimer and a Myo4p monomer (Section 2.4.4). This SHE-core complex has a molecular weight of approximately 500 kDa. If full-length Myo4p and six light chains per neck are taken into account, the SHE complex, including two *ASH1-E3* zip-code elements of 77 nucleotides, has a molecular weight of approximately 880 kDa.

In summary, the She2p tetramer provides a scaffold for dimerization of Myo4p (Figure 3.4 C). This result is consistent with the previous finding that a single transport complex purified from yeast cells contains at least two Myo4p molecules (Chung and Takizawa 2010). Recently, rotary shadowing EM confirmed that two Myo4p molecules associate with one She2p tetramer (Krementsova et al. 2011). The consequences of cargo-mediated dimerization of Myo4p for its transport activity are discussed below (page 83).

*Efficient complex assembly requires oligomerization of She2p and She3p*

She3p binds with its C-terminus to the helix E region of She2p (Section 2.2.5-2.2.8). One SHE-core complex contains four molecules of She2p (one tetramer) and four molecules of She3p (two dimers). Therefore, it is likely that one She3p C-terminus binds per helix E region. In contrast to dimeric full-length She3p, the monomeric She3p C-terminus (residues 334-425) did not form a complex with She2p in SEC (Table 2.1). This result suggests that She3p dimerization might stabilize binding to She2p. However, it cannot be ruled out that the C-terminus of She3p lacks additional She2p binding sites required for full binding affinity.

The mutation L130Y interferes with She2p tetramerization via the upper surface region (Müller et al. 2009). *In vitro* pull-down (Table 2.2 and Figure S4) as well as co-immunoprecipitation from yeast cells (Müller et al. 2009) revealed that She2p (L130Y) binds less efficiently to She3p than wild-type She2p. Thus, the association of two She2p dimers into a tetramer seems to stabilize binding of She3p. The dimeric nature of She3p might explain this observation. One She3p dimer might be able to simultaneously bind to both She2p dimers in the tetramer (Figure 3.4 C). Since She3p interacts with the helix E region of She2p and with zip-code RNA, it is tempting to speculate that the She3p dimer closes like a latch over the extended RNA-binding surface of She2p.

*RNAs with multiple zip-code elements induce higher-order assembly of SHE-core complexes*

Several localizing transcripts, like *ASH1*, *WSC2*, *DNM1*, and *YLR434* mRNA contain two or more zip-code elements (Chartrand et al. 1999; Gonzalez et al. 1999; Jambhekar et al. 2005). In addition, the She2p tetramer binds two zip-code RNAs simultaneously. When SHE-core complexes were reconstituted with a fusion RNA containing two zip-code elements, large mRNPs with variable size were formed (Section 2.4.5). Thus, interaction of bivalent She2p with bi- or multivalent RNAs induces multimerization of transport complexes (Figure 3.4 D). This finding provides a molecular explanation for the assembly and co-transport of several different mRNAs in one mRNP (Lange et al. 2008). It is also

consistent with the observation that overexpression of *ASH1* mRNA leads to fewer, but larger particles in the cell (Bertrand et al. 1998; Lange et al. 2008).

The formation of higher-order mRNPs has also been described for *oskar* mRNA in *Drosophila* (Hachet and Ephrussi 2004; Chekulaeva et al. 2006; Besse et al. 2009). Polypyrimidine tract-binding protein and Bruno mediate *oskar* mRNA oligomerization and assembly into large mRNPs that are required for translational repression. Similarly, clustering of SHE complexes might also contribute to translational silencing of *ASH1* mRNA. Recently, the discovery that *oskar* mRNA itself dimerizes via base-pairing of a stem-loop in its 3' UTR added another level of complexity to mRNP assembly (Jambor et al. 2011). Such RNA-mediated dimerization has previously been reported for *bicoid* mRNA (Ferrandon et al. 1997; Wagner et al. 2001). Thus, mRNA dimerization might be a common mechanism involved in the assembly and coordinated transport of mRNAs. If localizing mRNAs from yeast also dimerize, remains to be shown.

#### *Complex assembly does not stimulate the ATPase activity of Myo4p*

Myosin V is a dimeric motor capable of processive movement (Trybus 2008). To prevent unnecessary energy consumption in the absence of cargo, the tail domain inhibits the ATPase activity of the motor domain (Section 1.1.8). Binding of the adapter protein melanophilin likely relieves auto-inhibition (Li et al. 2005). Auto-inhibition of Myo4p might not be required, since the She3p:Myo4p co-complex contains only a single Myo4p monomer, which is not processive (Dunn et al. 2007; Hodges et al. 2008).

Neither She3p nor the co-complex of She3p, She2p, and zip-code RNA stimulated the actin-activated ATPase activity of Myo4p (Section 2.4.6). She3p did also not induce stimulation in a previous study (Hodges et al. 2008). Moreover, residues involved in auto-inhibition of MyoVa are not conserved in Myo4p (Heuck et al. 2010). The available data argues against auto-inhibition of Myo4p. As a consequence, SHE-complex assembly does not strongly influence the actin-activated ATPase activity of Myo4p.

*Cargo-mediated Myo4p dimerization might induce processive transport*

Most myosin V motors form stable dimers that move processively along actin filaments (Section 1.1.7) (Trybus 2008). In contrast, Myo4p forms a single-headed, non-processive complex with She3p. As shown in this thesis, dimerization of Myo4p is mediated by the interaction with its cargo, i.e. the She2p tetramer bound to zip-code RNA. Such cargo-mediated dimerization has also been described for myosin VI motors. Similar to Myo4p, myosin VI is a monomer in isolation (Lister et al. 2004). Binding to the adapter proteins optineurin or Dab2 triggers dimerization of myosin VI and enables kinetic gating as well as processive transport to the minus-end of actin filaments (Phichith et al. 2009; Yu et al. 2009). Similarly, cargo-induced dimerization might induce processive movement of Myo4p. A previous study reported that a chimeric myosin with the motor domain of yeast Myo4p dimerized by the neck and rod of mouse Myo5a moved processively (Krementsova et al. 2006). Thus, the Myo4p motor domain has all kinetic and structural properties required for processivity. While this thesis was written, Trybus and colleagues showed that a complex of She2p, She3p, Myo4p, CaM, and myosin light chain indeed moves processively in a hand-over-hand fashion (Krementsova et al. 2011).

Most molecular motors for cargo transport form stable dimers via coiled-coils (Section 1.1.5-1.1.7). Dimerization is a prerequisite for kinetic gating of the two heads and processive movement of the motor. It is unclear if kinetic gating of Myo4p occurs in the SHE complex. Coordination of both Myo4p heads would require the transmission of strain via She3p and She2p. Alternatively, the two Myo4p copies in the SHE complex might interact directly due to the high local concentration.

Coordinated dimeric motors display only half the actin-activated ATPase rate per motor domain when compared to the same motor in a monomeric state, since intramolecular strain between the two heads inhibits the ATPase cycle of one head at any given time. This effect on the ATPase rate has been observed for cargo-induced dimerization of monomeric myosin VI (Phichith et al. 2009). In contrast, only a modest reduction in the ATPase activity of Myo4p was observed

in the presence of stoichiometric amounts of She3p, She2p and zip-code RNA (Section 2.4.6). This observation argues against kinetic gating of Myo4p in the SHE complex. Recently, it has been suggested that kinetic gating might not be essential for processive movement, if the motor heads have a high duty ratio (i.e. the motor is strongly bound to actin most of the time of its catalytic cycle) (Krementsova et al. 2011). Furthermore, coupling of multiple motors to one cargo might counterbalance the lack of kinetic gating. This notion is supported by a recent study that investigated movement of myosin VI on an actin cytoskeleton derived from fish keratinocytes (Sivaramakrishnan and Spudich 2009). Four myosin VI monomers (non-processive, no gating) coupled to a nanosphere supported continuous transport in a similar manner as two artificially dimerized myosin VI motors (processive, gated).

*mRNA-mediated Myo4p multimerization might enhance sustained transport in vivo*

In the presence of bi- or multivalent RNAs, SHE complexes cluster into large particles (Section 2.4.5). Several previous findings indicate that such mRNA-mediated multimerization of Myo4p might enhance sustained transport. For instance, Myo4p-containing particles purified from yeast cells only supported continuous movement in an *in vitro* single-molecule assay, when they contained at least three Myo4p molecules (Dunn et al. 2007). In agreement with this observation, coupling of multiple Myo4p motors to one quantum dot induced sustained movement *in vitro* (Hodges et al. 2008).

The efficiency of *ASH1* mRNA localization *in vivo* increases with the number of zip-code elements per transcript (Chartrand et al. 2002). However, RNAs containing only a single zip-code element still localize to the bud of a yeast cell, albeit with low efficiency (Long et al. 1997; Chartrand et al. 1999; Gonzalez et al. 1999; Chartrand et al. 2002). Such a monovalent mRNA recruits only two Myo4p molecules (Section 2.4.4). This might be sufficient for mRNA transport to the bud if a highly processive Myo4p dimer is formed within the SHE complex. Alternatively, endogenous multivalent transcripts might induce formation of

higher-order mRNPs with multiple Myo4p motors and the monovalent RNA under investigation would be able to hitchhike on these particles. Takizawa and colleagues investigated the effect of multiple Myo4p motors *in vivo* by tethering a She3p fusion protein directly to stem-loop containing RNAs (Chung and Takizawa 2010). When the number of Myo4p molecules per RNA was increased, transport was more efficient. However, even eight artificially tethered motors did not yet approach the efficiency of wild-type *ASH1*-mRNA transport. Since She2p was not present in the artificial system, She2p-mediated Myo4p dimerization was likely missing for full transport activity.

Single-molecule experiments with reconstituted complexes will be necessary to clarify if dimerization of Myo4p in the SHE complex is sufficient for sustained movement or if higher-order assembly of SHE complexes via multivalent mRNAs is required. Since the incorporation of multiple motors prevents premature dissociation from actin filaments, it seems likely that such large particles at least enhance mRNA transport. In addition, simultaneous transport of several mRNAs by one mRNP might provide a cost-efficient way for the cell to localize a set of functionally related transcripts in a coordinated fashion.

#### *Model of SHE-core complex assembly*

In summary, the following model emerges for assembly and regulation of the SHE complex. In the nucleus, She2p interacts with its two RNA-binding sites with two zip-code elements of localizing mRNAs (Figure 3.4 A). The cytoplasmic motor complex is built up of a She3p dimer and a Myo4p monomer (Figure 3.4 B). This single-headed complex is not able to mediate sustained transport on its own (Dunn et al. 2007; Hodges et al. 2008).

When the mRNA:She2p complex enters the cytoplasm, it recruits two She3p:Myo4p motor complexes (Figure 3.4 C). It is unclear if both Myo4p copies interact directly in the SHE complex. The ATPase activity of the two heads does not seem to be coordinated by kinetic gating. However, She2p-induced dimerization of Myo4p enables processive movement of Myo4p *in vitro* (Krementsova et al. 2011). The interaction between She2p and She3p is

substantially stabilized in the presence of zip-code RNA (Section 3.1). Intriguingly, the same interaction mediates Myo4p dimerization. Thus, activation of Myo4p transport is directly coupled to the specific incorporation of localizing mRNAs.

In the presence of transcripts with multiple zip-code elements, high-order assembly of SHE complexes occurs (Figure 3.4 D). This step may lead to large mRNPs of variable size containing different mRNAs and multiple Myo4p dimers. Most likely, such higher-order assembly enhances the efficiency of mRNA transport and helps to coordinate localization of different transcripts.

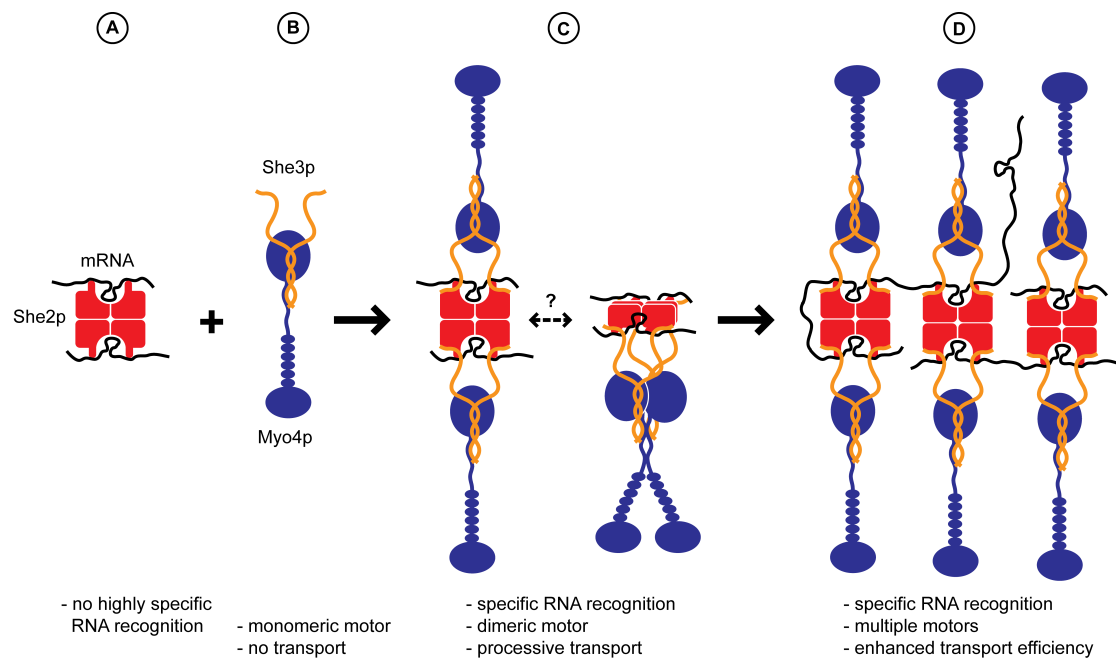


**Figure 3.4: Model of stepwise SHE-core complex assembly.** **A)** In the nucleus, one She2p tetramer (red) binds two zip-code RNAs (black). Two extended regions between the helices E on each side of the tetramer are crucial for RNA-binding. In the presence of transcripts with two or more zip-code elements, higher-order assembly, as shown in D, might occur already at this stage. **B)** In the cytoplasm, one Myo4p monomer (blue) forms a constitutive co-complex with one She3p dimer (orange). The N-terminal coiled-coil of She3p mediates dimerization as well as interaction with the Myo4p C-terminus. The single-headed motor complex is unable to promote successive transport (Dunn et al. 2007; Hodges et al. 2008). **C)** After nuclear export of the RNA:She2p co-complex, it assembles with two motor complexes, forming the SHE-core complex. The C-terminus of She3p binds directly to zip-code RNA and the helix E regions of She2p. This interaction ensures highly specific RNA recognition and incorporates two Myo4p copies into one mRNA. She2p-mediated dimerization of Myo4p likely enables processive transport of the SHE-core complex (Krementsova et al. 2011). Whether the two Myo4p copies are located on distant sides of the tetramer (left cartoon) or if they are in contact (right cartoon) is not known. **D)** Transcripts with two or more zip-code elements induce multimerization of SHE-core complexes. Since the She2p tetramer has two RNA-binding sites, several RNAs can be incorporated and large mRNPs of variable size can be formed. Such higher-order mRNPs contain multiple Myo4p motors that most likely enhance sustained transport *in vitro* and *in vivo* (Dunn et al. 2007; Hodges et al. 2008; Chung and Takizawa 2010).

## 4 MATERIALS & METHODS

### 4.1 Consumables and chemicals

All common chemicals were ordered from Roth, Merck, and Sigma-Aldrich, unless stated otherwise. Enzymes and nucleotides for molecular biology as well as loading dyes and molecular weight standards for gel electrophoresis were purchased from Fermentas, New England Biolabs, and Invitrogen. Components for bacterial growth media were obtained from Becton Dickinson. Insect cell media were ordered from Invitrogen and Thermo Scientific. Liquid chromatography was performed with equipment and columns from GE Healthcare.  $\gamma$ -<sup>32</sup>P-ATP for radioactive labeling of RNAs was obtained from Hartmann Analytic. Crystallization screens and tools were purchased from Hampton Research and Qiagen. DNA and RNA oligonucleotides were ordered from Thermo Scientific.

### 4.2 Oligonucleotides

#### 4.2.1 DNA oligonucleotides for cloning

Name	Sequence (5'→3')
01	GCGAGTCTGAATAGGGCGTATCCAC
06	GCTCGGTACCTACGTACTCGAGTCG
011	AAACGATCGATCTTCATCTCCATCTCCCTC
012	AAACGATCGATCTTGATCTCATCTTGCCAC
013	AAACGATCGAGAGAATTGATACATGGATAACTGAATC
014	AAACGATCGAGAGAAATGTACAATTGTTTCGTG
036	AAACGATCGTTGCGAATAGAGACATTCTATCG
037	TTTCGATCGTTGCTTTGAGATTTTGTTCTTAG
044	AAACGATCGTATGTTAAAATACGCGAAGAAGTG
045	TTTCGATCGTATTTTGATTATTAGTTAAGTTGGGTATAC
048	AAACCGGGATGAGCAAAGACAAAGATATCAAAG
049	TTTGAATTCCTAGTGATGGTGATGGTGATGGGATTGGGCCCCGTG
083	GGATCCATGGGTTCTATTCCAAAATCTGCATC
096	AAACGGCCGAGAGAATTGATACATGGATAACTGAATC
0101	AAACCGGCCAAGAGAAATGTACAATTGTTTCGTG
0106	GGCCTGAATCTCTTTCAACTAATAAGAGACATTATCAGGCCGC
0107	GGCCTGATAATGTCTCTTATTAGTTGAAAGAGATTCA
0108	GGCCGATAACTGAATCTCTTTCAACTAATAAGAGACATTATCGGCCGC

Name	Sequence (5'→3')
0109	GGCCGATAATGTCTCTTATTAGTTGAAAGAGATTCAGTTATC
0120	AAAGGATCCATGAGAAACGATGAGAAGATTAGTAATAAAG
0122	AAAGGATCCATGGGTAATAGCAGTAACAATAAAAAG
0126	AAACGGCCGATGGATAACTGAATCTCTTTCAAC
0127	AAACCGCGCCAATTGTTTCGTGATAATGTCTC
0134	AAACGGCCGGTCTCTCTGGTTAGACCAGATCTGAGCCTGGGAGCTCTCTGGCTAACTAGGGA ACCTGGCCGCGGAAA
0135	TTTCCGCGCCAGGTTCCCTAGTTAGCCAGAGAGCTCCCAGGCTCAGATCTGGTCTAACCAGA GAGACCCGCGCGTTT
0151	CTATACTGCGGAGCCTTTGCTGTC
0152	GACAGCAAAGGCTCCGCAGTATAG
0153	GTAACAATAAAAGAAGAGAATTCTATACTGCG
0154	CGCAGTATAGAATTCTCTTCTTTTATTGTTAC
0155	CCAAAATCTGCAGAGCCGGTTTTGCCTGG
0156	CCAGGCAAAACCGGCTCTGCAGATTTTGG
0157	CATTAAATGCGCAGATGCGGCCGCAACGAATATCGG
0158	CCGATATTCGTTGCGGCCGCATCTGCGCATTTAATG
0159	GAATATCGGAGAAGCTGCTAATATCTTCTTGC
0160	GCAAGAAGATATTAGCAGCTTCTCCGATATTC
0162	CATCCCCGGTTGCGCCTGGTGCTAAAAGAACTGC
0163	GCAGTTC'TTTTAGCACCAGGCGCAACCGGGATG
0164	GTAATAGCAGTAACAATAAAGAAAGAAGTTTCTATACTG
0165	CAGTATAGAACTTCTTCTTATTGTTACTGCTATTAC
0171	GAAACTGATAATATCGCCGCGCAGGAGATTC'TTC
0172	GAAGAATCTCCTGCGCGCGATATTATCAGTTTC
0173	CTGATAATATCTTCTTGGCGGGCTCTTCTGTCAACTC
0174	GAGTTGACAGGAAGAGCCGCGCAAGAAGATATTATCAG
0180	AAACGGCCCGCTAACATAATTAGAGAATTGATACATGGATAACTGAATC
0181	GATTTCAGTTATCCATGTATCAATTCTCTATATGTTAGAGAAATGTACAATTGTTTCGTG
0182	CACGAAACAATTGTACATTTCTCTAACATATAGAGAATTGATACATGGATAACTGAATC
0183	AAACCGCGCCACCTTCTATAGAGAAATGTACAATTGTTTCGTG
0190	AAACGGCCGGATGCTGGAGTGAAGAATGTCACGAACAATTC'AAGACAACCGAATCCTCTTCC TCTTCATCTGGCCGCGGAAA
0191	TTTCCGCGCCAGATGAAGAGGAAGAGGATTCGGTTGTCTTAGAATTGTTTCGTGACATTCTTC ACTCCAGCATCCGGCCGTTT
0198	CTGGTCTAACCAGAGAGACCATATGTTAGAGAAATGTACAATTGTTTCGTG
0199	CACGAAACAATTGTACATTTCTCTAACATATGGTCTCTCTGGTTAGACCAG
0200	TTTCCGCGGCCACCTTCTATGGTTCCTAGTTAGCCAGAG
0211	AAAGGATCCATGCCACTGTGTGAG
0212	AAATCTAGATTAGACTTTAATTTTAGCAAGG
0213	AAACCCGGGATGCCACTGTGTGAG
0214	AAACCATGGTTAGACTTTAATTTTAGCAAGG
AH-02 <sup>(1)</sup>	AAAGGATCCAAGCAAAGGCAAGAGTACG
AH-04 <sup>(1)</sup>	AAACTCGAGTTATTTTCTGTCTAATTTTATAAT
AH-06 <sup>(1)</sup>	AAAGGATCCATGTCGGACCAGGATAATACC
MM-S2-1 <sup>(2)</sup>	TTACTCGAGTCAGTTTTTCAATTTACCAAAATTG
MM-S2-22 <sup>(2)</sup>	TAACTCGAGTTTGTTCATGCCATTTAGTAGCGAC
MM-S2-27 <sup>(2)</sup>	AAAGGATCCATGGATATCAAAGTCACTCCTGG
MM-SC-5 <sup>(2)</sup>	AAACGGCCGGAGACAGTAGAGAATTGATAC
MM-SC-6 <sup>(2)</sup>	AAACCGCGGTTTTTATTTGTAGTTTATTTAGC

<sup>(1)</sup> Heuck 2009

<sup>(2)</sup> Müller 2009

4.2.2 DNA oligonucleotides to generate templates for *in vitro* transcription

Name	RNA	Sequence (5'→3')	Template produced by
Tx-10 <sup>(1)</sup>	ASH1-E3-118	<b>TAATACGACTCACTATAGGG</b> GACAGTAGAGAATTGATACATGG	PCR
Tx-11 <sup>(1)</sup>		TTTTTATTTGTAGTTTATTTAGC	
0204	ASH1-E3-77	<b>TAATACGACTCACTATAGGG</b> GAGAGAATTGATACATGGATAACTG	PCR
0205		AGAGAAATGTACAATTGTTTCG	
0137	ASH1-E3-51	<b>TAATACGACTCACTATAGGG</b> GAGATGGATAACTGAATCTCTTTCAACTAATAAGAGACATTATCACGAAACAAT	Hybridization
0138		ATTGTTTCGTGATAATGTCTCTTATTAGTTGAAAGAGATTCAGTTATCCATCT <b>CCCTATAGTGAGTCGTATTA</b>	
0139	ASH1-E3-51 (Δ1786-1802)	<b>TAATACGACTCACTATAGGG</b> GAGATGGATAACTGAATCGAAAGACATTATCACGAAACAAT	Hybridization
0140		ATTGTTTCGTGATAATGTCTTTTCGATTTCAGTTATCCATCT <b>CCCTATAGTGAGTCGTATTA</b>	
0141	ASH1-E3-51 (Δ1782-1804)	<b>TAATACGACTCACTATAGGG</b> GAGATGGATAACTGGAAACAATTATCACGAAACAAT	Hybridization
0142		ATTGTTTCGTGATAATGTTTCCAGTTATCCATCT <b>CCCTATAGTGAGTCGTATTA</b>	
Tx-28 <sup>(1)</sup>	HIV-1 TAR	<b>TAATACGACTCACTATAGGG</b> GTCTCTCTGGTTAGACCAGATCTGAGCCTGGGAGCTCTCTGGCTAACTAGGGAACC	Hybridization
Tx-29 <sup>(1)</sup>		GGTTCCTTAGTTAGCCAGAGAGCTCCAGGCTCAGATCTGGTCTAACCAGAGAGACC <b>CCCTATAGTGAGTCGTATTA</b>	

Bold: T7 promoter sequence.

<sup>(1)</sup> Müller 2009

## 4.2.3 RNA oligonucleotides

Chemically synthesized RNAs were ordered from Thermo Scientific / Dharmacon in a 2'-ACE-protected form. The RNA was deprotected as described by the manufacturer and dried by centrifugal evaporation. Before use, the RNA was dissolved in buffer (20 mM HEPES/NaOH (pH 7.4), 200 mM NaCl, and 2 mM MgCl<sub>2</sub> in Diethylpyrocarbonate (DEPC)-treated Millipore H<sub>2</sub>O) and refolded by heating to 80 °C for 5 min followed by cooling to 25 °C over 18 min in a thermal cyclor.

## MATERIALS & METHODS

RNA	Base no. relative to start codon	Sequence (5'→3')	Produced by
ASH1-E3-51	1771-1821	AUGGAUAACUGAAUCUCUUUCAACUAAUAAGAG ACAUUAUCACGAAACAAU	Chemical synthesis
ASH1-E3-51 (Δ1786-1802)	1771-1821 (Δ1786-1802)	AUGGAUAACUGAAUC <u>GAAAG</u> ACAUUAUCACGAA ACAAU	Chemical synthesis
ASH1-E3-118 <sup>(1)</sup>	1750-1867	<u>GGG</u> GAGACAGUAGAGAAUUGAUACAUGGAUAACU GAAUCUCUUUCAACUAAUAAGAGACAUUAUCAC GAAACAAUUGUACAUUUCUCUCCUUGUCUGUGC UAAAUAACUACAAAUA AAAA	<i>In vitro</i> transcription
ASH1-E3-77	1758-1834	<u>GGGAG</u> AGAGAAUUGAUACAUGGAUAACUGAAUC UCUUUCAACUAAUAAGAGACAUUAUCACGAAAC AAUUGUACAUUUCUCU	<i>In vitro</i> transcription
ASH1-E3-51	1771-1821	<u>GGGAG</u> AUGGAUAACUGAAUCUCUUUCAACUAAU AAGAGACAUUAUCACGAAACAAU	<i>In vitro</i> transcription
ASH1-E3-51 (Δ1786-1802)	1771-1821 (Δ1786-1802)	<u>GGGAG</u> AUGGAUAACUGAAUC <u>GAAAG</u> ACAUUAUC ACGAAACAAU	<i>In vitro</i> transcription
ASH1-E3-51 (Δ1782-1804)	1771-1821 (Δ1782-1804)	<u>GGGAG</u> AUGGAUAACUG <u>GAAAC</u> AUUAUCACGAA CAAU	<i>In vitro</i> transcription
HIV-1 TAR <sup>(1)</sup>		<u>GGG</u> GUCUCUCUGGUUAGACCAGAUUCUGAGCCUG GGAGCUCUCUGGCUAACUAGGGAACC	<i>In vitro</i> transcription
ASH1-E3-118-tRNA	1750-1867	GGCUACGUAGCUCAGUUGGUUAGAGCAGCGGCC GGAGACAGUAGAGAAUUGAUACAUGGAUAACUG <u>AAUCUCUUUCAACUAAUAAGAGACAUUAUCACG</u> <u>AAACAAUUGUACAUUUCUCUCCUUGUCUGUGCU</u> <u>AAAUAACUACAAAUA AAAA</u> CCGCGGGUCACAG GUUCGAAUCCCGUCGUAGCCACCA	Expression in <i>E. coli</i>
ASH1-E3-77-tRNA	1758-1834	GGCUACGUAGCUCAGUUGGUUAGAGCAGCGGCC GAGAGAAUUGAUACAUGGAUAACUGAAUCUCUU <u>UCAACUAAUAAGAGACAUUAUCACGAAACAAU</u> <u>GUACAUUUCUCUUGGCCGCGGGUCACAGGUUCG</u> AAUCCCGUCGUAGCCACCA	Expression in <i>E. coli</i>
ASH1-E3-51-tRNA	1771-1821	GGCUACGUAGCUCAGUUGGUUAGAGCAGCGGCC GAUGGAUAACUGAAUCUCUUUCAACUAAUAAGA <u>GACAUUAUCACGAAACAAUUGGCCGCGGGUCAC</u> AGGUUCGAAUCCCGUCGUAGCCACCA	Expression in <i>E. coli</i>
ASH1-E3-38-tRNA	1774-1811	GGCUACGUAGCUCAGUUGGUUAGAGCAGCGGCC GAUAACUGAAUCUCUUUCAACUAAUAAGAGACA <u>UUAUCGGCCGCGGGUCACAGGUUCGAAUCCCGU</u> CGUAGCCACCA	Expression in <i>E. coli</i>
ASH1-E3-33-tRNA	1780-1812	GGCUACGUAGCUCAGUUGGUUAGAGCAGCGGCC <u>UGAAUCUCUUUCAACUAAUAAGAGACAUUAUCA</u> GGCCGCGGGUCACAGGUUCGAAUCCCGUCGUAG CCACCA	Expression in <i>E. coli</i>
IST2-tRNA	2716-2777	GGCUACGUAGCUCAGUUGGUUAGAGCAGCGGCC GGAUGCUGGAGUGAAGAAUGUCACGAACAAUUC <u>UAAGACAACCGAAUCCUCUCCUUCUUCUUCUGG</u> CCGCGGGUCACAGGUUCGAAUCCCGUCGUAGCC ACCA	Expression in <i>E. coli</i>
HIV-1 TAR-tRNA		GGCUACGUAGCUCAGUUGGUUAGAGCAGCGGCC GGGUCUCUCUGGUUAGACCAGAUUCUGAGCCUGG <u>GAGCUCUCUGGCUAACUAGGGAACCUUGGCCGCG</u> GGUCACAGGUUCGAAUCCCGUCGUAGCCACCA	Expression in <i>E. coli</i>
2x-ASH1-E3-77-tRNA	1758-1834	GGCUACGUAGCUCAGUUGGUUAGAGCAGCGGCC <u>GCCGUAACAUAAU</u> UAGAGAAUUGAUACAUGGAU <u>AACUGAAUCUCUUUCAACUAAUAAGAGACAUUA</u> <u>UCACGAAACAAUUGUACAUUUCUCUAACAUUAU</u> GAGAAUUGAUACAUGGAUAACUGAAUCUCUUUC AACUAAUAAGAGACAUUAUCACGAAACAAUUGU ACAUUUCUCU <u>AUAGAAGG</u> UGGCCGCGGGUCACA GGUUCGAAUCCCGUCGUAGCCACCA	Expression in <i>E. coli</i>

RNA	Base no. relative to start codon	Sequence (5'→3')	Produced by
<i>ASH1</i> -E3-77/ HIV-1 TAR-tRNA	1758-1834	GGCUACGUAGCUCAGUUGGUUAGAGCAGCGGCC <b>GCCGUAACAUAUUU</b> AGAGAAUUGAUACAUGGAU <u>AACUGAAUCUCUUUCAACUAAUAAGAGACAUUA</u> <u>UCACGAAACAAUUGUACAUUUCUCUAACAUAUG</u> <u>GUCUCUCUGGUUAGACCAGAUCUGAGCCUGGGA</u> <u>GCUCUCUGGCUAACUAGGGAACCAUAGAAGGUG</u> GCCGCGGGUCACAGGUUCGAAUCCCGUCGUAGC CACCA	Expression in <i>E. coli</i>

Bold & underlined: Linker sequence resulting from *in vitro* transcription.

Italic & underlined: GAAA tetraloop sequence replacing the distal loop of *ASH1*-E3.

Underlined: Zip-code sequences inserted into the anticodon stem of Met-tRNA.

Bold: Three-way junction sequence from the Twort intron (Lescoute and Westhof 2006).

<sup>(1)</sup> Müller 2009

### 4.3 Plasmids

All created plasmids are based on one of the following vectors:

Name	Application	Tag	Source
pGex-6P-1	Bacterial expression of proteins	N-terminal GST	GE Healthcare
pET28a	Bacterial expression of proteins	N-terminal 6xHis	Merck
pETM40	Bacterial expression of proteins	N-terminal MBP	EMBL Heidelberg, modified by Dr. Alexander Heuck
pFastBac Dual	Insect cell expression of proteins		Invitrogen
pFastBac DM	Insect cell expression of proteins		Berger et al. 2004
pBSM	Bacterial expression of RNAs	Met-tRNA	Ponchon et al. 2009
pH203 (pMIH- $\Delta$ int- <i>rrnB</i> )	Transfer of rRNA operon B ( <i>rrnB</i> ) into <i>M. smegmatis</i> strain SZ0637		Dr. Sven Hobbie (Hobbie et al. 2007)

#### 4.3.1 Plasmids for protein expression in *E. coli*

Name	Insert	Vector	Primer	Mutagenesis primer	Restriction sites
pShe2p <sup>(1)</sup>	She2p	pGex-6P-1			BamHI, EcoRI
pRH118	She2p (E183A D184A G185A)	pShe2p		0157, 0158	BamHI, EcoRI
pRH119	She2p (T191A D192A)	pShe2p		0159, 0160	BamHI, EcoRI
pRH138	She2p (F195A L196A)	pShe2p		0171, 0172	BamHI, EcoRI
pRH139	She2p (Q197A E198A I199A)	pShe2p		0173, 0174	BamHI, EcoRI
pRH82	She2(6-246)	pGex-6P-1	MM-S2-27, MM-S2-1		BamHI, XhoI
pMM5 <sup>(2)</sup>	She2p(6-240) $\Delta$ Cys	pGex-6P-1	MM-S2-27, MM-S2-22		BamHI, XhoI
pAH2 <sup>(3)</sup>	She3p(1-234)	pET28a			
pRH83	She3p(274-425)-6xHis	pGex-6P-1	0120,049		BamHI,EcoRI
pRH85	She3p(334-425)-6xHis	pGex-6P-1	0122,049		BamHI,EcoRI
pRH136	She3p(334-425)-6xHis	petM40	0122, 049		BamHI, EcoRI

## MATERIALS & METHODS

Name	Insert	Vector	Primer	Mutagenesis primer	Restriction sites
pRH73	She3p(354-425)-6xHis	pGex-6P-1	083,049		BamHI,EcoRI
pRH137	She3(354-425)-6xHis	petM40	083,049		BamHI, EcoRI
pAH7 <sup>(3)</sup>	Myo4p(978-1471)	pGex-6P-1	AH-02, AH-04		BamHI, XhoI

<sup>(1)</sup> origin unknown

<sup>(2)</sup> Müller 2009

<sup>(3)</sup> Heuck 2009

### 4.3.2 Plasmids for protein expression in insect cells

Name	Insert	Vector	Primer	Mutagenesis primer	Restriction sites
pRH27	She3p-6xHis / She2p	pFastBac Dual	AH-06, 049 / 048, MM-S2-1		BamHI, EcoRI / SmaI, XhoI
pRH130	She3p(R341E)-6xHis / She2p	pRH27		0164, 0165	BamHI, EcoRI / SmaI, XhoI
pRH113	She3p(S348E)-6xHis / She2p	pRH27		0151, 0152	BamHI, EcoRI / SmaI, XhoI
pRH114	She3p(S343E S361E)- 6xHis / She2p	pRH27		0153, 0154 / 0155, 0156	BamHI, EcoRI / SmaI, XhoI
pRH129	She3p(L364A V367A)- 6xHis / She2p	pRH27		0162, 0163	BamHI, EcoRI / SmaI, XhoI
pRH162 <sup>(1)</sup>	FLAG-Myo4p / CaM / She4p / She3p-6xHis	pFastBac DM	0211, 0212 / 0213, 0214		BamHI, NotI / NcoI, XhoI / BamHI, XbaI / SmaI, NcoI

<sup>(1)</sup> partially based on pAH154 created by Dr. Alexander Heuck

### 4.3.3 Plasmids for expression of tRNA-tagged RNAs in *E. coli*

Name	Insert	Vector	Primer	Mutagenesis Primer	Restriction sites
pRH89	ASH1-E3-118	pBSM	MM-SC-5, MM-SC-6		EagI, SacII
pRH60	ASH1-E3-77	pBSM	096,0101		EagI, SacII
pRH90	ASH1-E3-51	pBSM	0126, 0127		EagI, SacII
pRH67	ASH1-E3-38	pBSM	0108,0109		EagI, SacII
pRH65	ASH1-E3-33	pBSM	0106,0107		EagI, SacII
pRH149	IST2	pBSM	0190, 0191		EagI, SacII
pRH99	HIV-TAR	pBSM	0134,0135		EagI, SacII
pRH145	2xASH1-E3-77	pBSM	0180, 0183	0181, 0182	EagI, SacII
pRH153	ASH1-E3-77/HIV-1 TAR	pBSM	0180, 0200	0198, 0199	EagI, SacII

#### 4.3.4 Plasmids for rRNA modification in *M. smegmatis*

Name	Insert	Vector	Primer	Mutagenesis primer	Restriction sites
pRH2	23SrRNA-Helix98-PvuI	pH203	01, 06	09, 010	NcoI, XbaI
pRH25	ASH1-E1	pRH2	044, 045		PvuI, PvuI
pRH21	ASH1-E2A	pRH2	036, 037		PvuI, PvuI
pRH5	ASH1-E2B	pRH2	011, 012		PvuI, PvuI
pRH6	ASH1-E3-77	pRH2	013, 014		PvuI, PvuI

#### 4.4 Bacterial strains

Strain	Species	Genotype	Source
XL1-Blue	<i>E. coli</i>	<i>recA1 endA1 gyrA96 thi-1 hsdR17 supE44 relA1 lac</i> [F' <i>proAB lacI<sup>q</sup>ZΔM15 Tn10</i> (Tet <sup>r</sup> )]	Agilent Technologies
BL21 Star (DE3)	<i>E. coli</i>	F- <i>ompT hsdSB</i> (rB <sup>-</sup> , mB <sup>-</sup> ) <i>gal dcm rne131</i> (DE3)	Invitrogen
DH10Bac	<i>E. coli</i>	F- <i>mcrA Δ(mrr-hsdRMS-mcrBC) Φ80lacZΔM15 ΔlacX74 recA1 endA1 araD139 Δ(ara, leu)7697 galU galK λ- rpsL nupG</i> /pMON14272 / pMON7124	Invitrogen
JM101	<i>E. coli</i>	<i>supE thi-1 Δ(lac-proAB)</i> [F' <i>traD36 proAB lacI<sup>q</sup>Z ΔM15</i> ]	Agilent Technologies
SZ0637	<i>M. smegmatis</i>	<i>ΔrrnA ΔrrnB attB::pMIG-sacB-rrnB<sup>2058G</sup></i>	Dr. Sven Hobbie (Hobbie et al. 2007)
RHM25	<i>M. smegmatis</i>	<i>ΔrrnA ΔrrnB attB::pMIH-Δint-rrnB(ASH1-E1)</i>	This study
RHM21	<i>M. smegmatis</i>	<i>ΔrrnA ΔrrnB attB::pMIH-Δint-rrnB(ASH1-E2A)</i>	This study
RHM5	<i>M. smegmatis</i>	<i>ΔrrnA ΔrrnB attB::pMIH-Δint-rrnB(ASH1-E2B)</i>	This study
RHM6	<i>M. smegmatis</i>	<i>ΔrrnA ΔrrnB attB::pMIH-Δint-rrnB(ASH1-E3-77)</i>	This study

#### 4.5 Insect cell lines

Cell line	Description	Source
Sf21	Derived from <i>Spodoptera frugiperda</i> ovarian cells. Used to isolate and propagate recombinant baculovirus stocks.	Invitrogen
High Five	Derived from the <i>Trichopulsia ni</i> cell line. Used to express recombinant proteins upon baculovirus infection.	Invitrogen

## 4.6 Media and supplements

Medium	Composition	Type of cells
LB	10 g/l Bacto tryptone, 5 g/l Bacto yeast extract, 5 g/l NaCl, pH 7.0 with NaOH, add 15 g/l Agar for plates	<i>E. coli</i>
2x TY	16 g/l Bacto tryptone, 10 g/l Bacto yeast extract, 5 g/l NaCl, pH 7.0 with NaOH	<i>E. coli</i>
SOC	20 g/l Bacto tryptone, 5 g/l Bacto yeast extract, 0.5 g/l NaCl, 2.5 mM KCl, 10 mM MgCl <sub>2</sub> , 20 mM glucose, pH 7.0 with NaOH	<i>E. coli</i> DH10Bac
Sf-900 III SFM (Invitrogen)	Protein-free insect cell culture medium	SF21 insect cells
HyClone SFX-Insect (Thermo Scientific)	Protein-free insect cell culture medium	High Five insect cells

Supplement	Stock solution	Final concentration	Purpose
Ampicillin	100 mg/ml	100 µg/ml	<i>E. coli</i> selection
Gentamycin	7 mg/ml	7 µg/ml	<i>E. coli</i> DH10Bac selection
Gentamycin	50 mg/ml	10 µg/ml	Insect cell culture
Hygromycin B	50 mg/ml	100 µg/ml	<i>M. smegmatis</i> selection (plates)
Hygromycin B	50 mg/ml	50 µg/ml	<i>M. smegmatis</i> selection (liquid culture)
Kanamycin	50 mg/ml	50 µg/ml	<i>E. coli</i> selection
Tetracyclin	10 mg/ml	10 µg/ml	<i>E. coli</i> DH10Bac selection
IPTG	1 M	0.25 mM	Induction (liquid culture)
IPTG	1 M	0.5 mM	Induction (plates)
Tween 80		0.05% (v/v)	Growth of <i>M. smegmatis</i>
X-gal	100 mg/ml	100 µg/ml	Substrate for blue/white selection on plates

## 4.7 Molecular biology

### 4.7.1 Molecular cloning

All standard molecular biology techniques were performed as described by Sambrook and Russel 2000. DNA fragments were amplified by polymerase chain reaction (PCR), analyzed by agarose gel electrophoresis (in 1x TBE, stained with GelRed stain (Biotium), and purified with the NucleoSpin gel and PCR clean-up kit (Macherey-Nagel). Restriction digestion of insert and vector DNA as well as ligation were performed according to the manufacturer's instructions (Fermentas, New England Biolabs). Point mutations were either introduced by

## MATERIALS & METHODS

PCR-based site-directed mutagenesis (Ho et al. 1989) or by using the QuickChange II site-directed mutagenesis kit (Agilent Technologies).

Chemically competent *E. coli* cells were prepared according to Hanahan 1983. Transformation of plasmid DNA was performed essentially as described (Sambrook and Russel 2000). Transformants were selected on LB agar plates supplemented with the respective antibiotics. A single colony was used to inoculate 5 ml LB medium supplemented with the respective antibiotics. After cultivation over night at 37 °C, the plasmid DNA was isolated using the NucleoSpin plasmid kit (Macherey-Nagel). The success of the cloning procedure was confirmed by DNA sequencing (Eurofins MWG Operon).

*E. coli* DH10Bac cells were transformed and selected as described for the Bac-to-Bac system (Invitrogen). Bacmid DNA was isolated by isopropanol precipitation and stored at 4 °C.

### 4.7.2 Transformation and selection of *M. smegmatis* cells

*M. smegmatis* cells were cultured in LB medium supplemented with 0.05% (v/v) Tween 80 (LB Tween) at 37 °C. To prepare electrocompetent cells, a 2 l culture with an OD<sub>600</sub> of 0.4 to 0.8 was prepared. The cells were chilled in ice water for 60 min and harvested at 4 °C for 20 min at 5000 x g. The cell pellet was washed successively in a total volume of 400 ml, 200 ml, 100 ml, and 50 ml 10% (v/v) glycerol. The final pellet (ca. 5 g wet mass) was resuspended in ca. 10 ml of 10% (v/v) glycerol. Aliquots of 100 µl were flash frozen in liquid nitrogen and stored at -80 °C.

Competent cells were thawed on ice and 1 µg of plasmid DNA was added per 100 µl cells. The cells were pulsed at 2.5 kV, 25 µF, and 1000 Ω in a 2 mm electroporation cuvette, immediately resuspended in 1 ml of prewarmed LB Tween, and shaken for two to three hours at 37 °C. Afterwards, cells were spread onto LB agar plates supplemented with 100 µg/ml hygromycin B and 5% (w/v) sucrose and incubated for at least three days at 37 °C. After restreaking,

successful integration into the genome was verified by colony PCR, cells were resuspended in 15% (v/v) glycerol and stored at -80 °C.

### **4.8 Protein expression and purification**

#### **4.8.1 Protein expression in *E. coli***

Colonies of freshly transformed BL21 Star (DE3) cells were used to inoculate 20 ml of LB supplemented with the respective antibiotics. After cultivation for 4 h at 37 °C, 3 l of prewarmed LB supplemented with the respective antibiotics (and with 2 g/l glucose, in case of maltose-binding protein (MBP)-fusion proteins) were inoculated with the preculture. At an OD<sub>600</sub> of ca. 0.3, the culture was cooled to 18 °C over 30-60 min. At an OD<sub>600</sub> of ca. 0.6, expression of the recombinant protein was induced by adding 0.25 mM Isopropyl-β-D-thiogalactopyranosid (IPTG). The cells were cultured at 18 °C and 140 rpm for ca. 15-17 h. Afterwards, cells were pelleted (4400 x g, 15 min, 4°C), resuspended in the respective buffer, and either flash frozen with liquid nitrogen and stored at -80 °C or directly used for purification.

The expression of Myo4p (978-1471) was improved by using 2x TY medium supplemented with 100 µg/ml ampicillin. In addition, 2% (v/v) ethanol was added just before induction.

#### **4.8.2 Protein expression in insect cells**

Recombinant baculovirus was prepared essentially as described for the Bac-to-Bac system (Invitrogen). In brief, 2 ml SF21 cells with a density of 0.4 x 10<sup>6</sup> cells/ml were transfected with 1-2 µg bacmid DNA using the FuGENE HD transfection reagent (Roche). After cultivation for at least four days at 27.5 °C, the supernatant (P0) of two transfections (4 ml) was used to infect 10 ml SF21 cells with a density of 1.4 x 10<sup>6</sup> cells/ml. After cultivation for four days at 27.5 °C and 95 rpm, the cells were centrifuged at 2000 x g, the supernatant (P1)

## MATERIALS & METHODS

was sterile filtered, and 2 ml thereof were used to infect 500 ml SF21 with a density of  $0.4 \times 10^6$  cells/ml. After cultivation for four days, cells were pelleted, the supernatant (P2) was sterile filtered and stored at 4 °C.

A culture of 500 ml High Five cells with a density of  $1 \times 10^6$  cells/ml were infected with 10-30 ml P2 virus supernatant and cultivated for 60-70 h at 27.5 °C. Afterwards, the cells were collected by centrifugation (2000 x g, 15 min, 4 °C), resuspended in the respective buffer, and either flash frozen with liquid nitrogen and stored at -80 °C or directly used for purification.

### **4.8.3 Purification of She2p, She3p (1-234), and Myo4p (978-1471)**

Wild-type and mutant She2p was purified essentially as described (Müller 2009), except that the glutathione S-transferase (GST)-tag was cleaved on the column. Purification of His-tagged She3p (1-234) and Myo4p (978-1471) was performed as previously described (Heuck 2009).

### **4.8.4 Purification of full-length She3p constructs**

All steps were carried out at 4 °C. The cell pellet of a 0.5-1 l culture was resuspended in S3-Ni-A1 buffer to a total volume of ca. 40 ml. One tablet of ethylenediaminetetraacetic acid (EDTA)-free protease inhibitor cocktail (Roche) and 0.4 mM phenylmethylsulfonyl fluoride (PMSF) was added. The cell suspension was lysed by sonication (3x 2 min, amplitude: 35%, output: 6). The lysate was cleared by centrifugation (39000 x g, 2x 20 min), filtered with a 2.7 µm filter and loaded on a HisTrap nickel sepharose column (GE Healthcare). The column was washed successively with S3-Ni-A1 buffer, S3-Ni-A2 buffer, and S3-Hep-A buffer. Protein was eluted directly on a HiTrap Q sepharose column attached to a HiTrap heparin sepharose column (both: GE Healthcare) with 60% S3-Ni-B and 40% S3-Hep-A buffer. The heparin column was washed with S3-Hep-A buffer, 15% S3-Hep-B buffer, and bound protein was eluted with 35% S3-Hep-B buffer. The protein was concentrated by ultrafiltration with an Amicon

## MATERIALS & METHODS

Ultra centrifugal filter (Millipore) and finally purified with a Superose 6 10/300 GL column (GE Healthcare) in S3-SEC buffer. Purified She3p was usually concentrated to 8-12 mg/ml by ultrafiltration. Aliquots were flash frozen in liquid nitrogen and stored at -80 °C. SDS-PAGE and UV-spectroscopy were used to analyze the quality of the purification. The ratio of absorbance at 260 nm and 280 nm was below 0.6 indicating that no contaminating nucleic acids were present.

S3-Ni-A1 buffer:	20 mM HEPES/NaOH (pH 7.8), 500 mM NaCl, 20 mM Imidazole
S3-Ni-A2 buffer:	20 mM HEPES/NaOH (pH 7.8), 1 M NaCl, 40 mM Imidazole
S3-Ni-B buffer:	20 mM HEPES/NaOH (pH 7.8), 200 mM NaCl, 500 mM Imidazole
S3-Hep-A buffer:	20 mM HEPES/NaOH (pH 7.8), 200 mM NaCl
S3-Hep-B buffer:	20 mM HEPES/NaOH (pH 7.8), 1 M NaCl, 2 mM EDTA, 2 mM DTT
S3-SEC buffer:	20 mM HEPES/NaOH (pH 7.8), 500 mM NaCl, 2 mM DTT

### 4.8.5 Purification of C-terminal She3p constructs

C-terminal She3p constructs were either purified via an N-terminal GST- or MBP-tag. In addition, a C-terminal 6x His-tag was present. All steps were carried out at 4 °C. The cell pellet was resuspended in S3C-GST-A1 buffer supplemented with EDTA-free protease inhibitor cocktail. The cell suspension was lysed by sonication (3x 4 min, amplitude: 35%, output: 6), the lysate was cleared by centrifugation (30000 x g, 30 min), and loaded on a GSTrap glutathione sepharose column (GE Healthcare). The column was washed successively with S3C-GST-A1 buffer, S3C-GST-A2 buffer, and again with S3C-GST-A1 buffer. A volume of 5 ml S3C-GST-A1 buffer supplemented with 100 µg PreScission protease (GE Healthcare) was applied to the column. After incubation at 4 °C for at least three hours, the cleaved protein was eluted directly on a HisTrap nickel sepharose column (GE Healthcare) with S3C-Ni-A buffer. The column was washed with 15% S3C-Ni-B buffer. Bound protein was eluted with S3C-Ni-B buffer, concentrated by ultrafiltration, and separated on a Superose 12 10/300 GL column (GE Healthcare) in S3C-SEC buffer. Pure fractions were pooled and concentrated by ultrafiltration. Since the She3p C-terminus shows no absorption at 280 nm, the concentration was estimated from sodium dodecyl sulfate

## MATERIALS & METHODS

polyacrylamide gel electrophoresis (SDS-PAGE) with Coomassie blue staining. Aliquots were flash frozen with liquid nitrogen and stored at -80 °C.

In the case of MBP-tagged She3p variants, the cell pellet was resuspended in S3C-MBP-A buffer supplemented with 5 mM EDTA and protease inhibitor cocktail. The lysate was loaded on a gravity flow column filled with amylose resin (New England Biolabs). The column was washed with S3C-MBP-A buffer, bound protein was eluted with S3C-MBP-B buffer, and loaded on a HisTrap nickel sepharose column (GE Healthcare). The following steps of the purification were performed as described above.

S3C-GST-A1 buffer:	20 mM HEPES/NaOH (pH 7.8), 500 mM NaCl
S3C-GST-A2 buffer:	20 mM HEPES/NaOH (pH 7.8), 1 M NaCl
S3C-MBP-A buffer:	20 mM HEPES/NaOH (pH 7.8), 200 mM NaCl
S3C-MBP-B buffer:	20 mM HEPES/NaOH (pH 7.8), 200 mM NaCl, 10 mM Maltose
S3C-Ni-A buffer:	20 mM HEPES/NaOH (pH 7.8), 500 mM NaCl, 20 mM Imidazole
S3C-Ni-B buffer:	20 mM HEPES/NaOH (pH 7.8), 500 mM NaCl, 500 mM Imidazole
S3C-SEC buffer:	20 mM HEPES/NaOH (pH 7.8), 200 mM NaCl

### 4.8.6 Purification of full-length Myo4p

All steps were carried out at 4 °C. The cell pellet of a 0.5-1 l culture was resuspended in M4-HB buffer to a total volume of ca. 40 ml and lysed by sonication (3x 2 min, amplitude: 35%, output: 6). The lysate was cleared by centrifugation (39000 x g, 2x 20 min), filtered with a 2.7 µM filter, and 1 ml ANTI-FLAG M2 affinity gel (Sigma-Aldrich) was added. The mixture was gently agitated for 60 min, transferred into a gravity flow column and washed with M4-FLAG-A buffer. Bound protein was eluted five times with 1 ml M4-FLAG-B buffer. The eluate was dialyzed two times against 1.5 l of ATPase buffer, followed by dialysis against 0.5 l ATPase buffer supplemented with 50% (v/v) glycerol. The protein was stored at -20 °C. The concentration of the protein was estimated by comparing the intensity of the Coomassie blue staining of Myo4p with known concentrations of bovine serum albumin (BSA) in an SDS-polyacrylamide gel.

## MATERIALS & METHODS

M4-HB buffer:	20 mM Imidazole (pH 7.5), 200 mM NaCl, 5 mM MgCl <sub>2</sub> , 1 mM EDTA, 1 mM EGTA, 7% (w/v) Sucrose, 1 mM PMSF, 3 mM ATP, 1 tablet EDTA-free protease inhibitor cocktail per 50 ml buffer
M4-FLAG-A buffer:	20 mM Imidazole (pH 7.5), 150 mM KCl, 5 mM MgCl <sub>2</sub> , 1 mM EDTA, 1 mM EGTA, 0.5 mM PMSF, 3 mM ATP, 1 tablet EDTA-free protease inhibitor cocktail per 50 ml buffer
M4-FLAG-B buffer:	20 mM Imidazole (pH 7.5), 150 mM KCl, 5 mM MgCl <sub>2</sub> , 1 mM EDTA, 1 mM EGTA, 0.5 mM PMSF, 0.1 mg/ml FLAG peptide, 1 tablet EDTA-free protease inhibitor cocktail per 50 ml buffer
ATPase buffer:	20 mM HEPES/NaOH (pH 7.8), 100 mM NaCl, 25 mM KCl, 2 mM MgCl <sub>2</sub> , 1 mM EGTA, 2 mM DTT

### 4.8.7 Purification of actin from rabbit muscle

Actin was purified from 5 g rabbit muscle acetone powder (Sigma-Aldrich, M6890). All steps were carried out at 4 °C. The frozen acetone powder was crushed into small pieces and actin was extracted 6-8 times. Therefore, the powder was covered with G-buffer, stirred for 20-30 min, and filtered with a compress. The first filtrate was discarded. All other filtrates were pooled and cleared by ultracentrifugation (Type 45 Ti rotor, 41 krpm, 30 min). The supernatant was supplemented with 800 mM KCl, 2 mM MgCl<sub>2</sub>, and 1 mM ATP, the pH was adjusted to 8, and polymerization of actin was allowed to proceed over night under slow stirring. F-actin was pelleted by ultracentrifugation (Type 45 Ti rotor, 41 krpm, 3 h). The pellets were washed with G-buffer and resuspended in 3-5 ml of G-buffer with a dounce homogenizer. The solution was dialyzed two times against 2 l of G-buffer. After ultracentrifugation (Type 70.1 Ti rotor, 44 krpm, 2 h) the supernatant contained the finally purified G-actin. The concentration was determined by absorption at 290 nm using an extinction coefficient of 26000 M<sup>-1</sup>cm<sup>-1</sup> (Abs 0.1% = 0.62). G-actin could be stored for up to two weeks at 4 °C when daily dialyzed against G-buffer supplemented with 0.02% (w/v) sodium azide. After polymerization (Section 4.11.15), F-actin could be flash frozen in liquid nitrogen and stored at -80 °C.

G-buffer: 2 mM TRIS/HCl (pH<sub>4°C</sub> 8), 0.2 mM CaCl<sub>2</sub>, 0.2 mM ATP, 0.5 mM DTT

## 4.9 RNA expression and purification

### 4.9.1 Expression and purification of tRNA-tagged RNAs

tRNA-tagged RNAs were expressed and purified essentially as described (Ponchon et al. 2009). In brief, 50  $\mu$ l JM101 cells were freshly transformed and directly used to inoculate 1 l of 2x TY medium containing 100  $\mu$ g/ml ampicillin without prior selection on plates. The culture was incubated at 37 °C and 140 rpm for 15-17 h. Cells were harvested by centrifugation (4400 x g, 15 min, 4 °C), resuspended in buffer RNA-HB, and either flash frozen with liquid nitrogen and stored at -80 °C or directly used for purification.

The RNA was isolated by phenol extraction followed by ethanol precipitation (Ponchon et al. 2009). Afterwards, anion exchange chromatography was performed. Either a SOURCE 15Q 4.6/100 PE column (GE Healthcare) or DNAPac PA100 (9 x 250 mm) column (Dionex) was used for this step. The precipitated RNA was dissolved in buffer RNA-Q-A, loaded onto the column, washed with 40% buffer RNA-Q-B (35% for small constructs, such as *ASH1-E3-33-tRNA* or *ASH1-E3-38-tRNA*), and eluted with a linear gradient from 40% (35%) to 100% RNA-Q-B buffer over 40 column volumes. Fractions were analyzed by 8% Urea-PAGE. Pure fractions were pooled and the buffer was exchanged by repeated ultrafiltration with RNA buffer. The concentration of the RNA was determined by the absorption at 254 nm ( $c = A_{254} \times 37 \mu\text{g/ml}$ ), the RNA was flash frozen in liquid nitrogen, and stored at -80 °C.

RNA-HB buffer: 10mM TRIS/HCl (pH<sub>4°C</sub> 7.4), 10mM Mg(OAc)<sub>2</sub> (autoclaved Millipore H<sub>2</sub>O)

RNA-Q-A buffer: 40 mM NaH<sub>2</sub>PO<sub>4</sub>/Na<sub>2</sub>HPO<sub>4</sub> (pH 7.0) (autoclaved Millipore H<sub>2</sub>O)

RNA-Q-B buffer: 40 mM NaH<sub>2</sub>PO<sub>4</sub>/Na<sub>2</sub>HPO<sub>4</sub> (pH 7.0), 1M NaCl (autoclaved Millipore H<sub>2</sub>O)

RNA buffer: 20 mM HEPES/NaOH (pH 7.4), 200 mM NaCl (DEPC-treated Millipore H<sub>2</sub>O)

### 4.9.2 *In vitro* transcription and RNA purification

RNase-free materials and reagents were used for all steps. DNA templates for *in vitro* transcription were either prepared by hybridization of DNA oligonucleotides or by PCR (Section 4.2.2). *In vitro* transcription was performed

## MATERIALS & METHODS

with the MEGAscript kit (Ambion) as described by the manufacturer. In brief, 200-500 nM template DNA was used per reaction, the mixture was incubated for 4 h at 37 °C, treated twice with 1 µl Fast-AP thermosensitive alkaline phosphatase (Fermentas) for 30 min at 37 °C, and once with TURBO DNase (Ambion) for 30 min at 37 °C. Afterwards, the RNA could be stored at -20 °C.

The RNA was separated by 10-15% native PAGE and RNA bands were visualized by UV-shadowing. The desired product was cut out, the gel was crushed into small pieces, covered with a solution containing 300 mM NaCl and 0.5 mM EDTA and incubated at 37 °C over night. The solution was filtered with an Ultrafree-MC centrifugal filter (Millipore). The buffer was exchanged to DEPC-treated Millipore H<sub>2</sub>O by ultrafiltration using Nanosep 3K centrifugal devices (Pall). The concentration of the RNA was determined by the absorption at 260 nm ( $c = A_{260} \times 33 \mu\text{g/ml}$ ) and the RNA was stored at -20 °C.

### 4.10 Ribosome expression and purification

A 60 ml preculture of LB containing 0.05% Tween (LB Tween) and 50 µg/ml hygromycin B was inoculated with the respective *M. smegmatis* strain from a glycerol stock and cultured at 37 °C for ca. 48 h until an OD<sub>600</sub> of 0.3-0.8 was reached. A flask with 3 l LB Tween without antibiotics was inoculated with 20 ml of the preculture and shaken at 37°C and 140 rpm for 27-31 h until an OD<sub>600</sub> of 0.4-0.6 was reached. The cells were pelleted (5000 x g, 15 min, 4 °C) resuspended in precooled 70S-HB buffer, and either flash frozen with liquid nitrogen and stored at -80 °C or directly used for purification.

Unless indicated otherwise all purification steps were carried out at 4 °C. The cell suspension was supplemented with 2 units DNase I (Fermentas) per 1 g of cell pellet. The cells were lysed 3-5 times with a microfluidizer at 10000-16000 psi. The lysate was cleared two times (30000 x g, 30 min) and 350 mM NH<sub>4</sub>Cl and 7 mM β-mercaptoethanol (β-ME) were added. The lysate was cleared again by ultracentrifugation (Type 70 Ti rotor, 36.6 krpm, 15 min) and 15 ml thereof were

## MATERIALS & METHODS

loaded per 9 ml sucrose cushion. The ribosomes were pelleted by ultracentrifugation (Type 70 Ti rotor, 36.6 krpm, 17 h), carefully washed three times with 70S buffer and dissolved in 70S buffer by gentle shaking. After centrifugation (9300 x g, 5 min) the absorption at 260 nm was measured. Up to 50  $A_{260}$  units were loaded per 10-40% (w/v) sucrose gradient in 70S buffer. After ultracentrifugation (SW 28 rotor, 16800 rpm, 16 h), the gradients were fractionated from top to bottom at room temperature. Fractions containing 70S ribosomes were pooled, the ribosomes were pelleted (Type 70 Ti, 36.6 krpm, 5 h), carefully washed three times with 70S buffer, and dissolved in 70S buffer by gentle shaking. After centrifugation (9300 x g, 5 min), the ribosome concentration was determined from the absorption at 260 nm ( $c = A_{260} \times 23 \text{ nM}$ ). The purity and integrity of 70S ribosomes was confirmed by SDS-PAGE, 1% (w/v) agarose gel electrophoresis, and analytical 10-40% (w/v) sucrose gradient centrifugation in 70S buffer (SW 40 rotor, 17.7 krpm, 16 h). Purified ribosomes were flash frozen in liquid nitrogen and stored at -80 °C.

All buffers were prepared with autoclaved Millipore H<sub>2</sub>O. RNase-free sucrose from Roth was used.

70S-HB buffer:	20 mM TRIS/HCl (pH 7.4), 100 mM NH <sub>4</sub> Cl, 10 mM MgCl <sub>2</sub> , 3 mM $\beta$ -ME
Sucrose cushion:	20 mM TRIS/HCl (pH 7.4), 350 mM NH <sub>4</sub> Cl, 10 mM MgCl <sub>2</sub> , 3 mM $\beta$ -ME, 1.1 M Sucrose
70S buffer:	20 mM HEPES/KOH (pH 7.4), 60 mM NH <sub>4</sub> Cl, 6 mM MgCl <sub>2</sub> , 3 mM $\beta$ -ME

### 4.11 Biochemistry

#### 4.11.1 Concentration determination

Unless stated otherwise, protein and nucleic acid concentrations were determined with a NanoDrop ND-1000 UV-Vis Spectrophotometer (Peqlab). Protein concentrations were calculated from the absorption at 280 nm according to the Lambert-Beer law. Molar extinction coefficients were determined with the ExPASy ProtParam tool (Gasteiger et al. 2003). The concentration of actin was determined from the absorption at 290 nm using a molar extinction coefficient of

26000 M<sup>-1</sup>cm<sup>-1</sup> (Abs 0.1% = 0.62). The concentration (c) of nucleic acids and ribosomes was calculated from the absorption at 260 or 254 nm as follows:

70S ribosomes ( <i>M. smegmatis</i> ):	$c = A_{260} \times 23 \text{ nM}$
<i>In vitro</i> transcribed RNAs:	$c = A_{260} \times 33 \text{ } \mu\text{g/ml}$
tRNA-tagged RNAs:	$c = A_{254} \times 37 \text{ } \mu\text{g/ml}$
ds DNA:	$c = A_{260} \times 50 \text{ } \mu\text{g/ml}$

### 4.11.2 Gel electrophoresis

Proteins were analyzed by sodium dodecyl sulfate polyacrylamide gel electrophoresis (SDS-PAGE) as described (Laemmli 1970). Depending on the size of the protein, 10-19% polyacrylamide gels were used. Gels were stained with Coomassie blue or SYPRO Orange (Sigma-Aldrich).

RNA was analyzed by native PAGE, denaturing Urea-PAGE, or agarose gel electrophoresis. Unless stated otherwise, electrophoresis was performed in 1x TBE. For Urea-PAGE, the polyacrylamide gel was supplemented with 8 M urea. Native loading dye was used for native PAGE and Urea-PAGE. Prior to separation on agarose gels, RNA samples were incubated in denaturing loading dye for 10 min at 70 °C. RNA gels were stained with Gel Red (Biotium).

10x TBE:	0.89 M TRIS, 0.89 M Boric acid, 20 mM EDTA
2x denaturing RNA loading dye:	95% Formamide, 0.025% SDS, 0.5 mM EDTA, 0.025% Xylene cyanol FF
6x native RNA loading dye:	60 mM Tris (pH 7.5), 60 % Glycerol

### 4.11.3 Circular dichroism spectroscopy.

Circular dichroism spectra were recorded with a Jasco J-810 spectropolarimeter at 20 °C. Proteins were diluted to 0.25-0.30 mg/ml with 10 mM NaH<sub>2</sub>PO<sub>4</sub>/Na<sub>2</sub>HPO<sub>4</sub> (pH 7.5) supplemented with 50 mM NaCl (She2p) or 200 mM NaCl (She3p). Measured spectra were averaged and corrected for the buffer. The secondary structure content was determined with the program K2d (Andrade et al. 1993).

#### 4.11.4 Chemical cross-linking of proteins

In a total volume of 22  $\mu$ l, 1-10  $\mu$ M of She3p or Myo4p were incubated with 45 mM 1-Ethyl-3-[3-dimethylaminopropyl]carbodiimide (EDC) and 45 mM N-Hydroxysuccinimide (NHS) in a buffer containing 20 mM HEPES/NaOH (pH 7.8) and 500 mM NaCl for 20 min at 25 °C. Afterwards, the sample was analyzed by SDS-PAGE and Coomassie blue staining.

#### 4.11.5 *In vitro* pull-down assay

In a total volume of 100  $\mu$ l, 10  $\mu$ M of She2p was mixed with 7.5  $\mu$ M His-tagged She3p in wash buffer. The mixture was centrifuged at 16100 x g and 4 °C for ten minutes to remove potential aggregates. After addition of 50  $\mu$ l nickel sepharose (GE Healthcare) and 200  $\mu$ l wash buffer, the mixture was gently agitated for 30-60 min at 4 °C. The nickel sepharose was pelleted by centrifugation (400 x g, 30 s, 4 °C), washed four times with 200  $\mu$ l and finally once with 50  $\mu$ l of wash buffer. Bound proteins were eluted with 50  $\mu$ l elution buffer. 1/10 of the input, 1/5 of the final wash, and 1/5 of the elution fraction were analyzed by SDS-PAGE and Coomassie blue staining.

Wash buffer: 20 mM HEPES/NaOH (pH 7.8), 200 mM NaCl, 2 mM MgCl<sub>2</sub>, 30 mM Imidazole

Elution buffer: 20 mM HEPES/NaOH (pH 7.8), 200 mM NaCl, 2 mM MgCl<sub>2</sub>, 750 mM Imidazole

#### 4.11.6 Analytical size-exclusion chromatography

Analytical size-exclusion chromatography (SEC) was performed at 4 °C using an ÄKTApurifier 10, a Superose 6 10/300 GL column (both GE Healthcare), and HNMD buffer as running buffer. Unless stated otherwise, the following concentrations were used: 8.5  $\mu$ M tRNA-tagged *ASH1-E3* RNA, 20  $\mu$ M She2p, 30  $\mu$ M She3p, and 15  $\mu$ M Myo4 (978-1471). The respective components were incubated in HNMD buffer for 5 min at room temperature, centrifuged (16100 x g, 4 °C, 10 min) to remove potential aggregates, and 100-300  $\mu$ l of the mixture were loaded onto the pre-equilibrated column at a flow rate of

0.5 ml/min. Collected fractions were analyzed by SDS-PAGE with Coomassie blue staining and 2% agarose gel electrophoresis with GelRed staining (Biotium).

HNMD buffer: 20 mM HEPES (pH 7.8), 200 mM NaCl, 2 mM MgCl<sub>2</sub>, 2 mM DTT

### **4.11.7 Density gradient centrifugation of SHE-core complexes**

In a total volume of 100  $\mu$ l, 30  $\mu$ M She2p, 30  $\mu$ M She3p, 15  $\mu$ M Myo4p (978-1471), and 15  $\mu$ M RNA (7.5  $\mu$ M in the case of 2x *ASH1*-E3-77-tRNA) were mixed in HNMD buffer and centrifuged (16100 x g, 4 °C, 20 min) to remove potential aggregates. After dynamic light scattering analysis (Section 4.11.8), the samples were loaded on 5-30% sucrose gradients in HNMD buffer and separated by ultracentrifugation (SW40 Ti rotor, 38 krpm, 15 h 30 min, 4 °C). Fractions were collected from the bottom to the top of the gradient using a peristaltic pump and analyzed on 10% SDS-polyacrylamide gels stained with Coomassie blue and on 1.5% agarose gels stained with GelRed (Biotium).

### **4.11.8 Dynamic light scattering**

Dynamic light scattering (DLS) was performed with a Viscotek 802 DLS instrument (Malvern) at 20 °C. At least ten intensity measurements for 4 s were averaged. The distribution of the hydrodynamic radius was determined from the autocorrelation function using the software OmniSIZE (Malvern). All samples showed one major species (>95% area), whose hydrodynamic radius is indicated.

### **4.11.9 Static light scattering**

Static light scattering (SLS) was performed with a Viscotek TDA 305 triple detector array (Malvern) coupled to an ÄKTApurifier 10 (GE Healthcare). The system was calibrated with 3.5 mg/ml BSA. Respective proteins and RNA were

## MATERIALS & METHODS

mixed in a stoichiometric or near-stoichiometric ratio at a total concentration of 1-5 mg/ml. The mixture was centrifuged (16100 x g, 4 °C, ≥ 10 min) to remove potential aggregates, and 100 µl thereof were separated on a SEC column at 4 °C with a flow rate of 0.5 ml/min. For Myo4p (978-1471) and for the She3p-His:Myo4p (978-1471) complex, a Superdex 200 10/300 GL column (GE Healthcare) in SLS buffer was used. All other samples were analyzed on a Superose 6 10/300 GL column (GE Healthcare) in HNMD buffer. The molecular weight of the sample was determined from the light scattering at right angle (RALS), the refractive index (RI), and the refractive index increment (dn/dc). A dn/dc value of 0.185 ml/g was used for proteins and a value of 0.170 ml/g for RNA (Rambo and Doudna 2004). For RNA:protein complexes, the dn/dc value was calculated according to the mass fraction ( $\omega$ ) of protein and RNA in the complex:

$$dn/dc = (\omega_{protein} \times 0.185 \text{ ml/g}) + (\omega_{RNA} \times 0.170 \text{ ml/g})$$

Accordingly, a dn/dc value of 0.182 ml/g was used for *ASH1-E3-51:She2p* and RNA:She2p:She3:Myo4p(978-1471). For tRNA-tagged zip-codes in complex with She2p, a dn/dc value of 0.178 was used. Data analysis was performed with the OmniSEC software (Malvern).

SLS buffer: 20 mM HEPES/NaOH (pH 7.8), 200 mM NaCl, 1 mM TCEP

### 4.11.10 Surface plasmon resonance

Surface plasmon resonance (SPR) experiments were performed with a Biacore 3000 system and a CM-5 chip (GE Healthcare) at 20 °C. HNMD buffer was used as running buffer. The proteins were centrifuged (16100 x g, 4 °C, 10 min) to remove potential aggregates and air bubbles. She3p was covalently attached to the chip surface by standard amine coupling. All binding signals were below 500 response units. Experiments were performed as duplicates and double referencing was applied. Kd values were obtained by fitting the steady-state SPR signals for varying She2p concentrations with the Langmuir isotherm.

#### 4.11.11 Isothermal titration calorimetry

Isothermal titration calorimetry (ITC) experiments were performed with an iTC200 isothermal titration calorimeter (GE Healthcare) at 20 °C. The very same ITC buffer preparation was used to purify both proteins by SEC and for subsequent dilution. Before measurement, the proteins were centrifuged (16100 x g, 4 °C, 10 min) to remove potential aggregates and air bubbles and the concentration was determined. A concentration of 10 µM Myo4p (978-1471) was used in the measuring cell and titrated with 220 µM She3p-His. The data was corrected for She3p-His titration into ITC buffer. The number of binding sites (N), the association constant (K<sub>a</sub>), and the change in enthalpy (ΔH) were obtained by fitting the data with the one-site binding model included in the MicroCal data analysis package based on the program Origin (OriginLab). The experiment was performed as duplicate.

ITC buffer: 20 mM HEPES/NaOH (pH 7.8), 500 mM NaCl, 1 mM TCEP

#### 4.11.12 Electrophoretic mobility shift assay

RNase-free materials and reagents were used for all steps. RNA oligonucleotides were radioactively labeled at the 5' end. In a total volume of 20 µl, 10 pmol dephosphorylated RNA oligonucleotide, 45 µCi (15 pmol)  $\gamma^{32}\text{P}$ -ATP (Hartmann Analytic, SRP-301), and 10 units T4 polynucleotide kinase (Fermentas) were incubated in reaction buffer A (Fermentas) for 45-90 min at 37 °C. The enzyme was inactivated for 10 min at 75 °C and the labeled RNA was separated from free nucleotides on a Sephadex G-25 Quick Spin column (Roche). The purified  $^{32}\text{P}$ -labeled RNA was diluted with DEPC-treated H<sub>2</sub>O to a total volume of 200 µl (final RNA concentration ca. 50 nM). The radiolabeled RNA was stored at -20 °C.

In a total volume of 20 µl, respective proteins at the indicated concentrations were incubated with 5 nM  $^{32}\text{P}$ -labeled RNA in HNMD buffer supplemented with 4% (v/v) glycerol and 30 µg/ml (EMSA with She2p and She3p) or 100 µg/ml yeast tRNA (EMSA with She3p) for 20 min at room temperature. For

stoichiometry determination, unlabeled RNA was added at the indicated concentration. The RNA:protein complexes were resolved on a native 4% polyacrylamide gel in 0.5x TBE for ca. 45 min at 80 V. Gels were scanned with a Storm Scanner (Amersham Biosciences).

### **4.11.13 UV cross-linking followed by mass spectrometry**

Ternary complexes of *ASH1*-E3-51 RNA, She2p, and She3p-His or She3p(334-425)-His were purified on a Superose 6 10/300 GL column (GE Healthcare) in HNMD buffer. Katharina Kramer and Prof. Henning Urlaub carried out all experimental steps following purification. In brief, 100 µg of the purified complex in a total volume of 200 µl were UV cross-linked for 10 min at 254 nm. The sample was digested with RNase A, RNase T1, and trypsin. Cross-linked peptides were enriched on a TiO<sub>2</sub> column (Luo et al. 2008; Kramer et al. 2011) and analyzed by nano liquid chromatography electrospray ionization mass spectrometry (Nano-LC-ESI-MS). Data analysis for the identification of cross-linked peptides was carried out essentially as described (Kramer et al. 2011). A detailed description of this method is given in Müller et al. 2011.

### **4.11.14 Quantitative mass spectrometry**

Complexes were purified by SEC in HNMD buffer (SHE-core complexes) or in SLS buffer (She3p:Myo4p complex). Care was taken that the complexes were saturated with all components. Dr. Lars Israel carried out all experimental steps following purification. In brief, 1-3 µg of the complex were incubated with 50 mM DTT for 60 min at room temperature followed by treatment with 10 mM iodoacetamide for 30 min at room temperature. Heavy-isotope labeled peptides (SpikeTides TQL, JPT Peptide Technologies) were dissolved in 40 mM ammonium bicarbonate. In a total volume of 50 µl, the pretreated sample was mixed with 0.5 pmol/µl of each peptide and the mixture was digested with 0.8 µg trypsin over night at 37 °C. 10 µl thereof (5 pmol of each heavy-isotope labeled

peptide) were analyzed by Nano-LC-ESI-MS/MS. Heavy and native light peptides were identified by search in a homemade database. The ratio of the peak areas in the MS scan was used to determine the amount of the respective light peptides in the sample. The MS analysis was performed twice for each purification and the results were averaged.

Peptide	Residues	Sequence
She2p peptide A	154-163	FSQWMIESLR*-Z
She2p peptide B	164-179	IGSNLLDLEVQFAIK*-Z
She2p peptide C	223-236	LSALDEEFDVVATK*-Z
She3p peptide	45-58	VIESLHDQIDMLTK*-Z
Myo4p peptide	1445-1464	YDTSAITQNSNTEGLATVSK*-Z

Amino acids labeled with the heavy isotopes <sup>15</sup>N and <sup>13</sup>C are marked with \*.  
Z: JPT-tag, cleaved by trypsin digestion

#### 4.11.15 Regenerative ATPase assay

The regenerative ATPase assay is based on an enzymatic system that regenerates hydrolyzed ATP under nicotinamide adenine dinucleotide (NADH) consumption (Norby 1988). The decay of NADH was measured spectroscopically with an Infinite M1000 PRO plate reader (Tecan). G-actin was polymerized to F-actin by incubation in 1x F-buffer supplemented with 10  $\mu$ M phalloidin (Sigma-Aldrich, P2141) for 30 min at room temperature. The ATPase assay was performed in a total volume of 50  $\mu$ l in 96-well plates (Greiner Bio-One, 675101) at 25 °C. The final reaction mixture contained ca. 35 nM Myo4p, 15  $\mu$ M F-actin, 1.2 mM NADH (Roche, 10107735001), 2 mM Phosphoenolpyruvic acid (Sigma-Aldrich, P7127), 10 U/ml Lactate dehydrogenase, 7.2 U/ml Pyruvate kinase (both Sigma-Aldrich, P0294), and 1 mM Mg-ATP (Sigma-Aldrich, A3377) in ATPase buffer. To investigate the effect of complex assembly, the mixture was supplemented by She3p, She2p, and RNA at the indicated concentrations. The ATPase assay was started by addition of Mg-ATP and the absorption of NADH was recorded at 340 nm for 60 min. In parallel, the same measurement was performed in the absence of Myo4p. Since only background NADH consumption was observed, the presence of active, contaminating ATPases can be excluded. The data was fit with a linear equation and the slope of the fit was corrected for the background NADH

consumption in each experiment. Since saturating concentrations of F-actin and ATP were used, the slope of the fit is proportional to the ATP turnover number and was used to calculate the relative ATPase activity with respect to Myo4p in the absence of any interaction partners.

10x F-buffer: 200 mM HEPES/NaOH (pH 7.8), 250 mM KCl, 20 mM MgCl<sub>2</sub>, 10 mM EGTA, 20 mM DTT

ATPase buffer: 20 mM Hepes/NaOH (pH 7.8), 100 mM NaCl, 25 mM KCl, 2 mM MgCl<sub>2</sub>, 1 mM EGTA, 2 mM DTT

### 4.11.16 Radioactive ATPase assay

The radioactive ATPase assay was performed in a total volume of 20 µl at 25 °C. The reaction mixture contained ca. 35 nM Myo4p, 15 µM F-actin, 1 mM Mg-ATP, and 2 nCi/µl  $\gamma^{32}\text{P}$ -ATP (Hartmann Analytic, SRP-301) in ATPase buffer. To investigate the effect of complex assembly, She3p, She2p, and RNA were added at the indicated concentrations. The assay was started by adding a premix of Mg-ATP and  $\gamma^{32}\text{P}$ -ATP. After 1, 15, 30, 45, and 60 min, the reaction was stopped by spotting 1µl of the mixture on a polyethylenimine-cellulose foil (Merck, 105579). Phosphate (P<sub>i</sub>) was separated from ATP by thin-layer chromatography in 1 M formic acid and 0.1% (w/v) LiCl. The thin-layer chromatography foil was scanned with a Storm Scanner and counts for ATP and P<sub>i</sub> were determined with the software ImageQuant (Amersham Biosciences). The amount (n) of hydrolyzed ATP at each time point was determined by the following formula:

$$n(\text{hydrolyzed ATP}) = \frac{\text{count}(P_i) \times n(\text{initial ATP})}{\text{count}(P_i) + \text{count}(ATP)}$$

The data was fit with a linear equation and the slope of the fit was corrected for the background ATP hydrolysis in the absence of Myo4p. The relative ATPase activity with respect to Myo4p alone was determined from the slope of the fit.

#### 4.11.17 Ribosome pelleting assay

In a final volume of 30  $\mu$ l, 0.4  $\mu$ M ribosomes, 2  $\mu$ M She2p, and 330  $\mu$ g/ml yeast tRNA were incubated in 70S-binding buffer for 10 min at room temperature. To determine the stoichiometry of binding, 0.4, 0.8, 1.2, and 1.6  $\mu$ M She2p were used. Binding of She2p and She3p was probed with 1  $\mu$ M of each protein. The sample was loaded on a 550  $\mu$ l sucrose cushion (70S-binding buffer supplemented by 0.75 M sucrose) in an 0.8 ml Ultra-Clear tube (Beckman-Coulter, 344090) and centrifuged (SW 55 rotor with adapter, 33 krpm, 3 h 45 min, 4 °C). Afterwards, the tube was flash frozen in liquid nitrogen and cut into halves. Proteins in the supernatant and the pellet fraction were precipitated with trichloroacetic acid, dissolved in 1x SDS-loading dye, and analyzed on a 15% SDS-polyarylamide gel. The gel was stained with SYPRO Orange (Sigma-Aldrich) and scanned (excitation: 488 nm, emission: 580 nm) with a Typhoon scanner (GE Healthcare).

70S-binding buffer: 20 mM HEPES/KOH (pH 7.4), 100 mM  $\text{NH}_4\text{Cl}$ , 6 mM  $\text{MgCl}_2$ , 3 mM  $\beta$ -ME

## 4.12 Structural biology

### 4.12.1 Crystallization

The ternary complex of She2p (6-246), She3p(334-425)-His, and either *ASH1*-E3-51 or *ASH1*-E3-51 ( $\Delta$ 1786-1802) was purified on a Superose 6 10/300 GL column (GE Healthcare) in HNMD buffer and concentrated by ultrafiltration. Initial crystallization screening was performed at the MPI Crystallization Facility (Martinsried, Germany) with a Phoenix crystallization robot (Art Robbins Instruments). Several commercially available and custom-made crystallization screens in 96 well format were tested. Crystallization was performed by sitting drop vapor diffusion with 100 nl sample and 100 nl precipitant solution at 20 °C. The final concentration of complex in the drop was ca. 1.1 mg/ml.

She2p (6-240, C-S) and She3p(354-425)-His were purified by SEC in S3C-SEC buffer. The proteins were mixed in approximately equimolar amounts and

concentrated by ultrafiltration. Initial crystallization screening was performed essentially as described. Refinement of the crystallization conditions was performed by hanging drop vapor diffusion with 1  $\mu$ l sample and 1  $\mu$ l precipitant solution at 4 °C and 20 °C. The final concentration of She2p in the drop was 2-3 mg/ml. Crystals usually appeared after 2-4 days. They were successively soaked with increasing concentrations of cryoprotectant in precipitant solution for 1-2 min and flash frozen in liquid nitrogen. The final concentration of cryoprotectant was 30% (v/v) glycerol or 20% (v/v) ethylene glycol. X-ray diffraction of the crystals was tested at ID 14-4 (ESRF, Grenoble, France).

### 4.12.2 Cryo-electron microscopy

Preparation of cryo-electron microscopy (cryo-EM) grids and data collection were performed by Charlotte Ungewickell, Dr. Otto Berninghausen, and Dr. Thomas Becker in the laboratory of Prof. Roland Beckmann. In brief, 46 nM zip-code ribosomes and 1.5  $\mu$ M She2p were incubated in 70S-binding buffer for 5 min at room temperature. Afterwards, the sample was applied to carbon-coated holey grids essentially as described (Wagenknecht et al. 1988). High-resolution data of *ASH1*-E3 zip-code ribosomes in complex with She2p were acquired with a Tecnai Polara F30 electron microscope (FEI) at 300 kV. Datasets were recorded under low-dose conditions with  $\sim 20$  electrons/ $\text{\AA}^2$  in a defocus range of 1.0-4.5  $\mu$ m. The micrographs were scanned with a Heidelberg drum scanner resulting in a pixel size of 1.2375  $\text{\AA}$ /pixel on the object scale. Low-resolution data were collected at 120 kV on a Tecnai G<sup>2</sup> Spirit electron microscope equipped with an Eagle 2k CCD camera (FEI) resulting in a pixel size of 3.308  $\text{\AA}$ /pixel.

#### 4.12.3 Calculation of single-particle cryo-EM reconstructions

Single-particle cryo-EM reconstructions were calculated with the software packages SPIDER and WEB (Frank et al. 1996). The contrast transfer function (CTF), the defocus value and the power spectrum for each micrograph were determined with SPIDER (Spirit data) or CTFFIND (Mindell and Grigorieff 2003) (Polara data). Power spectra were visualized with WEB and micrographs with power spectra indicating high drift or astigmatism were removed from the dataset. Single particles in the micrographs were identified automatically by the template matching method using SIGNATURE (Chen and Grigorieff 2007). These particles were inspected manually and images showing ribosome aggregates, ice, or contaminating particles were removed.

The preselected particles were aligned to a reference structure by projection matching. For alignment of wild-type *M. smegmatis* ribosomes, a cryo-EM reconstruction of the *Pyrococcus furiosus* ribosome was used as initial reference. The final reconstruction of the wild-type *M. smegmatis* ribosome was used as initial reference for the alignment of zip-code ribosomes. A total of 83 reference projections (15° increments) were calculated and corrected for the CTF of the respective micrograph. Each particle was compared with each reference projection by translational and rotational alignment of the particle image. The reference projection fitting best to a given particle was identified by the cross-correlation coefficient.

The micrographs were grouped into several defocus groups and three-dimensional reconstructions were calculated for each defocus group by backprojection in Fourier space. After correction for the average defocus value and the number of particles of each defocus group, the sub-reconstructions were merged to generate the initial three-dimensional reconstruction. To determine the resolution of the reconstruction, the dataset was randomly divided in halves and the resulting reconstructions were compared along shells in Fourier space (Frank 2002). The resolution was determined from the resulting Fourier Shell Correlation (FSC) curve at a cutoff of 0.5 (0.5 FSC criterion).

## MATERIALS & METHODS

The initial reconstruction was filtered according to its resolution and refined in an iterative process using the reconstruction of the current round as a reference for the next round of alignment. After each refinement cycle, backprojection in real space was performed. In the case of Polara data, initial alignment was done with three-fold decimated particle images. The decimation was decreased to two-fold with improving resolution. Final reconstructions were filtered according to their resolution with the Gaussian filter.

<b>Sample</b>	<b>Resolution (0.5 FSC criterion)</b>	<b>Number of particles</b>	<b>Microscope</b>
wt-70S ( <i>M. smegmatis</i> )	20 Å	7494	Spirit
ASH1-E3-70S	25 Å	7113	Spirit
ASH1-E3-70S:She2p	24 Å	4433	Spirit
ASH1-E3-70S:She2p	10 Å	~60000	Polara

Visualization of three-dimensional reconstructions and docking of crystal structures was done with UCSF CHIMERA (Pettersen et al. 2004).

## 5 ABBREVIATIONS

°C	Degree Celsius	EM	Electron microscopy
x g	Times standard gravity	EMSA	Electrophoretic mobility shift assay
β-ME	β-mercaptoethanol	ER	Endoplasmic reticulum
μ	Micro	ESI	Electrospray ionization
Å	Angstrom	F-actin	Filamentous actin
A <sub>254</sub>	Absorption at 254 nm	FISH	Fluorescence <i>in situ</i> hybridization
A <sub>260</sub>	Absorption at 260 nm	FSC	Fourier shell correlation
aa	Amino acid	g	Gram
Abs 0.1%	Absorption of a 0.1% (w/v) protein solution	G-actin	Globular actin
ADP	Adenosine diphosphate	GTD	Globular tail domain
ATP	Adenosine triphosphate	GST	Glutathione S-transferase
BicD	Bicaudal-D	IPTG	Isopropyl-β-D-thiogalactopyranosid
BSA	Bovine serum albumin	HEPES	Hydroxyethyl piperazine-ethanesulfonic acid
CaM	Calmodulin	hnRNP K	Heterogeneous nuclear ribonucleoprotein K
CaMKIIα	Ca <sup>2+</sup> /calmodulin-dependent protein kinase II α	HO endo-nuclease	Homothallic switching endonuclease
<i>C. albicans</i>	<i>Candida albicans</i>	k	Kilo
CD	Circular dichroism	Kd	Equilibrium dissociation constant
Ck2	Casein kinase 2	KH	hnRNP K homology
Cryo-EM	Cryo-electron microscopy	KHC	Kinesin heavy chain
C-terminus	Carboxy-terminus	Khd1p	KH-domain protein 1
CTF	Contrast transfer function	KLC	Kinesin light chain
DEPC	Diethylpyrocarbonate	l	Liter
DHC	Dynein heavy chain	LB	Lysogeny broth
DLS	Dynamic light scattering	LC	Liquid chromatography
DNA	Deoxyribonucleic acid	m	Milli
dn/dc	Refractive index increment	M	Molar
dsRBD	Double-stranded RNA-binding domain	MBP	Maltose-binding protein
<i>E. coli</i>	<i>Escherichia coli</i>	min	Minutes
EDC	1-Ethyl-3-[3-dimethyl-aminopropyl]carbodiimide	mRNA	Messenger RNA
EDTA	Ethylenediaminetetraacetic acid	MS	Mass spectrometry
Egl	Egalitarian	<i>M. smegmatis</i>	<i>Mycobacterium smegmatis</i>

## ABBREVIATIONS

n	Nano	UTR	Untranslated region
NADH	Nicotinamide adenine dinucleotide	UV	Ultraviolet
n.d.	Not determined	v/v	Volume per volume
NHS	N-Hydroxysuccinimide	wt	Wild type
N-terminus	Amino-terminus	w/v	Weight per volume
OD <sub>600</sub>	Optical density at 600 nm	X-gal	5-bromo-4-chloro-indolyl-galactopyranoside
PAGE	Polyacrylamide gel electrophoresis	Yck1p	Yeast casein kinase 1
PCR	Polymerase chain reaction		
pH	Potentia hydrogenii	<u>Amino acids</u>	
PMSF	Phenylmethylsulfonyl fluoride	A (Ala)	Alanine
PUF	Pumilio family	C (Cys)	Cysteine
Puf6p	Pumilio-homology domain family protein 6	D (Asp)	Aspartic acid
psi	Pound per square inch	E (Glu)	Glutamic acid
RALS	Right angle light scattering	F (Phe)	Phenylalanine
RI	Refractive index	G (Gly)	Glycine
RNA	Ribonucleic acid	H (His)	Histidine
RNAP II	RNA polymerase II	I (Ise)	Isoleucine
rpm	Revolutions per minute	K (Lys)	Lysine
RRM	RNA recognition motif	L (Leu)	Leucine
rRNA	Ribosomal RNA	M (Met)	Methionine
S	Svedberg	N (Asn)	Asparagine
<i>S. cerevisiae</i>	<i>Saccharomyces cerevisiae</i>	P (Pro)	Proline
SDS	Sodium dodecyl sulfate	Q (Gln)	Glutamine
SEC	Size-exclusion chromatography	R (Arg)	Arginine
SHE	Swi5p-dependent HO expression	S (Ser)	Serine
SHE-core complex	Complex containing She2p, She3p, Myo4p, and zip-code RNA	T (Thr)	Threonine
SLS	Static light scattering	V (Val)	Valine
SPR	Surface plasmon resonance	W (Trp)	Tryptophan
TCEP	Tris-(2-carboxyethyl)-phosphine hydrochloride	Y (Tyr)	Tyrosine
TGF	Transforming growth factor		
TRIS	Tris-(hydroxymethyl)-aminomethane	<u>Bases</u>	
tRNA	Transfer RNA	A	Adenine
		C	Cytosine
		G	Guanine
		T	Thymine
		U	Uracil

## 6 SUPPLEMENTARY INFORMATION

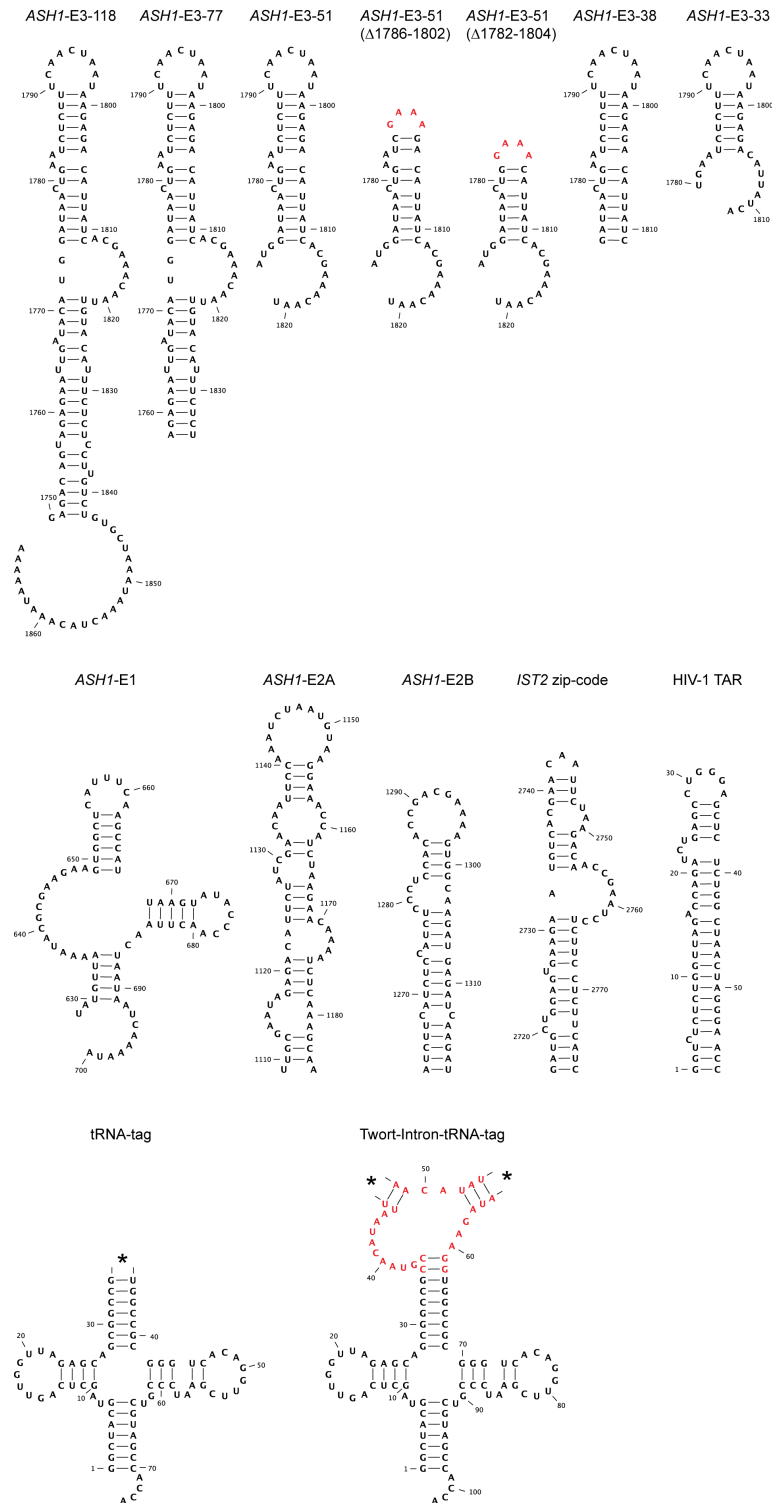


**Figure S1: Secondary structure predictions of RNAs used in this study.** The modeled GAAA tetraloops that are not part of the native *ASH1-E3* sequence and the sequence of the Twort intron are highlighted in red. “\*” marks positions where zip-code elements were fused to the tRNA-tag. Numbering of *ASH1* and *IST2* zip-code elements is with respect to the first base of the start codon. Predictions were prepared with the program CLC RNA Workbench ([www.clcbio.com](http://www.clcbio.com)), which uses a modified version of the algorithm developed by Zuker (Zuker 1989).

# SUPPLEMENTARY INFORMATION

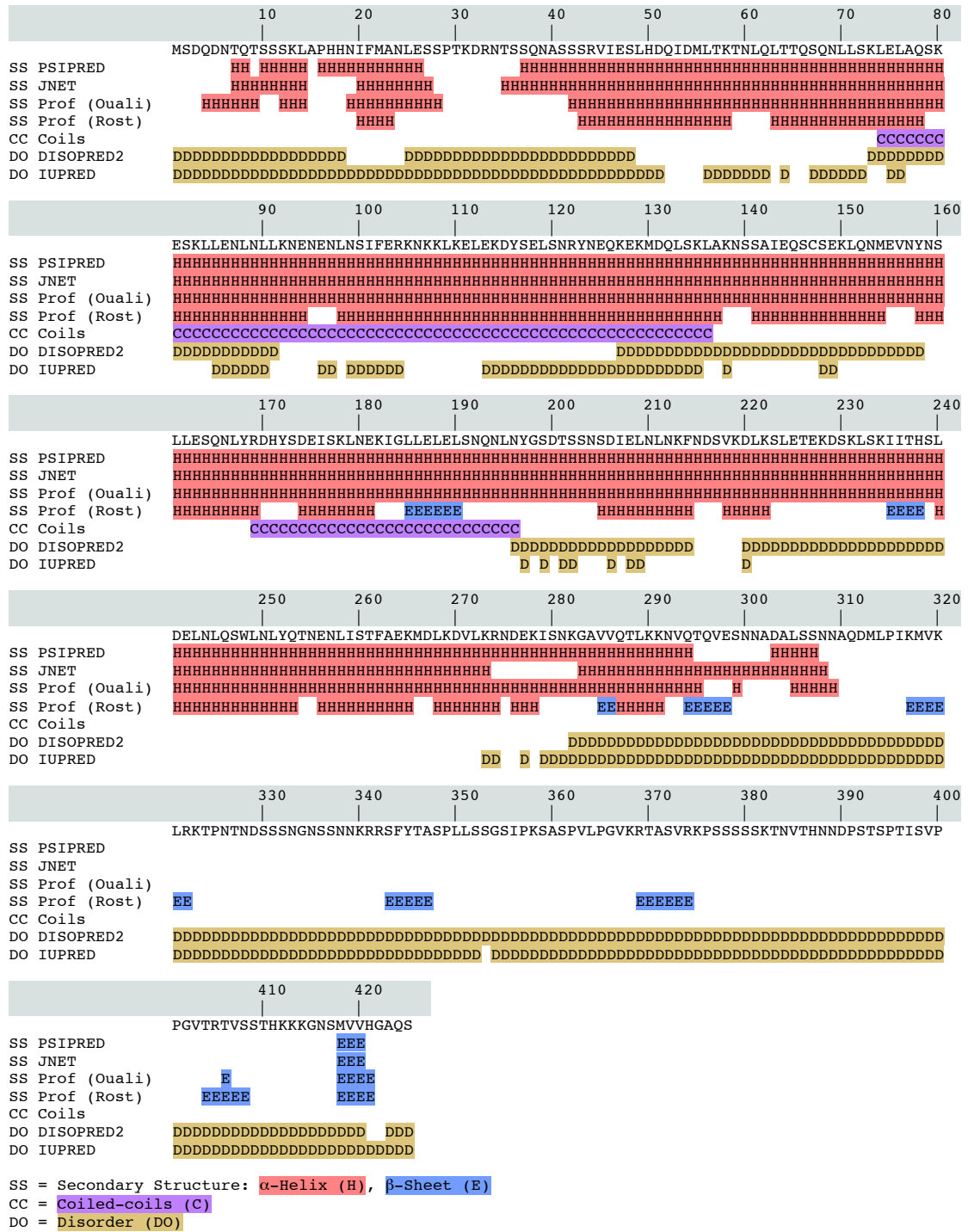


**Figure S2: Secondary structure prediction of She3p.** The prediction was prepared with the program Quick2D (Biegert et al. 2006) using different prediction algorithms for secondary structure (SS), coiled-coils (CC), and disordered (DO) regions. Structural features are color-coded.

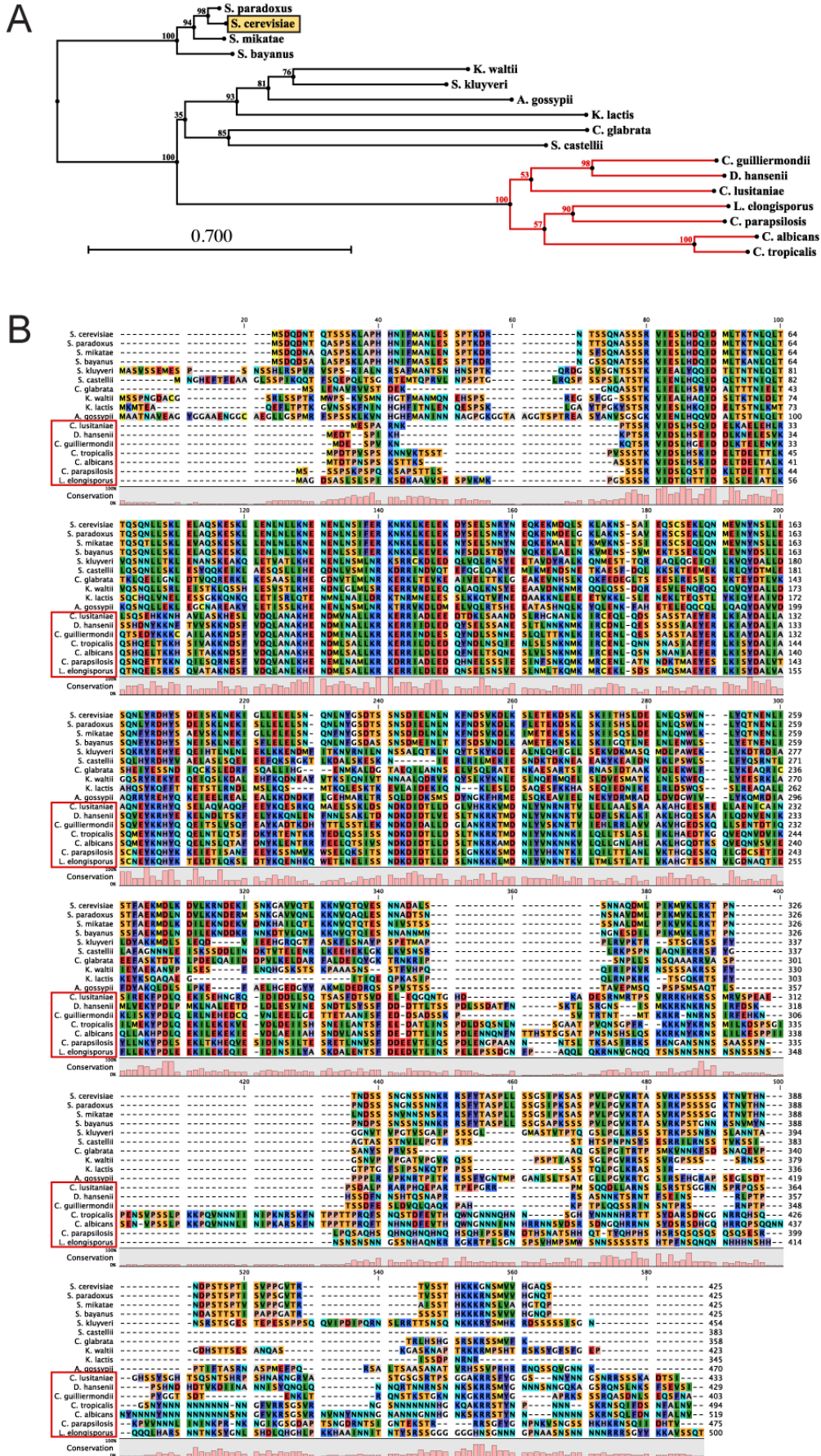
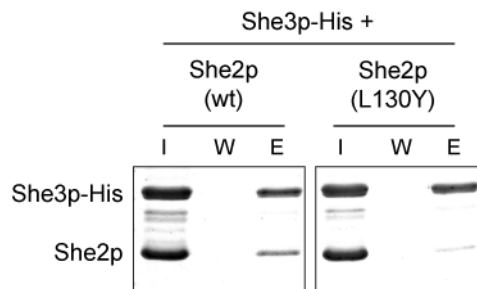


Figure S3: Alignment of She3p protein sequences from different yeast species.

## SUPPLEMENTARY INFORMATION

**A)** Evolutionary tree with bootstrap analysis. Species without a clear She2p homolog cluster in a separate branch (indicated in red). Bootstrap values are given above nodes. **B)** Sequence alignment of She3p from different yeast species. Yeast species without a clear She2p homolog are indicated by a red box. Amino acid properties are color-coded. The alignment was performed via Fungal Genome Search using WU-BLAST2 ([www.yeastgenome.org](http://www.yeastgenome.org)). Based on this alignment, the phylogenetic tree (Neighbor Joining algorithm) and alignment representation were prepared using the CLC Sequence Viewer ([www.clcbio.com](http://www.clcbio.com)). The figure was taken from Müller et al. 2011.



**Figure S4: Disruption of the She2p tetramer impairs binding to She3p.** In a pull-down experiment with immobilized His-tagged She3p, the tetramer mutant She2p (L130Y) (Müller et al. 2009) co-eluted less efficiently than wild-type She2p (I: input, W: final wash, E: elution).

## 7 REFERENCES

- Ainger, K., Avossa, D., Morgan, F., Hill, S.J., Barry, C., Barbarese, E., and Carson, J.H. 1993. Transport and localization of exogenous myelin basic protein mRNA microinjected into oligodendrocytes. *J Cell Biol* 123(2): 431-441.
- Akhmanova, A. and Hammer, J.A. 2010. Linking molecular motors to membrane cargo. *Curr Opin Cell Biol* 22(4): 479-487.
- Andrade, M.A., Chacon, P., Merelo, J.J., and Moran, F. 1993. Evaluation of secondary structure of proteins from UV circular dichroism spectra using an unsupervised learning neural network. *Protein Eng* 6(4): 383-390.
- Aronov, S., Gelin-Licht, R., Zipor, G., Haim, L., Safran, E., and Gerst, J.E. 2007. mRNAs encoding polarity and exocytosis factors are cotransported with the cortical endoplasmic reticulum to the incipient bud in *Saccharomyces cerevisiae*. *Mol Cell Biol* 27(9): 3441-3455.
- Atlas, R., Behar, L., Sapoznik, S., and Ginzburg, I. 2007. Dynamic association with polysomes during P19 neuronal differentiation and an untranslated-region-dependent translation regulation of the tau mRNA by the tau mRNA-associated proteins IMP1, HuD, and G3BP1. *J Neurosci Res* 85(1): 173-183.
- Barral, J.M., Hutagalung, A.H., Brinker, A., Hartl, F.U., and Epstein, H.F. 2002. Role of the myosin assembly protein UNC-45 as a molecular chaperone for myosin. *Science* 295(5555): 669-671.
- Beach, D.L., Thibodeaux, J., Maddox, P., Yeh, E., and Bloom, K. 2000. The role of the proteins Kar9 and Myo2 in orienting the mitotic spindle of budding yeast. *Curr Biol* 10(23): 1497-1506.
- Becalska, A.N. and Gavis, E.R. 2009. Lighting up mRNA localization in *Drosophila* oogenesis. *Development* 136(15): 2493-2503.
- Berger, I., Fitzgerald, D.J., and Richmond, T.J. 2004. Baculovirus expression system for heterologous multiprotein complexes. *Nat Biotechnol* 22(12): 1583-1587.
- Bertrand, E., Chartrand, P., Schaefer, M., Shenoy, S.M., Singer, R.H., and Long, R.M. 1998. Localization of *ASH1* mRNA particles in living yeast. *Mol Cell* 2(4): 437-445.
- Besse, F. and Ephrussi, A. 2008. Translational control of localized mRNAs: restricting protein synthesis in space and time. *Nat Rev Mol Cell Biol* 9(12): 971-980.
- Besse, F., Lopez de Quinto, S., Marchand, V., Trucco, A., and Ephrussi, A. 2009. *Drosophila* PTB promotes formation of high-order RNP particles and represses oskar translation. *Genes Dev* 23(2): 195-207.
- Bevilacqua, P.C. and Blose, J.M. 2008. Structures, kinetics, thermodynamics, and biological functions of RNA hairpins. *Annu Rev Phys Chem* 59: 79-103.
- Biegert, A., Mayer, C., Remmert, M., Soding, J., and Lupas, A.N. 2006. The MPI Bioinformatics Toolkit for protein sequence analysis. *Nucleic Acids Res* 34(Web Server issue): W335-339.
- Blasius, T.L., Cai, D., Jih, G.T., Toret, C.P., and Verhey, K.J. 2007. Two binding partners cooperate to activate the molecular motor Kinesin-1. *J Cell Biol* 176(1): 11-17.
- Bobola, N., Jansen, R.P., Shin, T.H., and Nasmyth, K. 1996. Asymmetric accumulation of Ash1p in postanaphase nuclei depends on a myosin and restricts yeast mating-type switching to mother cells. *Cell* 84(5): 699-709.
- Böhl, F., Kruse, C., Frank, A., Ferring, D., and Jansen, R.P. 2000. She2p, a novel RNA-binding protein tethers *ASH1* mRNA to the Myo4p myosin motor via She3p. *EMBO J* 19(20): 5514-5524.
- Borovinskaya, M.A., Pai, R.D., Zhang, W., Schuwirth, B.S., Holton, J.M., Hirokawa, G., Kaji, H., Kaji, A., and Cate, J.H. 2007. Structural basis for aminoglycoside inhibition of bacterial ribosome recycling. *Nat Struct Mol Biol* 14(8): 727-732.
- Bramham, C.R. and Wells, D.G. 2007. Dendritic mRNA: transport, translation and function. *Nat Rev Neurosci* 8(10): 776-789.
- Bramham, C.R., Worley, P.F., Moore, M.J., and Guzowski, J.F. 2008. The immediate early gene *arc/arg3.1*: regulation, mechanisms, and function. *J Neurosci* 28(46): 11760-11767.
- Bullock, S.L. 2011. Messengers, motors and mysteries: sorting of eukaryotic mRNAs by cytoskeletal transport. *Biochem Soc Trans* 39(5): 1161-1165.

## REFERENCES

- Bullock, S.L. and Ish-Horowicz, D. 2001. Conserved signals and machinery for RNA transport in *Drosophila* oogenesis and embryogenesis. *Nature* 414(6864): 611-616.
- Bullock, S.L., Nicol, A., Gross, S.P., and Zicha, D. 2006. Guidance of bidirectional motor complexes by mRNA cargoes through control of dynein number and activity. *Curr Biol* 16(14): 1447-1452.
- Bullock, S.L., Ringel, I., Ish-Horowicz, D., and Lukavsky, P.J. 2010. A'-form RNA helices are required for cytoplasmic mRNA transport in *Drosophila*. *Nat Struct Mol Biol* 17(6): 703-709.
- Cannone, J.J., Subramanian, S., Schnare, M.N., Collett, J.R., D'Souza, L.M., Du, Y., Feng, B., Lin, N., Madabusi, L.V., Muller, K.M. et al. 2002. The comparative RNA web (CRW) site: an online database of comparative sequence and structure information for ribosomal, intron, and other RNAs. *BMC Bioinformatics* 3: 2.
- Carter, A.P., Cho, C., Jin, L., and Vale, R.D. 2011. Crystal structure of the dynein motor domain. *Science* 331(6021): 1159-1165.
- Chao, J.A., Patskovsky, Y., Patel, V., Levy, M., Almo, S.C., and Singer, R.H. 2010. ZBP1 recognition of beta-actin zipcode induces RNA looping. *Genes Dev* 24(2): 148-158.
- Chartrand, P., Meng, X.H., Hüttelmaier, S., Donato, D., and Singer, R.H. 2002. Asymmetric sorting of ash1p in yeast results from inhibition of translation by localization elements in the mRNA. *Mol Cell* 10(6): 1319-1330.
- Chartrand, P., Meng, X.H., Singer, R.H., and Long, R.M. 1999. Structural elements required for the localization of *ASH1* mRNA and of a green fluorescent protein reporter particle in vivo. *Curr Biol* 9(6): 333-336.
- Chartrand, P., Singer, R.H., and Long, R.M. 2001. RNP localization and transport in yeast. *Annu Rev Cell Dev Biol* 17: 297-310.
- Chekulaeva, M., Hentze, M.W., and Ephrussi, A. 2006. Bruno acts as a dual repressor of oskar translation, promoting mRNA oligomerization and formation of silencing particles. *Cell* 124(3): 521-533.
- Chen, J.Z. and Grigorieff, N. 2007. SIGNATURE: a single-particle selection system for molecular electron microscopy. *J Struct Biol* 157(1): 168-173.
- Chung, S. and Takizawa, P.A. 2010. Multiple Myo4 motors enhance *ASH1* mRNA transport in *Saccharomyces cerevisiae*. *J Cell Biol* 189(4): 755-767.
- Condeelis, J. and Singer, R.H. 2005. How and why does *beta-actin* mRNA target? *Biol Cell* 97(1): 97-110.
- Cosma, M.P. 2004. Daughter-specific repression of *Saccharomyces cerevisiae* HO: Ash1 is the commander. *EMBO Rep* 5(10): 953-957.
- Deng, Y., Singer, R.H., and Gu, W. 2008. Translation of *ASH1* mRNA is repressed by Puf6p-Fun12p/eIF5B interaction and released by CK2 phosphorylation. *Genes Dev* 22(8): 1037-1050.
- Diaconu, M., Kothe, U., Schlunzen, F., Fischer, N., Harms, J.M., Tonevitsky, A.G., Stark, H., Rodnina, M.V., and Wahl, M.C. 2005. Structural basis for the function of the ribosomal L7/12 stalk in factor binding and GTPase activation. *Cell* 121(7): 991-1004.
- Dienstbier, M., Boehl, F., Li, X., and Bullock, S.L. 2009. Egalitarian is a selective RNA-binding protein linking mRNA localization signals to the dynein motor. *Genes Dev* 23(13): 1546-1558.
- Du, T.G., Jellbauer, S., Müller, M., Schmid, M., Niessing, D., and Jansen, R.P. 2008. Nuclear transit of the RNA-binding protein She2p is required for translational control of localized *ASH1* mRNA. *EMBO Rep* 9: 781-787.
- Dunn, B.D., Sakamoto, T., Hong, M.S., Sellers, J.R., and Takizawa, P.A. 2007. Myo4p is a monomeric myosin with motility uniquely adapted to transport mRNA. *J Cell Biol* 178(7): 1193-1206.
- Elson, S.L., Noble, S.M., Solis, N.V., Filler, S.G., and Johnson, A.D. 2009. An RNA transport system in *Candida albicans* regulates hyphal morphology and invasive growth. *PLoS Genet* 5(9): e1000664.
- Elvira, G., Wasiak, S., Blandford, V., Tong, X.K., Serrano, A., Fan, X., del Rayo Sanchez-Carbente, M., Servant, F., Bell, A.W., Boismenu, D. et al. 2006. Characterization of an RNA granule from developing brain. *Mol Cell Proteomics* 5(4): 635-651.
- Estrada, P., Kim, J., Coleman, J., Walker, L., Dunn, B., Takizawa, P., Novick, P., and Ferro-Novick, S. 2003. Myo4p and She3p are required for cortical ER inheritance in *Saccharomyces cerevisiae*. *J Cell Biol* 163(6): 1255-1266.

## REFERENCES

- Farina, K.L., Hüttelmaier, S., Musunuru, K., Darnell, R., and Singer, R.H. 2003. Two ZBP1 KH domains facilitate beta-actin mRNA localization, granule formation, and cytoskeletal attachment. *J Cell Biol* 160(1): 77-787.
- Ferrandon, D., Elphick, L., Nüsslein-Volhard, C., and St Johnston, D. 1994. Stauf protein associates with the 3'UTR of *bicoid* mRNA to form particles that move in a microtubule-dependent manner. *Cell* 79(7): 1221-1232.
- Ferrandon, D., Koch, I., Westhof, E., and Nüsslein-Volhard, C. 1997. RNA-RNA interaction is required for the formation of specific *bicoid* mRNA 3' UTR-STAUFIN ribonucleoprotein particles. *EMBO J* 16(7): 1751-1758.
- Forget, A. and Chartrand, P. 2011. Cotranscriptional assembly of mRNP complexes that determine the cytoplasmic fate of mRNA. *Transcription* 2(2): 86-90.
- Forrest, K.M. and Gavis, E.R. 2003. Live imaging of endogenous RNA reveals a diffusion and entrapment mechanism for nanos mRNA localization in *Drosophila*. *Curr Biol* 13(14): 1159-1168.
- Frank, J. 2001. Cryo-electron microscopy as an investigative tool: the ribosome as an example. *Bioessays* 23(8): 725-732.
- Frank, J. 2002. Single-particle imaging of macromolecules by cryo-electron microscopy. *Annu Rev Biophys Biomol Struct* 31: 303-319.
- Frank, J., Radermacher, M., Penczek, P., Zhu, J., Li, Y., Ladjadj, M., and Leith, A. 1996. SPIDER and WEB: processing and visualization of images in 3D electron microscopy and related fields. *J Struct Biol* 116(1): 190-199.
- Gagnon, J.A. and Mowry, K.L. 2011. Molecular motors: directing traffic during RNA localization. *Crit Rev Biochem Mol Biol* 46(3): 229-239.
- Gasteiger, E., Gattiker, A., Hoogland, C., Ivanyi, I., Appel, R.D., and Bairoch, A. 2003. ExPASy: The proteomics server for in-depth protein knowledge and analysis. *Nucleic Acids Res* 31(13): 3784-3788.
- Gautreau, D., Cote, C.A., and Mowry, K.L. 1997. Two copies of a subelement from the Vg1 RNA localization sequence are sufficient to direct vegetal localization in *Xenopus* oocytes. *Development* 124(24): 5013-5020.
- Gennerich, A. and Vale, R.D. 2009. Walking the walk: how kinesin and dynein coordinate their steps. *Curr Opin Cell Biol* 21(1): 59-67.
- Giorgi, C. and Moore, M.J. 2007. The nuclear nurture and cytoplasmic nature of localized mRNPs. *Semin Cell Dev Biol* 18(2): 186-193.
- Git, A. and Standart, N. 2002. The KH domains of *Xenopus* Vg1RBP mediate RNA binding and self-association. *RNA* 8(10): 1319-1333.
- Gonsalvez, G.B., Lehmann, K.A., Ho, D.K., Stanitsa, E.S., Williamson, J.R., and Long, R.M. 2003. RNA-protein interactions promote asymmetric sorting of the *ASH1* mRNA ribonucleoprotein complex. *RNA* 9(11): 1383-1399.
- Gonsalvez, G.B., Little, J.L., and Long, R.M. 2004. *ASH1* mRNA anchoring requires reorganization of the Myo4p/She3p/She2p transport complex. *J Biol Chem* 279: 46286-46294.
- Gonsalvez, G.B., Urbinati, C.R., and Long, R.M. 2005. RNA localization in yeast: moving towards a mechanism. *Biol Cell* 97(1): 75-86.
- Gonzalez, I., Buonomo, S.B., Nasmyth, K., and von Ahsen, U. 1999. *ASH1* mRNA localization in yeast involves multiple secondary structural elements and Ash1 protein translation. *Curr Biol* 9(6): 337-340.
- Gonzalez-Reyes, A., Elliott, H., and St Johnston, D. 1995. Polarization of both major body axes in *Drosophila* by gurken-torpedo signalling. *Nature* 375(6533): 654-658.
- Gu, W., Deng, Y., Zenklusen, D., and Singer, R.H. 2004. A new yeast PUF family protein, Puf6p, represses *ASH1* mRNA translation and is required for its localization. *Genes Dev* 18(12): 1452-1465.
- Hachet, O. and Ephrussi, A. 2004. Splicing of oskar RNA in the nucleus is coupled to its cytoplasmic localization. *Nature* 428(6986): 959-963.
- Hamilton, R.S. and Davis, I. 2007. RNA localization signals: deciphering the message with bioinformatics. *Semin Cell Dev Biol* 18(2): 178-185.
- Hanahan, D. 1983. Studies on transformation of *Escherichia coli* with plasmids. *J Mol Biol* 166(4): 557-580.
- Handa, N., Nureki, O., Kurimoto, K., Kim, I., Sakamoto, H., Shimura, Y., Muto, Y., and Yokoyama, S. 1999. Structural basis for recognition of the *tra* mRNA precursor by the Sex-lethal protein. *Nature* 398(6728): 579-585.

## REFERENCES

- Hasegawa, Y., Irie, K., and Gerber, A.P. 2008. Distinct roles for Khd1p in the localization and expression of bud-localized mRNAs in yeast. *RNA* 14(11): 2333-2347.
- Heuck, A. 2009. Characterization of a myosin transport complex from yeast. *PhD thesis*.
- Heuck, A., Du, T.G., Jellbauer, S., Richter, K., Kruse, C., Jaklin, S., Muller, M., Buchner, J., Jansen, R.P., and Niessing, D. 2007. Monomeric myosin V uses two binding regions for the assembly of stable translocation complexes. *Proc Natl Acad Sci USA* 104(50): 19778-19783.
- Heuck, A., Fetka, I., Brewer, D.N., Huls, D., Munson, M., Jansen, R.P., and Niessing, D. 2010. The structure of the Myo4p globular tail and its function in ASH1 mRNA localization. *J Cell Biol* 189(3): 497-510.
- Ho, S.N., Hunt, H.D., Horton, R.M., Pullen, J.K., and Pease, L.R. 1989. Site-directed mutagenesis by overlap extension using the polymerase chain reaction. *Gene* 77(1): 51-59.
- Hobbie, S.N., Kalapala, S.K., Akshay, S., Bruell, C., Schmidt, S., Dabow, S., Vasella, A., Sander, P., and Bottger, E.C. 2007. Engineering the rRNA decoding site of eukaryotic cytosolic ribosomes in bacteria. *Nucleic Acids Res* 35(18): 6086-6093.
- Hodges, A.R., Kremmentsova, E.B., and Trybus, K.M. 2008. She3p binds to the rod of yeast myosin V and prevents it from dimerizing, forming a single-headed motor complex. *J Biol Chem* 283(11): 6906-6914.
- Hogan, D.J., Riordan, D.P., Gerber, A.P., Herschlag, D., and Brown, P.O. 2008. Diverse RNA-binding proteins interact with functionally related sets of RNAs, suggesting an extensive regulatory system. *PLoS Biol* 6(10): e255.
- Holt, C.E. and Bullock, S.L. 2009. Subcellular mRNA localization in animal cells and why it matters. *Science* 326(5957): 1212-1216.
- Irie, K., Tadauchi, T., Takizawa, P.A., Vale, R.D., Matsumoto, K., and Herskowitz, I. 2002. The Khd1 protein, which has three KH RNA-binding motifs, is required for proper localization of ASH1 mRNA in yeast. *EMBO J* 21(5): 1158-1167.
- Jambhekar, A. and DeRisi, J.L. 2007. Cis-acting determinants of asymmetric, cytoplasmic RNA transport. *RNA* 13(5): 625-642.
- Jambhekar, A., McDermott, K., Sorber, K., Shepard, K.A., Vale, R.D., Takizawa, P.A., and DeRisi, J.L. 2005. Unbiased selection of localization elements reveals cis-acting determinants of mRNA bud localization in *Saccharomyces cerevisiae*. *Proc Natl Acad Sci USA* 102: 18005-18010.
- Jambor, H., Brunel, C., and Ephrussi, A. 2011. Dimerization of oskar 3' UTRs promotes hitchhiking for RNA localization in the *Drosophila* oocyte. *RNA* 17(12): 2049-2057.
- Jansen, R.P., Dowzer, C., Michaelis, C., Galova, M., and Nasmyth, K. 1996. Mother cell-specific HO expression in budding yeast depends on the unconventional myosin myo4p and other cytoplasmic proteins. *Cell* 84(5): 687-697.
- Kaan, H.Y., Hackney, D.D., and Kozielski, F. 2011. The structure of the kinesin-1 motor-tail complex reveals the mechanism of autoinhibition. *Science* 333(6044): 883-885.
- Kanai, Y., Dohmae, N., and Hirokawa, N. 2004. Kinesin transports RNA: isolation and characterization of an RNA-transporting granule. *Neuron* 43(4): 513-525.
- Karcher, R.L., Roland, J.T., Zappacosta, F., Huddleston, M.J., Annan, R.S., Carr, S.A., and Gelfand, V.I. 2001. Cell cycle regulation of myosin-V by calcium/calmodulin-dependent protein kinase II. *Science* 293(5533): 1317-1320.
- Kardon, J.R. and Vale, R.D. 2009. Regulators of the cytoplasmic dynein motor. *Nat Rev Mol Cell Biol* 10(12): 854-865.
- Kertesz, M., Wan, Y., Mazor, E., Rinn, J.L., Nutter, R.C., Chang, H.Y., and Segal, E. 2010. Genome-wide measurement of RNA secondary structure in yeast. *Nature* 467(7311): 103-107.
- Kim-Ha, J., Webster, P.J., Smith, J.L., and Macdonald, P.M. 1993. Multiple RNA regulatory elements mediate distinct steps in localization of oskar mRNA. *Development* 119(1): 169-178.
- King, M.L., Messitt, T.J., and Mowry, K.L. 2005. Putting RNAs in the right place at the right time: RNA localization in the frog oocyte. *Biol Cell* 97(1): 19-33.
- Kislauskis, E.H., Zhu, X., and Singer, R.H. 1994. Sequences responsible for intracellular localization of beta-actin messenger RNA also affect cell phenotype. *J Cell Biol* 127(2): 441-451.
- Kramer, K., Hummel, P., Hsiao, H.H., Luo, X., Wahl, M., and Urlaub, H. 2011. Mass-spectrometric analysis of proteins cross-linked to 4-thio-uracil- and 5-bromo-uracil-substituted RNA. *Int J Mass Spectrom* 304(2-3): 184-194.
- Krauss, J., Lopez de Quinto, S., Nusslein-Volhard, C., and Ephrussi, A. 2009. Myosin-V regulates oskar mRNA localization in the *Drosophila* oocyte. *Curr Biol* 19(12): 1058-1063.

## REFERENCES

- Krementsova, E.B., Hodges, A.R., Bookwalter, C.S., Sladewski, T.E., Travaglia, M., Sweeney, H.L., and Trybus, K.M. 2011. Two single-headed myosin V motors bound to a tetrameric adapter protein form a processive complex. *J Cell Biol* 195(4): 631-641.
- Krementsova, E.B., Hodges, A.R., Lu, H., and Trybus, K.M. 2006. Processivity of chimeric class V myosins. *J Biol Chem* 281(9): 6079-6086.
- Kruse, C., Jaedicke, A., Beaudouin, J., Böhl, F., Ferring, D., Güttler, T., Ellenberg, J., and Jansen, R.P. 2002. Ribonucleoprotein-dependent localization of the yeast class V myosin Myo4p. *J Cell Biol* 159(6): 971-982.
- Kugler, J.M. and Lasko, P. 2009. Localization, anchoring and translational control of oskar, gurken, bicoid and nanos mRNA during Drosophila oogenesis. *Fly (Austin)* 3(1): 15-28.
- Laemmli, U.K. 1970. Cleavage of structural proteins during the assembly of the head of bacteriophage T4. *Nature* 227(5259): 680-685.
- Landers, S.M., Gallas, M.R., Little, J., and Long, R.M. 2009. She3p possesses a novel activity required for ASH1 mRNA localization in *Saccharomyces cerevisiae*. *Eukaryot Cell* 8(7): 1072-1083.
- Lange, S., Katayama, Y., Schmid, M., Burkacky, O., Brauchle, C., Lamb, D.C., and Jansen, R.P. 2008. Simultaneous transport of different localized mRNA species revealed by live-cell imaging. *Traffic* 9(8): 1256-1267.
- Latham, V.M., Yu, E.H., Tullio, A.N., Adelstein, R.S., and Singer, R.H. 2001. A Rho-dependent signaling pathway operating through myosin localizes *beta-actin* mRNA in fibroblasts. *Curr Biol* 11(13): 1010-1016.
- Lecuyer, E., Yoshida, H., Parthasarathy, N., Alm, C., Babak, T., Cerovina, T., Hughes, T.R., Tomancak, P., and Krause, H.M. 2007. Global analysis of mRNA localization reveals a prominent role in organizing cellular architecture and function. *Cell* 131(1): 174-187.
- Lehmann, R. and Nusslein-Volhard, C. 1986. Abdominal segmentation, pole cell formation, and embryonic polarity require the localized activity of oskar, a maternal gene in Drosophila. *Cell* 47(1): 141-152.
- Leontis, N.B. and Westhof, E. 2003. Analysis of RNA motifs. *Curr Opin Struct Biol* 13(3): 300-308.
- Lescoute, A. and Westhof, E. 2006. Topology of three-way junctions in folded RNAs. *RNA* 12(1): 83-93.
- Leung, K.M., van Horck, F.P., Lin, A.C., Allison, R., Standart, N., and Holt, C.E. 2006. Asymmetrical beta-actin mRNA translation in growth cones mediates attractive turning to netrin-1. *Nat Neurosci* 9(10): 1247-1256.
- Li, J.F. and Nebenfuhr, A. 2008. The tail that wags the dog: the globular tail domain defines the function of myosin V/XI. *Traffic* 9(3): 290-298.
- Li, X.D., Ikebe, R., and Ikebe, M. 2005. Activation of myosin Va function by melanophilin, a specific docking partner of myosin Va. *J Biol Chem* 280(18): 17815-17822.
- Li, X.D., Jung, H.S., Mabuchi, K., Craig, R., and Ikebe, M. 2006. The globular tail domain of myosin Va functions as an inhibitor of the myosin Va motor. *J Biol Chem* 281(31): 21789-21798.
- Li, X.D., Jung, H.S., Wang, Q., Ikebe, R., Craig, R., and Ikebe, M. 2008. The globular tail domain puts on the brake to stop the ATPase cycle of myosin Va. *Proc Natl Acad Sci U S A* 105(4): 1140-1145.
- Lister, I., Schmitz, S., Walker, M., Trinick, J., Buss, F., Veigel, C., and Kendrick-Jones, J. 2004. A monomeric myosin VI with a large working stroke. *EMBO J* 23(8): 1729-1738.
- Liu, J., Taylor, D.W., Krementsova, E.B., Trybus, K.M., and Taylor, K.A. 2006. Three-dimensional structure of the myosin V inhibited state by cryoelectron tomography. *Nature* 442(7099): 208-211.
- Long, R.M., Gu, W., Lorimer, E., Singer, R.H., and Chartrand, P. 2000. She2p is a novel RNA-binding protein that recruits the Myo4p-She3p complex to ASH1 mRNA. *EMBO J* 19(23): 6592-6601.
- Long, R.M., Gu, W., Meng, X., Gonsalvez, G., Singer, R.H., and Chartrand, P. 2001. An exclusively nuclear RNA-binding protein affects asymmetric localization of ASH1 mRNA and Ash1p in yeast. *J Cell Biol* 153(2): 307-318.
- Long, R.M., Singer, R.H., Meng, X., Gonzalez, I., Nasmyth, K., and Jansen, R.P. 1997. Mating type switching in yeast controlled by asymmetric localization of ASH1 mRNA. *Science* 277(5324): 383-387.
- Lord, M., Sladewski, T.E., and Pollard, T.D. 2008. Yeast UCS proteins promote actomyosin interactions and limit myosin turnover in cells. *Proc Natl Acad Sci U S A* 105(23): 8014-8019.

## REFERENCES

- Lu, H., Kremontsova, E.B., and Trybus, K.M. 2006. Regulation of myosin V processivity by calcium at the single molecule level. *J Biol Chem* 281(42): 31987-31994.
- Luo, X., Hsiao, H.H., Bubunenko, M., Weber, G., Court, D.L., Gottesman, M.E., Urlaub, H., and Wahl, M.C. 2008. Structural and functional analysis of the E. coli NusB-S10 transcription antitermination complex. *Mol Cell* 32(6): 791-802.
- MacDougall, N., Clark, A., MacDougall, E., and Davis, I. 2003. Drosophila gurken (TGF $\alpha$ ) mRNA localizes as particles that move within the oocyte in two dynein-dependent steps. *Dev Cell* 4(3): 307-319.
- Martel, C., Dugre-Brisson, S., Boulay, K., Breton, B., Lapointe, G., Armando, S., Trepanier, V., Duchaine, T., Bouvier, M., and Desgroseillers, L. 2010. Multimerization of Staufen1 in live cells. *RNA* 16(3): 585-597.
- Martin, K.C. and Ephrussi, A. 2009. mRNA localization: gene expression in the spatial dimension. *Cell* 136(4): 719-730.
- Martin, K.C. and Zukin, R.S. 2006. RNA trafficking and local protein synthesis in dendrites: an overview. *J Neurosci* 26(27): 7131-7134.
- Matadeen, R., Sergiev, P., Leonov, A., Pape, T., van der Sluis, E., Mueller, F., Osswald, M., von Knoblauch, K., Brimacombe, R., Bogdanov, A. et al. 2001. Direct localization by cryo-electron microscopy of secondary structural elements in Escherichia coli 23 S rRNA which differ from the corresponding regions in Haloarcula marismortui. *J Mol Biol* 307(5): 1341-1349.
- Meignin, C. and Davis, I. 2010. Transmitting the message: intracellular mRNA localization. *Curr Opin Cell Biol* 22(1): 112-119.
- Micklem, D.R., Adams, J., Grunert, S., and St Johnston, D. 2000. Distinct roles of two conserved Staufen domains in oskar mRNA localization and translation. *EMBO J* 19(6): 1366-1377.
- Mili, S., Moissoglu, K., and Macara, I.G. 2008. Genome-wide screen reveals APC-associated RNAs enriched in cell protrusions. *Nature* 453(7191): 115-119.
- Miller, S., Yasuda, M., Coats, J.K., Jones, Y., Martone, M.E., and Mayford, M. 2002. Disruption of dendritic translation of CaMKII $\alpha$  impairs stabilization of synaptic plasticity and memory consolidation. *Neuron* 36(3): 507-519.
- Mindell, J.A. and Grigorieff, N. 2003. Accurate determination of local defocus and specimen tilt in electron microscopy. *J Struct Biol* 142(3): 334-347.
- Müller, M. 2009. Characterization of She2p-dependent mRNP assembly in Saccharomyces cerevisiae. *PhD thesis*.
- Müller, M., Heuck, A., and Niessing, D. 2007. Directional mRNA transport in eukaryotes: lessons from yeast. *Cell Mol Life Sci* 64: 171-180.
- Müller, M., Heym, R.G., Mayer, A., Kramer, K., Schmid, M., Cramer, P., Urlaub, H., Jansen, R.P., and Niessing, D. 2011. A cytoplasmic complex mediates specific mRNA recognition and localization in yeast. *PLoS Biol* 9(4): e1000611.
- Müller, M., Richter, K., Heuck, A., Kremmer, E., Buchner, J., Jansen, R.P., and Niessing, D. 2009. Formation of She2p tetramers is required for mRNA binding, mRNP assembly, and localization. *RNA* 15(11): 2002-2012.
- Münchow, S., Ferring, D., Kahlina, K., and Jansen, R.P. 2002. Characterization of Candida albicans ASH1 in Saccharomyces cerevisiae. *Curr Genet* 41(2): 73-81.
- Navarro, C., Puthalakath, H., Adams, J.M., Strasser, A., and Lehmann, R. 2004. Egalitarian binds dynein light chain to establish oocyte polarity and maintain oocyte fate. *Nat Cell Biol* 6: 381-383.
- Neuman-Silberberg, F.S. and Schupbach, T. 1993. The Drosophila dorsoventral patterning gene gurken produces a dorsally localized RNA and encodes a TGF  $\alpha$ -like protein. *Cell* 75(1): 165-174.
- Nielsen, J., Kristensen, M.A., Willemoes, M., Nielsen, F.C., and Christiansen, J. 2004. Sequential dimerization of human zipcode-binding protein IMP1 on RNA: a cooperative mechanism providing RNP stability. *Nucleic Acids Res* 32(14): 4368-4376.
- Niessing, D., Huttelmaier, S., Zenklusen, D., Singer, R.H., and Burley, S.K. 2004. She2p is a novel RNA binding protein with a basic helical hairpin motif. *Cell* 119(4): 491-502.
- Norby, J.G. 1988. Coupled assay of Na<sup>+</sup>,K<sup>+</sup>-ATPase activity. *Methods Enzymol* 156: 116-119.
- Oeffinger, M., Wei, K.E., Rogers, R., Degrasse, J.A., Chait, B.T., Aitchison, J.D., and Rout, M.P. 2007. Comprehensive analysis of diverse ribonucleoprotein complexes. *Nat Methods* 4(11): 951-956.

## REFERENCES

- Olivier, C., Poirier, G., Gendron, P., Boisgontier, A., Major, F., and Chartrand, P. 2005. Identification of a conserved RNA motif essential for She2p recognition and mRNA localization to the yeast bud. *Mol Cell Biol* 25(11): 4752-4766.
- Paquin, N., Menade, M., Poirier, G., Donato, D., Drouet, E., and Chartrand, P. 2007. Local Activation of Yeast ASH1 mRNA Translation through Phosphorylation of Khd1p by the Casein Kinase Yck1p. *Mol Cell* 26(6): 795-809.
- Pashkova, N., Jin, Y., Ramaswamy, S., and Weisman, L.S. 2006. Structural basis for myosin V discrimination between distinct cargoes. *EMBO J* 25: 693-700.
- Perez-Canadillas, J.M. 2006. Grabbing the message: structural basis of mRNA 3'UTR recognition by Hrp1. *EMBO J* 25(13): 3167-3178.
- Pettersen, E.F., Goddard, T.D., Huang, C.C., Couch, G.S., Greenblatt, D.M., Meng, E.C., and Ferrin, T.E. 2004. UCSF Chimera--a visualization system for exploratory research and analysis. *J Comput Chem* 25(13): 1605-1612.
- Phichith, D., Travaglia, M., Yang, Z., Liu, X., Zong, A.B., Safer, D., and Sweeney, H.L. 2009. Cargo binding induces dimerization of myosin VI. *Proc Natl Acad Sci U S A* 106(41): 17320-17324.
- Ponchon, L., Beauvais, G., Nonin-Lecomte, S., and Dardel, F. 2009. A generic protocol for the expression and purification of recombinant RNA in Escherichia coli using a tRNA scaffold. *Nat Protoc* 4(6): 947-959.
- Ponchon, L. and Dardel, F. 2007. Recombinant RNA technology: the tRNA scaffold. *Nat Methods* 4(7): 571-576.
- Powrie, E.A., Zenklusen, D., and Singer, R.H. 2011. A nucleoporin, Nup60p, affects the nuclear and cytoplasmic localization of ASH1 mRNA in *S. cerevisiae*. *RNA* 17(1): 134-144.
- Rambo, R.P. and Doudna, J.A. 2004. Assembly of an active group II intron-maturase complex by protein dimerization. *Biochemistry* 43(21): 6486-6497.
- Reck-Peterson, S.L., Provance, D.W., Jr., Mooseker, M.S., and Mercer, J.A. 2000. Class V myosins. *Biochim Biophys Acta* 1496(1): 36-51.
- Reck-Peterson, S.L., Tyska, M.J., Novick, P.J., and Mooseker, M.S. 2001. The yeast class V myosins, Myo2p and Myo4p, are nonprocessive actin-based motors. *J Cell Biol* 153(5): 1121-1126.
- Rook, M.S., Lu, M., and Kosik, K.S. 2000. CaMKIIalpha 3' untranslated region-directed mRNA translocation in living neurons: visualization by GFP linkage. *J Neurosci* 20(17): 6385-6393.
- Ross, A.F., Oleynikov, Y., Kislauskis, E.H., Taneja, K.L., and Singer, R.H. 1997. Characterization of a beta-actin mRNA zipcode-binding protein. *Mol Cell Biol* 17(4): 2158-2165.
- Sambrook, J. and Russel, D.W. 2000. Molecular Cloning: A Laboratory Manual. *Cold Spring Harbor Laboratory*.
- Schmid, M., Jaedicke, A., Du, T.-D., and Jansen, R.-P. 2006. Coordination of endoplasmic reticulum and mRNA localization to the yeast bud. *Curr Biol* 16(15): 1538-1543.
- Sellers, J.R. and Veigel, C. 2006. Walking with myosin V. *Curr Opin Cell Biol* 18(1): 68-73.
- Shahbadian, K. and Chartrand, P. 2011. Control of cytoplasmic mRNA localization. *Cell Mol Life Sci*.
- Sharma, S., Ding, F., and Dokholyan, N.V. 2008. iFoldRNA: three-dimensional RNA structure prediction and folding. *Bioinformatics* 24(17): 1951-1952.
- Shen, Z., Paquin, N., Forget, A., and Chartrand, P. 2009. Nuclear Shuttling of She2p Couples ASH1 mRNA Localization to its Translational Repression by Recruiting Loc1p and Puf6p. *Mol Biol Cell* 20(8): 2265-2275.
- Shen, Z., St-Denis, A., and Chartrand, P. 2010. Cotranscriptional recruitment of She2p by RNA pol II elongation factor Spt4-Spt5/DSIF promotes mRNA localization to the yeast bud. *Genes Dev* 24(17): 1914-1926.
- Shepard, K.A., Gerber, A.P., Jambhekar, A., Takizawa, P.A., Brown, P.O., Herschlag, D., DeRisi, J.L., and Vale, R.D. 2003. Widespread cytoplasmic mRNA transport in yeast: identification of 22 bud-localized transcripts using DNA microarray analysis. *Proc Natl Acad Sci USA* 100(20): 11429-11434.
- Shi, H. and Blobel, G. 2010. UNC-45/CRO1/She4p (UCS) protein forms elongated dimer and joins two myosin heads near their actin binding region. *Proc Natl Acad Sci U S A* 107(50): 21382-21387.
- Sil, A. and Herskowitz, I. 1996. Identification of asymmetrically localized determinant, Ash1p, required for lineage-specific transcription of the yeast *HO* gene. *Cell* 84(5): 711-722.

## REFERENCES

- Sivaramakrishnan, S. and Spudich, J.A. 2009. Coupled myosin VI motors facilitate unidirectional movement on an F-actin network. *J Cell Biol* 187(1): 53-60.
- Slagter-Jager, J.G., Allen, G.S., Smith, D., Hahn, I.A., Frank, J., and Belfort, M. 2006. Visualization of a group II intron in the 23S rRNA of a stable ribosome. *Proc Natl Acad Sci U S A* 103(26): 9838-9843.
- Spahn, C.M., Grassucci, R.A., Penczek, P., and Frank, J. 1999. Direct three-dimensional localization and positive identification of RNA helices within the ribosome by means of genetic tagging and cryo-electron microscopy. *Structure* 7(12): 1567-1573.
- Spudich, J.A. and Watt, S. 1971. The regulation of rabbit skeletal muscle contraction. I. Biochemical studies of the interaction of the tropomyosin-troponin complex with actin and the proteolytic fragments of myosin. *J Biol Chem* 246(15): 4866-4871.
- St Johnston, D. 2005. Moving messages: the intracellular localization of mRNAs. *Nat Rev Mol Cell Biol* 6: 363-375.
- St Johnston, D., Brown, N.H., Gall, J.G., and Jantsch, M. 1992. A conserved double-stranded RNA-binding domain. *Proc Natl Acad Sci U S A* 89(22): 10979-10983.
- Steward, O., Wallace, C.S., Lyford, G.L., and Worley, P.F. 1998. Synaptic activation causes the mRNA for the IEG Arc to localize selectively near activated postsynaptic sites on dendrites. *Neuron* 21(4): 741-751.
- Takizawa, P.A., DeRisi, J.L., Wilhelm, J.E., and Vale, R.D. 2000. Plasma membrane compartmentalization in yeast by messenger RNA transport and a septin diffusion barrier. *Science* 290(5490): 341-344.
- Takizawa, P.A., Sil, A., Swedlow, J.R., Herskowitz, I., and Vale, R.D. 1997. Actin-dependent localization of an RNA encoding a cell-fate determinant in yeast. *Nature* 389(6646): 90-93.
- Takizawa, P.A. and Vale, R.D. 2000. The myosin motor, Myo4p, binds *ASH1* mRNA via the adapter protein, She3p. *Proc Natl Acad Sci USA* 97(10): 5273-5278.
- Tang, F., Kauffman, E.J., Novak, J.L., Nau, J.J., Catlett, N.L., and Weisman, L.S. 2003. Regulated degradation of a class V myosin receptor directs movement of the yeast vacuole. *Nature* 422(6927): 87-92.
- Taylor, K.A. 2007. Regulation and recycling of myosin V. *Curr Opin Cell Biol* 19(1): 67-74.
- Thio, G.L., Ray, R.P., Barcelo, G., and Schupbach, T. 2000. Localization of gurken RNA in Drosophila oogenesis requires elements in the 5' and 3' regions of the transcript. *Dev Biol* 221(2): 435-446.
- Thirumurugan, K., Sakamoto, T., Hammer, J.A., 3rd, Sellers, J.R., and Knight, P.J. 2006. The cargo-binding domain regulates structure and activity of myosin 5. *Nature* 442(7099): 212-215.
- Toi, H., Fujimura-Kamada, K., Irie, K., Takai, Y., Todo, S., and Tanaka, K. 2003. She4p/Dim1p interacts with the motor domain of unconventional myosins in the budding yeast, *Saccharomyces cerevisiae*. *Mol Biol Cell* 14(6): 2237-2249.
- Trybus, K.M. 2008. Myosin V from head to tail. *Cell Mol Life Sci* 65(9): 1378-1389.
- Tyska, M.J. and Mooseker, M.S. 2003. Myosin-V motility: these levers were made for walking. *Trends Cell Biol* 13(9): 447-451.
- Urbinati, C.R., Gonsalvez, G.B., Aris, J.P., and Long, R.M. 2006. Loc1p is required for efficient assembly and nuclear export of the 60S ribosomal subunit. *Mol Genet Genomics* 276(4): 369-377.
- Urlaub, H., Kuhn-Holsken, E., and Luhrmann, R. 2008. Analyzing RNA-protein crosslinking sites in unlabeled ribonucleoprotein complexes by mass spectrometry. *Methods Mol Biol* 488: 221-245.
- Vale, R.D. 2003a. Myosin V motor proteins: marching stepwise towards a mechanism. *J Cell Biol* 163(3): 445-450.
- Vale, R.D. 2003b. The molecular motor toolbox for intracellular transport. *Cell* 112(4): 467-480.
- Vale, R.D. and Milligan, R.A. 2000. The way things move: looking under the hood of molecular motor proteins. *Science* 288(5463): 88-95.
- Wagenknecht, T., Grassucci, R., and Frank, J. 1988. Electron microscopy and computer image averaging of ice-embedded large ribosomal subunits from *Escherichia coli*. *J Mol Biol* 199(1): 137-147.
- Wagner, C., Palacios, I., Jaeger, L., St Johnston, D., Ehresmann, B., Ehresmann, C., and Brunel, C. 2001. Dimerization of the 3'UTR of bicoid mRNA involves a two-step mechanism. *J Mol Biol* 313(3): 511-524.

## REFERENCES

- Walker, M.L., Burgess, S.A., Sellers, J.R., Wang, F., Hammer, J.A., 3rd, Trinick, J., and Knight, P.J. 2000. Two-headed binding of a processive myosin to F-actin. *Nature* 405(6788): 804-807.
- Wang, X. and Tanaka Hall, T.M. 2001. Structural basis for recognition of AU-rich element RNA by the HuD protein. *Nat Struct Biol* 8(2): 141-145.
- Welte, M.A. 2004. Bidirectional transport along microtubules. *Curr Biol* 14(13): R525-537.
- Wesche, S., Arnold, M., and Jansen, R.P. 2003. The UCS domain protein She4p binds to myosin motor domains and is essential for class I and class V myosin function. *Curr Biol* 13(9): 715-724.
- Wilkie, G.S. and Davis, I. 2001. Drosophila wingless and pair-rule transcripts localize apically by dynein-mediated transport of RNA particles. *Cell* 105(2): 209-219.
- Yao, J., Sasaki, Y., Wen, Z., Bassell, G.J., and Zheng, J.Q. 2006. An essential role for beta-actin mRNA localization and translation in Ca<sup>2+</sup>-dependent growth cone guidance. *Nat Neurosci* 9(10): 1265-1273.
- Yokoyama, T. and Suzuki, T. 2008. Ribosomal RNAs are tolerant toward genetic insertions: evolutionary origin of the expansion segments. *Nucleic Acids Res* 36(11): 3539-3551.
- Yu, C., Feng, W., Wei, Z., Miyanoiri, Y., Wen, W., Zhao, Y., and Zhang, M. 2009. Myosin VI undergoes cargo-mediated dimerization. *Cell* 138(3): 537-548.
- Zaessinger, S., Busseau, I., and Simonelig, M. 2006. Oskar allows nanos mRNA translation in Drosophila embryos by preventing its deadenylation by Smaug/CCR4. *Development* 133(22): 4573-4583.
- Zimyanin, V., Lowe, N., and St Johnston, D. 2007. An oskar-dependent positive feedback loop maintains the polarity of the Drosophila oocyte. *Curr Biol* 17(4): 353-359.
- Zuker, M. 1989. On finding all suboptimal foldings of an RNA molecule. *Science* 244(4900): 48-52.

## **PUBLICATIONS & PRESENTATIONS**

### **Parts of this work have been published:**

Müller, M.\*, Heym, R.G.\*, Mayer, A., Kramer, K., Schmid, M., Cramer, P., Urlaub, H., Jansen, R.P., and Niessing, D. 2011. A cytoplasmic complex mediates specific mRNA recognition and localization in yeast. *PLoS Biol* 9(4): e1000611.

\* These authors contributed equally to this work.

### **Parts of this work have been presented at international conferences:**

#### **Selected talks:**

RNA 2011, 16th Annual Meeting of the RNA Society, Kyoto (Japan)

3rd International Gene Center/SFB646 Symposium, 2011, Munich (Germany)

Heym, R.G., Müller, M., Mayer, A., Kramer, K., Schmid, M., Cramer, P., Urlaub, H., Jansen, R.P., and Niessing, D. A cytoplasmic complex mediates specific mRNA recognition and localization in yeast.

#### **Posters:**

EMBO Practical Course on Computational RNA Biology, 2010, Cargèse (France)

The Complex Life of mRNA: From Synthesis to Decay, 2010, EMBL, Heidelberg (Germany)

Heym, R.G., Müller, M., Beckmann, R., and Niessing, D. Assembly of the cytoplasmic *ASH1* mRNP.

#### **Other publications:**

Heym, R.G. and Niessing, D. 2011. Principles of mRNA transport in yeast. *Cell Mol Life Sci*.

Unterreitmeier, S., Fuchs, A., Schaffler, T., Heym, R.G., Frishman, D., and Langosch, D. 2007. Phenylalanine promotes interaction of transmembrane domains via GxxxG motifs. *J Mol Biol* 374(3): 705-718.

Dietz, H., Bornschlöggl, T., Heym, R., König, F. and Rief, M. 2007. Programming protein self assembly with coiled coils. *New J Phys* 9, 424.

## ACKNOWLEDGEMENTS

Viele Menschen haben zu dieser Arbeit beigetragen. Ihnen möchte ich an dieser Stelle herzlich danken. Dierk Niessing danke ich für sein großes Engagement. Er hat mich stets unterstützt, gefördert und mit seinen Impulsen wesentlich zum Gelingen dieser Arbeit beigetragen. Außerdem gab er mir die nötige Freiheit eigene Ideen und Interessen einzubringen.

Roland Beckmann möchte ich für die Betreuung dieser Arbeit als erster Gutachter und für seine Unterstützung bei allen Cryo-EM Experimenten danken. Bei Klaus Förstemann, Karl-Peter Hopfner, Petra Wendler und Thomas Becker bedanke ich mich für ihre guten Ideen und Anregungen bei den TAC-Meetings.

Zahlreiche Kooperationen haben diese Arbeit grundlegend beeinflusst. Charlotte Ungewickell, Otto Berninghausen und Thomas Becker danke ich für ihre Hilfe in Sachen Cryo-EM. Bei Katharina Kramer, Henning Urlaub und Lars Israel bedanke ich mich für ihre massenspektrometrischen Analysen. Erik Böttger und seiner Arbeitsgruppe danke ich für die Unterstützung bei der Modifikation und Reinigung der *M. smegmatis* Ribosomen.

Mein Dank gilt auch allen aktuellen und ehemaligen "Niessings". Besonders Alex Heuck und Daniela Hüls möchte ich für hilfreiche Diskussionen und ihre Unterstützung danken. Sigrun Jaklin bin ich besonders dankbar, dass sie mir einen Großteil der Klonierungsarbeit abgenommen hat und außerdem immer für gute Stimmung im Labor gesorgt hat. Marisa Müller danke ich für die erfolgreiche Zusammenarbeit bei der Charakterisierung spezifischer RNA-Bindung, Annika Niedner für die kostbare *ASH1* mRNA und Sebastian Brück für die tatkräftige Unterstützung während seines Praktikums.

Zu guter Letzt möchte ich meiner Familie für ihren großen Rückhalt danken. Mein größter Dank gilt Lisa, die mich durch alle Höhen und Tiefen begleitet hat.